Materials & Design 244 (2024) 113077

Contents lists available at ScienceDirect

Materials & Design

journal homepage: www.elsevier.com/locate/matdes

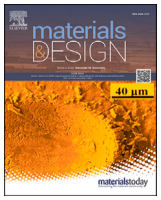

Towards a fracture mechanics-based fatigue assessment of lattice structures obtained from additive manufacturing of metallic powders

Francesco Collini, Giovanni Meneghetti *

University of Padova, Department of Industrial Engineering, via Venezia 1, 35131, Padova, Italy

ARTICLE INFO

Keywords:
Additive manufacturing
Lattice structures
Defect-tolerant fatigue design
Linear Elastic Fracture Mechanics
Notch-Stress Intensity Factor

ABSTRACT

Additive Manufacturing (AM) technologies are at the forefront of technological development in machine design as they allow the production of complex parts with high stiffness-to-weight ratios, such as lattice structures, that conventional production processes cannot manufacture. Despite the advantages of AM and lattice structures, their potential is currently limited by concerns related to their fatigue strength due to process-related intrinsic defects. Considering that fatigue is a leading cause of mechanical failures that require costly maintenance, the interest in understanding the fatigue strength of AMed lattice structures is evident.

This work explores the applicability of the Linear Elastic Fracture Mechanics (LEFM) for predicting the fatigue limit of lattice structures, building on the positive results obtained for AMed fully-dense materials. It includes a literature review of the experimental fatigue analysis of lattice structures, highlighting the experimental evidence of the fundamental role of AM defects and notches on the fatigue strength of AMed lattice structures. The main conclusions are that AMed lattice structures should be considered defective and notched materials, and the fatigue assessment should be performed with LEFM-based approaches. Lastly, this paper validates LEFM-based predictions against 400+ experimental data for AMed materials from the literature, including small-sized specimens and lattice structures.

1. Introduction

The increasing demand from the industry for light but reliable and stiff structures is propelling the development of Additive Manufacturing (AM) technologies of metallic materials, especially in the automotive, biomedical, and aerospace industries.

AM for metallic materials is a cutting-edge technology that builds parts layer by layer, creating complex geometries that may be impossible to achieve with conventional subtractive processes. The most common technologies for metallic materials can be divided into two categories: Powder Bed Fusion (PBF) and Direct Energy Deposition (DED). As depicted in Fig. 1, the process involves the melting and subsequent rapid solidification of metallic powders using an input energy source, usually a laser or an electron beam. In PBF processes, Fig. 1 a), a scraper distributes a thin layer of powder across the build area, and the laser (or electron beam) selectively scans and melts the powder to form the desired geometry layer by layer. In contrast, DED processes, Fig. 1 b), deliver the powder through a nozzle, which is simultaneously melted by the energy source to build the part. PBF processes are conducted in a highly controlled environment, resulting in finer, more precise parts. This method is particularly advantageous for producing small, intricate components such as lattice structures. On the other hand, DED is more suitable for creating larger parts, as the nozzle and energy source can be mounted on robotic arms, leading to a seemingly infinite building volume or building on top of already existing parts. Among the possibilities AM offers, lattice structures (or cellular structures, metamaterials, architected materials, stochastic materials, and trabecular structures), in particular, stand out. These structures are obtained by the repetition in the space of a Unit Cell (UC, or Elementary Cell) of struts and nodes or thin sheets and, at the apparent macroscopic scale, are characterized by mechanical properties different from that of the base material.

Lattice structures can be classified into two different categories depending on their architecture:

- strut-based lattice structures, composed of nodes connected by struts, which can be further divided into (i) stretching-dominated if, by replacing all the nodes with spherical joints and considering the struts as links, the UC does not exhibit internal degrees of freedom; (ii) else, bending-dominated.

* Corresponding author.
E-mail address: giovanni.meneghetti@unipd.it (G. Meneghetti).

https://doi.org/10.1016/j.matdes.2024.113077
Received 21 April 2024; Received in revised form 4 June 2024; Accepted 7 June 2024
Available online 18 June 2024

List of symbols

E or E_0, E_{lattice}	Young's modulus of the base material and of the homogeneous material associated with the lattice structure at the apparent macroscopic scale, respectively
ρ or ρ_0	Density of the base material and of the homogeneous material associated with the lattice structure at the apparent macroscopic scale, respectively
γ	singularity exponent of the stress field ahead of notches and cracks
K_{I}	Stress Intensity Factor (SIF)
K_{I}^{v}	Notch-Stress Intensity Factor (N-SIF)
ΔK_{th}	threshold SIF
$\Delta K_{\text{th}}^{\text{v}}$	threshold N-SIF
$\Delta K_{\text{th,LC}}$	fatigue crack propagation threshold for long cracks
K_{tg}	elastic stress concentration factor referred to the gross section of the specimen
a_0	El Haddad-Smith-Topper material constant
a	reference dimension of a crack or notch size
$\sqrt{\text{area}}$	square root of the area of a defect projected onto the plane perpendicular to the maximum principal stress
a_{eff}	effective crack size
α, α_γ	geometric shape factor for a component containing a crack or a notch, respectively
σ_{g}	remote gross nominal stress
$\Delta\sigma_{\text{g}}$	range of the remote gross nominal stress
$\Delta\sigma_{\text{g,th}}$	threshold range of the remote gross nominal stress
$\Delta\sigma_0$	plain specimen fatigue limit (in terms of stress range)
HV	Vickers Hardness
N_{f}	number of cycles to failure
σ_{Y}	yield strength of the material
R	force ratio

List of acronyms

AB	As-Built
AD	As-Designed
ALM	Atzori-Lazzarin-Meneghetti
AM	Additive Manufacturing
AMed	Additively Manufactured
BD	Building Direction
DS	Down Skin
EHST	El Haddad-Smith-Topper
FCIS	Fatigue Crack Initiation Site
HIP	Hot Isostatic Pressing
LOF	Lack Of Fusion
LEFM	Linear Elastic Fracture Mechanics
NPC	Non-Propagating Crack
N-SIF	Notch-Stress Intensity Factor
PBF, L-PBF, EB-PBF	Powder Bed Fusion, Laser-PBF, Electron Beam-PBF, respectively
SIF	Stress Intensity Factor
UC	Unit Cell
US	Upper Skin

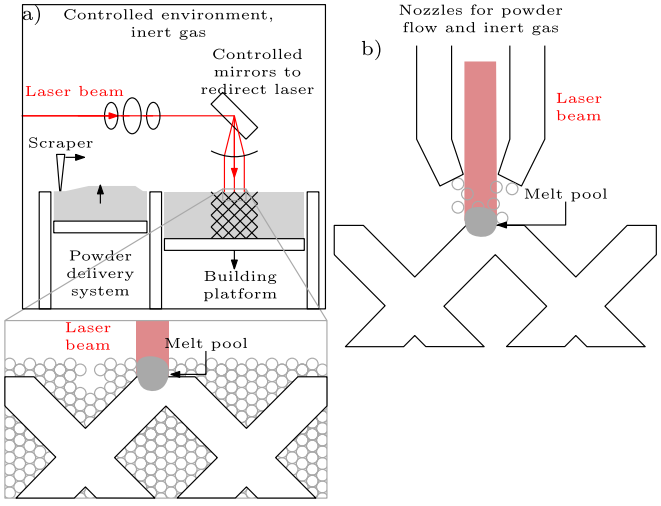

Fig. 1. Schematic representation of the AM processes for metallic materials; a) PBF processes, b) DED process.

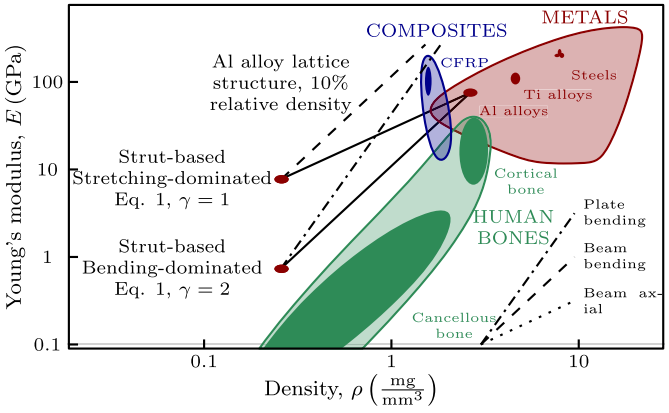

Fig. 2. Materials selection diagram for optimal stiffness-to-weight ratio; data for metals and composites materials from ANSYS Granta Material Selector, data for human bones from [1]. Optimal selection curves in the bottom right are $\frac{E}{\rho}$ for beams under axial loading, $\frac{E}{\rho^2}$ for beams under bending loading, and $\frac{E}{\rho^3}$ for plates under bending loading.

- sheet-based lattice structures if their UC is made of thin plates, which can be subdivided into open and closed cells.

The growing engineering interest in lattice structures over the past few decades can be explained by analyzing the relationships proposed by Ashby and Deshpande in [2] between the elastic modulus and the density of lattice structures at the apparent macroscopic scale (subscript lattice) and the base material that they are made of (subscript 0):

$$\frac{E_{\text{lattice}}}{E_0} = \text{const.} \left(\frac{\rho_{\text{lattice}}}{\rho_0} \right)^{\gamma} \tag{1}$$

where: $\gamma = 1$ for stretching-dominated structures, while $\gamma = 2$ for bending-dominated structures. Leary et al. [3], showed that equation (1) is capable of capturing the behavior of lattice structures; however, large scatter bands are required (const. $= 0.1 \div 4$), mainly due to the manufacturing defects. Concerning Fig. 2, note that

1. lattice structures allow to obtain stiffness-to-weight ratios competitive with those of composite materials. This, combined with the high geometry freedom of the AM process, renders this class of structures particularly suitable for producing light, stiff, and reliable structures [4];
2. the lower the relative density of the lattice structure ($\rho_{\text{rel}} = \frac{\rho_{\text{lattice}}}{\rho_0}$), the higher the stiffness-to-weight ratio, thus, for a given stiffness target and UC size, the smaller individual features, the lighter the structure. At the current state-of-the-art, powder-based AM technologies can manufacture features on the scale of approximately 100 μm; as a result, sheet-based UCs are larger than struts-based.

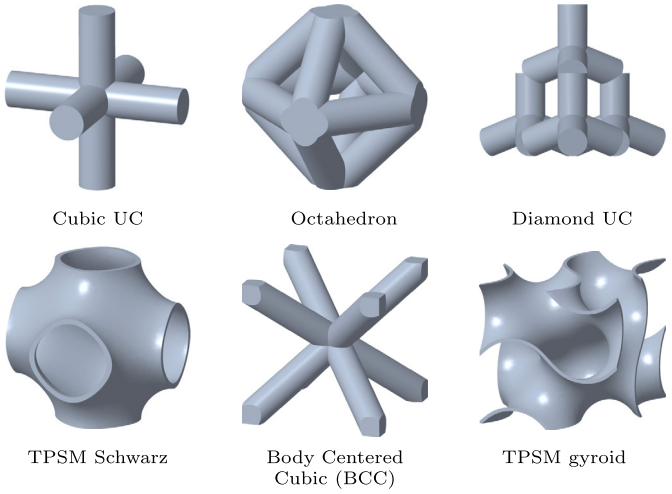

Fig. 3. Topology of some common UCs adopted in the literature.

Recent developments with different technologies allow the manufacturing of significantly smaller parts in the range of $\approx 1 \div 100$ nm [5,6].

3. the ability to replicate the stiffness of the human bone, combined with that of producing materials with negative Poisson's ratio on the apparent macroscopic scale (auxetic lattice structures), significantly increases the bio-compatibility for bone implants by reducing the bone shielding phenomenon and favoring the osseointegration [7–9]. Additionally, the geometry freedom enables the production of patient-specific bone implants, further increasing their bio-compatibility.

Furthermore, lattice structures can be designed to assess multiple functions simultaneously; some relevant examples from the literature are: load-carrying heat exchangers [10]; bone implants storing antibiotic drugs in the voids of the lattice structure [11], a novel leading edge of an airplane wing capable of withstanding the aerodynamic loads and bird-strikes, while also integrating the anti-ice system functions [12]. For further readings on the possible applications of lattice structures, the interested reader is referred to [3,13,14].

The specific industrial application, the design targets, and technology limitations guide the selection of the proper UC architecture. The rules of thumb are: sheet-based lattice structures are better suited for heat exchangers given their high surface-to-volume ratio – although size limitation may lead to struts-based lattice structures with higher surface-to-volume ratios; avoid building struts of size below $0.2 \div 0.3$ mm, and features with orientation angle below $30 \div 35°$deg; introduce smooth transitions from fully-dense portions to lattice structures to reduce stress concentrations at the transition region. The most common UCs found in the literature are reported in Fig. 3. Achieving the optimal selection may involve design optimization procedures (e.g., topology optimization, lattice optimization) to tailor the lattice architecture to the desired mechanical characteristics that are currently available in commercial FE software.

Currently, the use of AMed lattice structures in critically loaded components is limited due to concerns related to their structural integrity, especially under fatigue loading, arising from AM process-specific peculiarities. In particular: (i) the pronounced surface roughness and the internal defects that may favor fatigue crack initiation and growth, (ii) the strong residual stresses in As-Built (AB) conditions, and (iii) the high defect sensitivity of AMed microstructures in AB conditions. These factors collectively contribute to the poor fatigue strength of AMed materials compared to their counterparts obtained by conventional processes. Moreover, the fatigue assessment is complex considering: (i) the potentially significant discrepancy between the As-Designed (AD) and As-Built (AB) geometry of the component [15–19], (ii) the inherently notched nature of lattice structure and the manufacturing defects leading to severe stress concentrations and local multiaxial stress fields, (iii) the unpredictability of the defect distribution based solely on process parameters and the geometry of the part, and (iv) the lack of regulations standardizing either the experimental testing of lattice structures and their fatigue assessment. Lastly, the possibility of structural health monitoring is minimal, and on this topic, the literature concerning real structures is scarce.

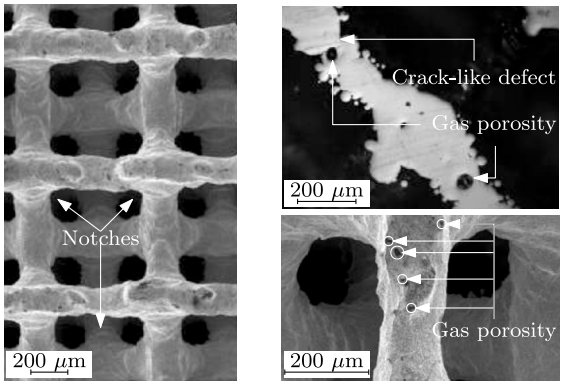

Fig. 4. Stress concentrations at strut junctions and defects such as internal voids and surface roughness; a) and c) adapted from [20] with permission from ELSEVIER; b) adapted from [21] with permission from ELSEVIER.

At the current state of the art, the fatigue assessment of AMed lattice structures is typically performed with a nominal approach. It requires the calculation of the applied nominal stresses, either considering the homogenized material associated with the lattice structure at the apparent macroscopic scale or employing the beam theory for individual struts. The obtained stresses are then compared with an experimentally calibrated $\sigma - N_f$ curve to estimate the component's fatigue life. The main limitation of the method is that it neglects the effects of the stress concentrations at: (i) the notches, such as strut junctions, and (ii) the defects inherent to the AM process, as illustrated in Fig. 4.

Experimental results show that lattice-structure fatigue cracks initiate from surface defects or internal defects close to the surface, characteristic of the AM process. Assuming the presence of Non-Propagating Cracks (NPC) originating from such defects at the fatigue limit (as experimentally seen for various metallic alloys typically used to produce lattice structures), the estimation of the fatigue limit should be performed with a local approach based on the Linear Elastic Fracture Mechanics (LEFM). In the literature, there are several successful applications of LEFM-based models for un-notched AMed materials (e.g., [22–33]) but very few for notched materials [31,34,35] and, to the best of the author's knowledge, none for lattice structures. Only a few studies have explored the use of methods based on the Theory of Critical Distances (TCD) [36–38] to lattice structures considering the presence of the AM defects.

The present work is based on extensive research of the relevant scientific literature on the fatigue strength of lattice structures, conducted by analyzing articles indexed in Scopus and Web of Science databases. The literature search focused on articles containing the following words in the title, abstract, and keywords: "lattice structures" OR "metamaterials" OR "architected materials" AND "fatigue", limiting the search to the fields "Fatigue Of Materials", "Fatigue", "Cracks" in Scopus and "Metallurgical Engineering", "Nanofibers, Scaffolds & Fabrication" and "Mechanics" in Web Of Science. Due to the scarcity of data available in the literature on the fatigue behavior of AMed lattice structures, the review also builds on previous knowledge on the fatigue behavior of metallic materials weakened by defects and notches, both conventionally and AMed.

The present article is organized as follows:

- Section 2 discusses the defects characteristic of the AM process, focusing on aspects detrimental to fatigue strength;
- Section 3 delves into the fatigue assessment of notched and defective materials, examining the competition between notches and defects;
- Section 4 provides a comprehensive review of the experimental analysis of fatigue behavior in AMed lattice structures;
- Section 5 proposes a validation of the Defect Tolerant models proposed in the theoretical background against data from the scientific literature for AMed materials and lattice structures, highlighting the potential of the approach;
- finally, in Section 6 the final remarks.

Although the design optimization of lattice structures and the optimization of process parameters are essential to taking advantage of the potential of AMed lattice structures, this article does not discuss these topics in detail. While a thorough analysis regarding the optimization of the process parameters is beyond the scope of the present work, it is the author's opinion that optimization procedures, at the current state of the art, often lack a fatigue design criterion that includes the material-microstructure-loading conditions system besides part's geometry. Nonetheless, the interested reader is referred to [39–45] for further insights into the fatigue design and optimization of UCs, and to [46,47] for a comprehensive review of guidelines on the design for additive.

2. Characteristic properties of AMed materials

At the current state of the art, Additive Manufacturing technologies cannot produce defect-free materials. Instead, AMed parts exhibit a series of peculiarities that are detrimental to their fatigue strength and pose challenges when performing the fatigue assessment:

- the pronounced surface roughness and large internal porosities that act as a stress raiser and thus promote fatigue crack initiation and growth;
- the presence of significant residual stresses, typically tensile near the outer surface, that are detrimental to the fatigue strength and alter the nominal stress field;
- the potentially notable discrepancy between the nominal As-Designed (AD) geometry and the As-Built (AB – i.e., the conditions of the parts when removed from the building platform before any post-processing treatment) geometry, altering the mechanical response from that of the nominal geometry.

This Section covers the aforementioned characteristic properties of AMed materials in AB conditions and how post-processing treatments can mitigate their effect. The microstructure of AMed materials and the quantitative influence of individual process parameters on the defect distribution are not discussed. Although these topics are valuable and relevant, they are beyond the scope of this review article and are better suited for dedicated analysis; only some qualitative notes on the influence of the most important process parameters are reported here.

2.1. Surface roughness and internal porosity

Although it is possible to improve the surface finish through machining processes (e.g., turning, milling, and grinding) or chemical etching, the surface roughness in AB conditions requires a thorough analysis for the following reasons:

- for specific applications, a pronounced surface roughness can be beneficial. For example, increased surface roughness is preferred in the biomedical field as it enhances the biocompatibility of bone implants [48];

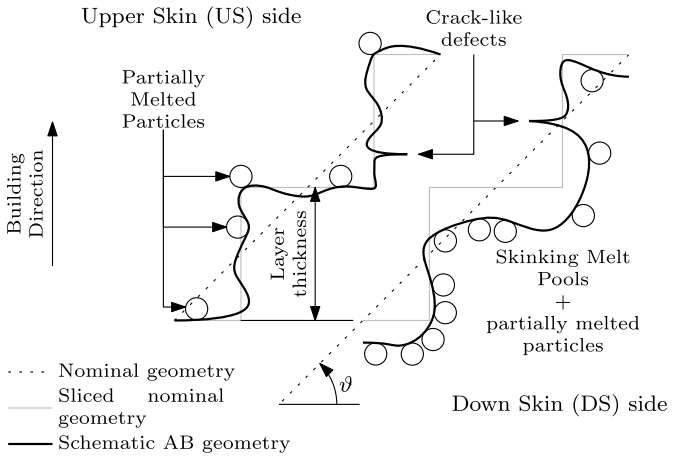

Fig. 5. Schematic representation of the surface roughness characteristic of AMed materials in AB conditions for inclined parts.

- complex geometries, such as lattice structures, prevent using mechanical machining, as reaching all parts of the structure may be difficult, if not impossible.

Concerning Fig. 5, various types of surface defects can be distinguished, including:

- partially melted powder particles, which tend to aggregate in the Down Skin (DS) side;
- defects caused by irregular stacking of successive material layers, leading to crack-like defects normal to the building direction, that are highly detrimental to the fatigue life [49];
- inclined parts exhibit a staircase-like surface due to the approximation made during the slicing operation, where the three-dimensional part is sliced into layers of constant thickness equal to the layer thickness. The magnitude of this phenomenon varies with the printing angle ϑ and layer thickness as depicted in Fig. 5;
- the increased surface roughness at the DS side, caused by the sinking of the melt material in the unmelted powders.

While surface defects, if present, typically govern fatigue behavior, it is also important to consider internal or sub-surface defects for the following reasons:

- internal porosities may emerge after treatments aimed at improving the surface finish, resulting in surface or sub-surface defects;
- for porosities, the thin bridge of material separating the pore from the surface could be broken in the early stages of the fatigue life of the component, leading to the formation of a large surface defect.

Concerning Fig. 6, two different internal void morphologies can be distinguished:

- nearly spherical pores, that can be classified as (i) gas porosity – in red in Fig. 6 – and (ii) keyhole porosity – in green in Fig. 6. The former is generally inherent to the AM process and difficult, if not impossible, to eliminate and small in size. The latter is larger, potentially traversing multiple layers, and tends to aggregate near the surface; it appears spherical in the core of the component while elongated near the outer surface [19,50]. Although fatigue crack may initiate at such porosity (e.g., [51] for lattice structures), it is rarely the leading cause of fatigue failure. Keyhole porosities are generally attributed to excessive laser power;
- voids with a flattened, almost planar geometry and irregular edges that can be connected directly to the outer surface, named Lack Of Fusion (LOF) defects – in blue in Fig. 6. Experimental evidence

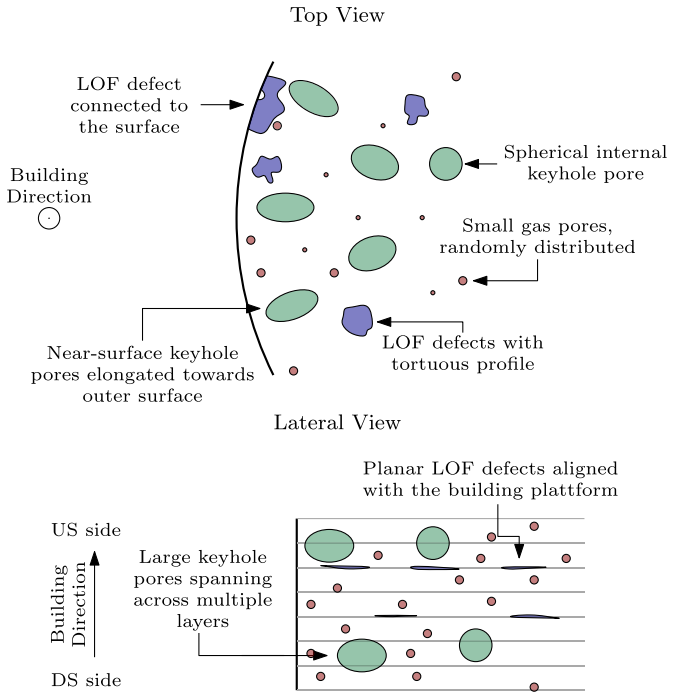

Fig. 6. Schematic representation of the internal porosities characteristic of AMed materials in AB conditions.

shows that this type of porosity is responsible for poor fatigue resistance and material anisotropy (e.g., [52])

It is worth mentioning that with recent advancements in PBF technology, it is now possible to produce components with relative porosity exceeding 99.9% and with rare LOFs (e.g., [53–55]).

2.1.1. Process parameters influence

The process parameters that mostly influence the surface finish and the internal porosity are:

- the orientation of the part with respect to the building direction;
- the laser power and speed, which effects are closely linked to layer thickness and the hatching distance;
- the absolute dimensions of the printed part;
- the powder properties, in particular, its geometry, size, and porosity;
- the printing strategy.

The following paragraphs qualitatively discuss the influence of the process parameters on the internal porosities and surface roughness, emphasizing potential issues specific to AMed lattice structures.

Fig. 7 a) plots the surface roughness measured by R_a or S_a depending on the building direction ϑ. The figure shows that: (i) the surface roughness on the US is almost constant to changes of the printing angle, and (ii) the surface roughness in the DS rapidly increases for $\vartheta < 45°$. Similarly, keyholes tend to aggregate near the DS, especially for reduced printing angle [19].

These phenomena are particularly evident in lattice structures, where horizontally, inclined, and vertically built features exhibit distinct defect distributions. Consequently, several authors suggest avoiding features with low printing angles to minimize the defectiveness of the final part. For example, the diamond UC, which enables the production of parts where the struts are printed with the same building angle of $\vartheta = 54.5°$, is preferred over the cubic UC with horizontally built struts (e.g., [69]).

To examine the combined influence of the laser power and scanning velocity, the energy density is defined as:

$$E_{vol} = g \cdot \frac{P}{vht} \tag{2}$$

where: P is the laser power, v is the scanning velocity, h, t are the hatching distance and the layer thickness, respectively, and g is the energy absorption factor. Fig. 7 b), inspired by the review article of Shao et al. [70], plots the relative density of the manufactured part ρ_{rel} to changes of the energy density E_{vol}; note that there exists a range of E_{vol} in which the relative density remains almost constant and > 99.9%. Regarding the surface roughness, higher energy densities lead to higher surface roughness at the DS and lower at the US [71]. Due to the smaller size of lattice structures, the building structure transfers

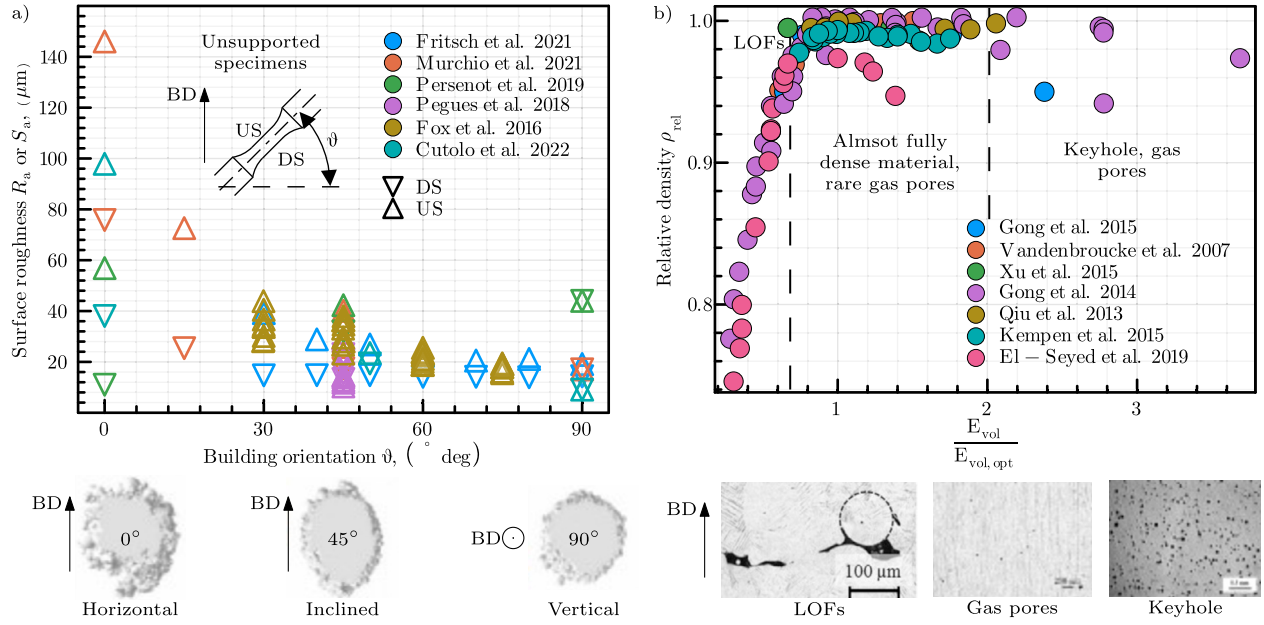

Fig. 7. Process parameters influence; a) effect of the building orientation on the surface roughness – experimental data from [19,56–60]; b) effect of the energy density on internal porosity – the x-axis plots the normalized energy density against the energy density leading to the maximum relative density, experimental data from [61–67]; subfigures from [59,64,65,68] reproduced with permissions from ELSEVIER.

less heat away from the melt pools; thus the process parameters used for lattice structures should have reduced energy densities compared to those for bulk, fully dense parts. In a recent study from Van Hooreweder et al., [72], they showed the effectiveness of multiple contour scanning for lattice structures with a diamond UC with struts diameters below 0.5 mm.

Lastly, various strategies involving in-situ laser remelting with varied process parameters and scanning strategies are being developed to reduce internal porosity, especially keyhole, improve the surface finish, and alter the residual stress field; notable examples are reported in [73–76].

2.1.2. Post-processing techniques

The most used processes to smoothen the surface and/or meet any dimensional tolerances are:

- mechanical machining, that is limited by the potential complexity of AMed parts: some surfaces may be unreachable by traditional tools, as is the case of lattice structures or hollow parts. Interestingly, machining processes alter the microstructure and introduce residual stresses in a thin layer of material near the machined surfaces [35,77];
- chemical, electrical, or electrochemical etching, that allows the removal of material from surfaces inaccessible to conventional tools and thus finds successful applications for complex geometries such as lattice structures or hollow parts. However, it cannot remove deeper defects, as observed by several authors (e.g., [49,78]), and primarily affects the outermost unit cells (UCs), becoming less effective deeper within larger lattice structures.

Note that porosities will likely emerge after material removal techniques (e.g., [24,79–81]); considering that the distribution of internal voids is not constant through the thickness of the part (e.g., [19]), attention should be paid to the thickness of material removed [81].

Performing the Hot Isostatic Pressing (HIP) process, which consists of a heat treatment in a high-pressure environment, leads to significant reductions in the internal porosity [58,62,68,82–95]. However, it is important to note that:

- the gas entrapped in the pores does not dissolve in the crystal lattice of the metallic material; therefore, porosities are not closed but significantly reduced in size (e.g., [68,84,95,96]).
- for near-surface pores, the elevated temperatures and high-pressure characteristic of the HIP process lead to the failure of the bridge of material separating the pores from the surface, preventing its closure [97,98]. Given the small scale of individual geometrical features of lattice structures, internal porosities are also near the surface, and several works highlighted the scarce effectiveness of HIP when compared to HT at similar temperatures [20,21];
- the elevated temperature and long hold periods required to close the pores may lead to the formation of coarse and soft microstructures. Consequently, additional heat treatments are often necessary to strengthen the material, during which pores can reopen, thus mitigating the effect of the HIP treatment (e.g., for AlSi10Mg, several authors [99–101] showed that the HIP treatment could be even counterproductive);

2.1.3. Characterization techniques

The characterization of surface roughness for traditional bulk structures typically employs optical or laser profilometers or digital microscopes. However, when the geometry is too complex, as in the case of lattice structures, μX-CT is usually preferred.

Regarding the characterization of internal porosities, various methodologies are available; the most established in the literature are: (i) the Archimedes method, which allows the measurement of the relative density without providing any information on the position, shape, and size of individual pores; (ii) fractographic analysis, by SEM, optical or digital microscopes, that are destructive techniques for characterizing the position and shape of individual pores, but not their volume; (iii) μX-CT, which is the most comprehensive method for the complete characterization of all defects; however, it is time-consuming, requires sophisticated equipment, and has limitations related to measurement depth and resolution.

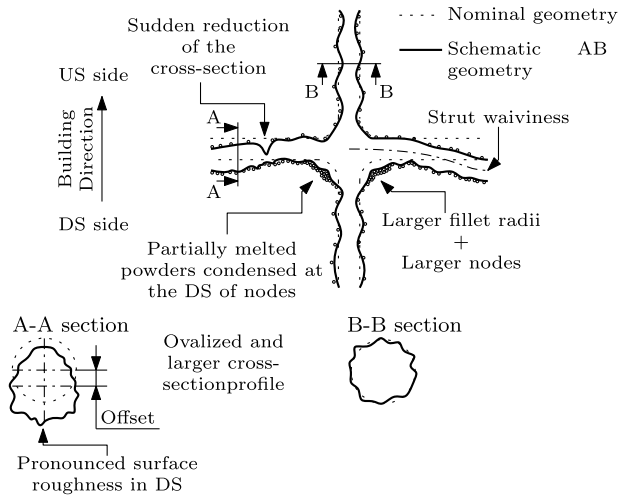

Fig. 8. Schematic representation of the geometry discrepancies for lattice structures.

2.2. Geometry discrepancy

Due to several factors, including (i) high surface roughness, (ii) staircase effect, and (iii) sinking of melt pools into the powder bed, the AB geometry always differs from the AD one. This is particularly critical for lattice structures, where the size of individual features is so small that such discrepancies can significantly alter the mechanical response of the component (e.g., [17,18,72,102–111]). Concerning Fig. 8, the following peculiarities can be distinguished:

- for the same nominal cross-section and process parameters, horizontally and inclined built struts typically have larger cross sections than vertically built ones [15,60,112];
- the cross-section is not constant and can show significant variations along its axis [69], with sudden reductions [16,17,59,113–115];
- horizontally and inclined built struts exhibit ovalized cross-sections, characterized by high surface roughness in the DS [103,113,116,117];
- the axis of AB struts may be different from that of the AD geometry, leading to a significant offset between the nominal axis and the geometric area center of the AB geometry [18,102,104];
- for strut-based lattice structures, nodes are typically larger than the nominal geometry [18,113].

These observations show that CAD models should be created considering the geometric distortion that occurs while manufacturing parts, a process known as compensation (e.g., [15,113]).

2.3. Residual stresses

The AM process is characterized by intense residual stress states in AB conditions intimately linked to the AM process. The high thermal gradients experienced by the material during the process lead to the rapid solidification of the melt without allowing sufficient time for the surrounding material to accommodate the solidification shrinkage. As a result, surface tensile residual stresses are obtained, that are detrimental to the component fatigue strength as they promote crack initiation and

growth. Experimental evidence shows that residual stresses in AB conditions can reach a significant fraction of the material's yield strength, especially near the outer surface of the component [31,118–121]. While in general performing a stress relief heat treatment may improve the fatigue strength of AMed materials (e.g., Ti-6Al-4V [122]), the changes introduced in the microstructure by the heat treatment could ultimately reduce the fatigue strength (e.g., [123] for an AlSi10Mg alloy).

2.4. Summary

At the current state of the art, the AM process cannot produce defect-free materials; instead, AMed materials are weakened by internal and surface defects. Such defects are characterized by a flattened crack-like geometry and tend to be aligned with the building platform. As a result, the mechanical properties of the produced materials are inherently anisotropic on a macroscopic scale.

Furthermore, the AB geometry always differs from the AD geometry (e.g., strut waviness, enlarged nodes, ovalized cross sections). Thus, the design of lattice structures should account for such defects, limiting, for example, the printing angles or the minimal size of individual struts.

3. Theoretical background

It is well-known that cracks, defects, and notches are particularly detrimental to the fatigue strength of metallic materials as they act as stress raisers, favoring fatigue crack initiation and growth [124]. Although the relationship between the size and severity of the stress raiser and the fatigue limit may seem intuitive – the larger the defect, the lower the fatigue limit – it deserves a dedicated discussion. These topics are particularly relevant for AMed lattice structures, given their notched nature and the defectiveness inherent to the AM process.

This Section introduces the fundamentals of the Linear Elastic Fracture Mechanics (LEFM) for predicting the fatigue limit of metallic materials weakened by cracks. It includes a detailed discussion of the non-conventional extensions of the LEFM for the fatigue assessment of defective and notched materials. Although the stress field in the proximity of nodes of lattice structures may be multiaxial, even under remote axial loading, the present Section does not discuss the multiaxial fatigue strength of metallic materials. The complexity of the topic requires dedicated analysis beyond the scope of this article.

This Section will not discuss the applications of LEFM-based fatigue analysis of lattice structures at the macroscopic apparent scale as in [125,126] and [127–129] for metallic foams and honeycombs; instead, it will discuss the applicability of LEFM to lattice structures analyzed at the scale of individual UCs and defects

3.1. Linear Elastic Fracture Mechanics and defect sensitivity

Methods for predicting the fatigue limit of defective materials based on the Linear Elastic Fracture Mechanics (LEFM) are derived from the analytical description of the local stress state in the neighborhood of mode I loaded cracks. Concerning Fig. 9, under the hypotheses of linear elasticity, the stress field is characterized by a singularity with singularity exponent $\gamma = 0.5$ uniquely described by a single scalar quantity called Stress Intensity Factor (SIF), K_I, that is linearly dependent to the remote stress field, σ_g, [130]. Based on these observations, a concept of similarity is implicitly assumed as highlighted by Ritchie and Suresh [131], according to which two different cracks in the same material-microstructure system, under the same loading conditions, subjected to the same SIF, will exhibit the same mechanical behavior. One can thus infer that: (i) the crack propagation rate depends only on the material properties, the force ratio R, and the SIF applied as formerly proposed in [132,133], and (ii) the threshold conditions can be uniquely identified by a threshold SIF range, ΔK_{th}. Taking advantage of the well-known relationship $K_I = \sigma_g \sqrt{\pi \cdot (\alpha^2 a)}$, the fatigue limit, $\Delta\sigma_{g,th}$, of any cracked component can be estimated as:

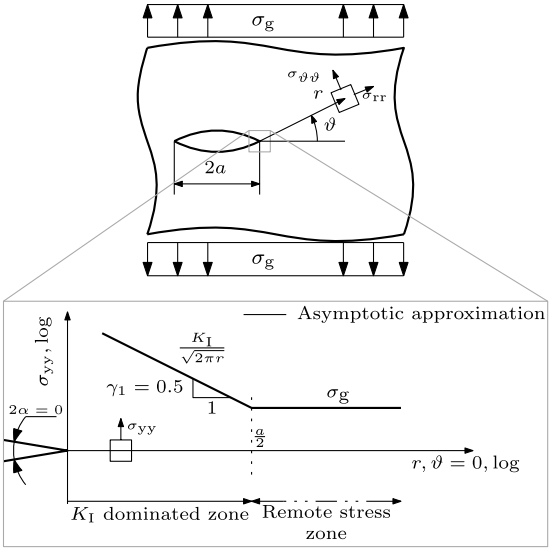

Fig. 9. LEFM reference system and schematic stress field along the crack bisector for a crack size $2a$ in an infinite plate.

$$\Delta\sigma_{g,th} = \frac{\Delta K_{th}}{\sqrt{\pi \cdot (\alpha^2 a)}} \tag{3}$$

where a is the crack size and α is a shape factor accounting for the crack geometry,[1] highlighting that there is a scale effect between the crack size a and the fatigue limit $\Delta\sigma_{g,th}$.

Paris and Erdogan, in the review article in 1963 [134], showed the validity of this assumption for the prediction of the fatigue crack propagation behavior of long cracks (black dashed line in Fig. 10 b)). However, experimental evidence shows this hypothesis does not hold for short cracks and would significantly overestimate the fatigue limit (grey region in Fig. 10 b)). In particular, the fatigue limit of materials weakened by short cracks (i.e., crack size approaching zero) approaches asymptotically that of the defect-free un-notched material as represented in the Kitagawa-Takahashi (KT) diagram 1979 [135,136]. The reduction in the threshold SIF range of short cracks is considered a characteristic of metallic materials, and there are several experimental evidence supporting this assumption for different metallic alloys (including steels and aluminum alloys, pure copper, Ni-based alloys e.g., [133,135–141]). Based on these observations, from now on, the threshold ΔK_{th} of long cracks will be referred to as $\Delta K_{th,LC}$ and is considered a material-microstructure-loading conditions property.

Understanding the transition from short-crack behavior to long-crack behavior has been a relevant research area for the past five decades and remains an ongoing topic. Various approaches have been proposed to address this issue, with the most common being phenomenological models that fit the experimental results and the two asymptotes of the KT diagram. Among these, both the El Haddad-Smith-Topper (HST) model [142,143] and the Atzorri-Lazzarin-Meneghetti (ALM) model [144,145] stand out, with the latter extending the former to cracks of any shape by introducing the effective crack size concept (i.e., introducing the shape factor α in the crack size):

$$\Delta\sigma_{g,th} = \frac{\Delta K_{th,LC}}{\sqrt{\pi \cdot (a_{eff} + a_0)}}, \begin{cases} a_{eff} = \alpha^2 \cdot a \\ a_0 = \frac{1}{\pi}\left(\frac{\Delta K_{th,LC}}{\Delta\sigma_0}\right) \end{cases} \tag{4}$$

[1] Several authors use $Y = \sqrt{\pi}\alpha$ instead of α.

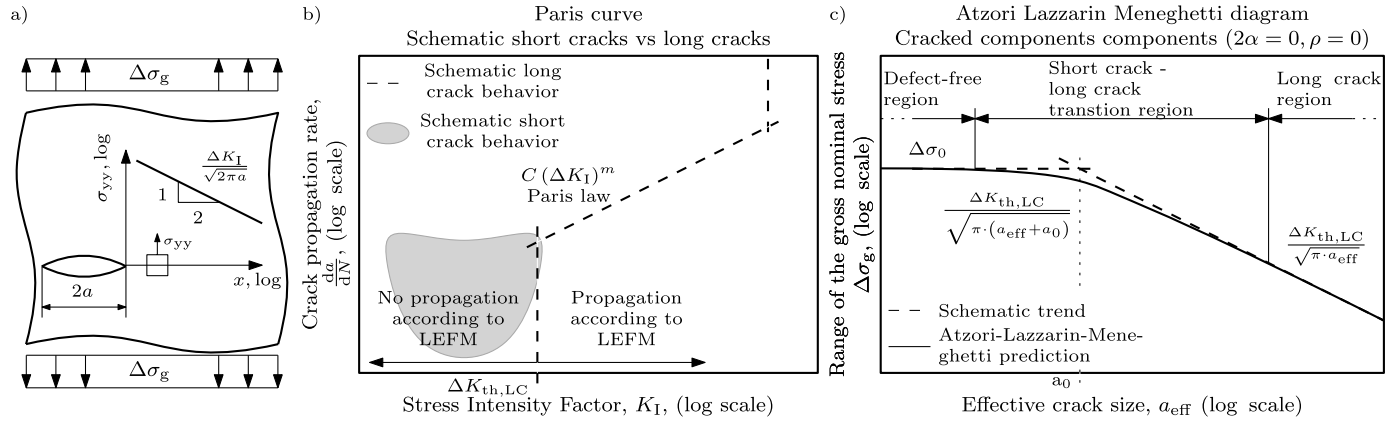

Fig. 10. Short crack vs long crack behavior; a) reference system and schematic stress field according to LEFM; b) crack propagation rate for long cracks and short cracks in a Paris diagram; c) schematic ALM diagram for cracked components $\left(K_{tg} \to \infty, 2\alpha = 0\right)$: prediction of the fatigue limit of cracked materials to changes of the crack size.

where a_0 is a material-microstructure-environment characteristic length (Fig. 10 c)). Other models aim to capture the physical phenomenon; the most common are the cyclic R-curve analysis, formerly proposed by Tanaka and Akinawa [146] ([147,148] for more recent developments), and Newman's modified strip yield model [149,150] ([151] for more recent developments). In this paper, the fatigue assessment is limited to the prediction of the threshold conditions with the ALM model, given (i) the simplicity, (ii) the generality of the analytical formulation, and (iii) the availability of the material properties required (i.e., $\Delta\sigma_0$, $\Delta K_{th,LC}$) either experimentally tested or estimated empirically. For applications of other DT models for the fatigue assessment of AMed fully dense materials, also in the finite life regime, the interested reader is directed to [152–157].

3.1.1. Formulation for defective materials

Studies conducted by Frost and Phillips on sharply notched steels and aluminum alloys [137,138,159] revealed the existence of fatigue cracks even at or below the fatigue limit, named Non-Propagating Cracks (NPCs). This experimental evidence, later confirmed for several metallic alloys with small artificial defects or notches (e.g., [160–165]), and materials with inclusions (e.g., [166]), leads to the following conclusions:

- two different threshold conditions can be distinguished [167]: (i) the threshold for crack initiation – at lower stress levels – and (ii) the condition of NPCs – at higher stress levels[2];
- small defects can be considered cracks for predicting the NPC threshold conditions, as formerly suggested by Usami and Shida 1979 for casting defects [168].

To apply LEFM for predicting the fatigue limit of defective materials, one should know the SIF of non-propagating cracks in threshold conditions initiated from the defects; however, this may be very complex due to the intricate geometry characteristic of AM defects. The most common approximation is the Murakami model [158,169,170], formerly proposed for the rapid estimation of the SIF of cracks with arbitrary shape and orientation between the principal loading direction and the crack plane in infinite bodies with Poisson's ratio $\nu = 0.3$, as schematized in Fig. 11:

$$K_I = \alpha\sigma_g \cdot \sqrt{\pi\sqrt{\text{area}}}, \begin{cases} \alpha = 0.65 \text{ surf.} \\ \alpha = 0.5 \text{ int.} \end{cases} \tag{5}$$

[2] Note that corrosive environments and, or variable amplitude loading may eliminate the threshold condition of NPCs.

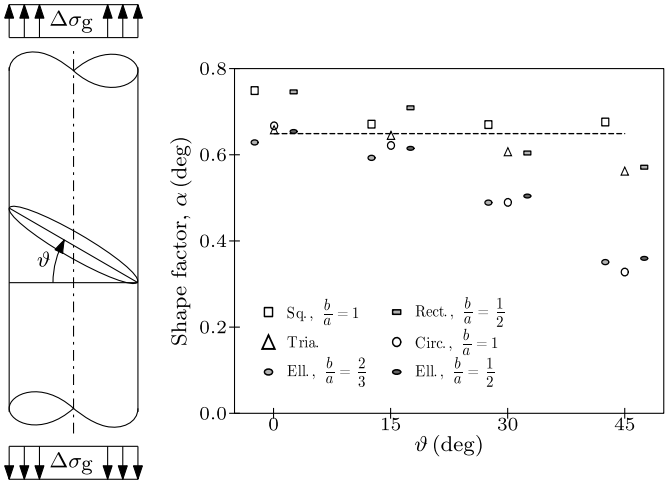

Fig. 11. Shape factor α of different crack geometries to changes of the angle ϑ between the crack plane and the principal loading direction; adapted from [158].

An alternative to the ALM model combined with Murakami's $\sqrt{\text{area}}$ SIF estimation model is the well-established Murakami's $\sqrt{\text{area}}$, HV model [171–173], valid only in the transition from short crack to long crack behavior.

3.2. Notch fatigue and notch sensitivity

The experimental results of Smith and Miller [167] on sharply notched specimens showed that notched metallic materials exhibit two different fatigue behaviors depending on the acuity of the notch and the material-microstructure-environment system: blunt notches – where the fatigue limit is determined by the elastic peak stress at the notch root – and sharp notches - where notches behave like long cracks of the same length. This difference between blunt and sharp notches is known as the notch sensitivity phenomenon and is considered a characteristic of metallic materials.

Atzori and Lazzarin 2001 [174] inferred a connection between the defect sensitivity, observed for short cracks and small defects, and the notch sensitivity, characteristic of sharp notches. This intuition was formalized in the Atzori-Lazzarin-Meneghetti diagram [144], where a single design curve for predicting the fatigue limit of U-notches of any shape and size (Fig. 12 b)) was proposed and validated against experimental data showing promising results.

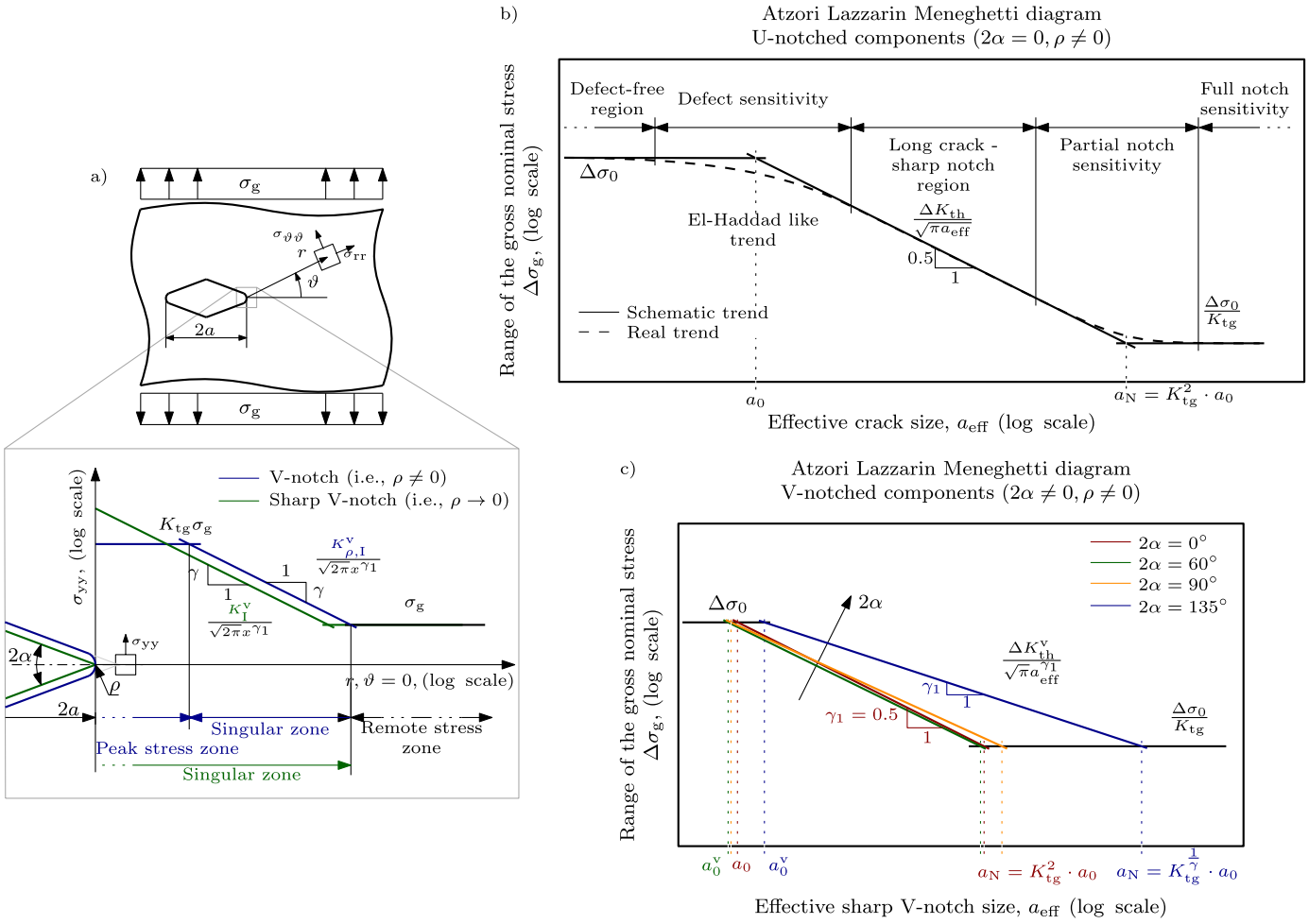

Fig. 12. Atzorri-Lazzarin-Meneghetti (ALM) diagram; a) reference system and schematic linear elastic stress field at the V-notch tip; b) ALM diagram for U-notched components [144]; c) ALM diagram for V-notched components [145]; adapted from [180].

Later, in [145], the diagram was extended to include also V-notches (Fig. 12 c)), taking advantage of the analytical analysis of the stress field of open V-notches from [175]. Concerning Fig. 12 a), the stress field ahead of the notch tip of severe V-notches (i.e., small notch tip radius, ρ, and large elastic stress concentration factors K_{tg}) can be approximated with good accuracy to that of a sharp V-notch (i.e., $\rho \to 0$), which is characterized by a singularity with a singularity exponent, γ_1, dependent on the V-notch opening angle (2α in Fig. 12 a) [176]) and that can be described uniquely by a scalar quantity referred to as Notch-Stress Intensity Factor (N-SIF, K^v_1, [177]). The interested reader is referred to [175,178,179] for a detailed stress field analysis ahead of sharp and rounded V-notches. Concerning Fig. 12 c), note that: (i) the obtained diagram diverges to the KT diagram for cracks, where $K_{tg} \to \infty$ and $\gamma_1 = 0.5$; (ii) the design curves obtained for open V-notches are formally identical to those of U-notches, with the only difference being the singularity exponent γ_1; (iii) different design curves are obtained for different V-notch opening angles (2α); (iv) the scale effect highlighted by the KT diagram is present also for U- and V-notches in the sharp-notch region, governed by the following equation:

$$\Delta\sigma_{g,th} = \frac{\Delta K^v_{I,th}}{\sqrt{\pi} a^{\gamma_1}_{eff}}, \quad a_{eff} = \alpha^{\frac{1}{\gamma_1}}_{\gamma_1} a \tag{6}$$

where: a_{eff} is the effective notch size of a notch in an infinite plate subjected to the same SIF. Considering that lattice structures can be designed to have very sharp notches, predictions based on the N-SIFs could be very effective since they would not require the analysis of defects.

3.3. Application of LEFM for AMed materials and lattice structures

The ALM combined with Murakami's $\sqrt{area}$ SIF estimation model, Equations (4) and (5) (or, similarly Murakami's $\sqrt{area}$, HV model), has extensively been applied for AMed materials, showing promising results for their fatigue limit prediction [22–26,31,33–35,49,52,58,77,93,94,121,181–195]. In the following paragraphs, the applicability of these models to AMed materials is further discussed, reporting the precautions required for the fatigue assessment of AM defects and potential issues peculiar to the small scale of lattice structures.

3.3.1. Estimation of $\sqrt{area}$ for irregularly shaped defects

Typical AM defects may have very complex shapes characterized by deep concavities, as depicted in Fig. 13 b), which are known to smoothen out, even at or below the fatigue limit due to the initiation and growth of NPCs [169,196,197]. To account for the presence of such NPCs, Murakami and Nasser, [169,196] suggested considering an effective crack obtained by smoothing the defect front (area dashed in red in Fig. 13 a)). Several researchers followed these guidelines for AMed materials (e.g., [52,93,94]). In contrast, others (e.g., [24,26,31,181]) considered the exact shape of the crack front, referred to as Beretta's guidelines from now on (area dashed in green in Fig. 13 a)). In the case of shallow cracks – characteristic of the surface roughness profile of

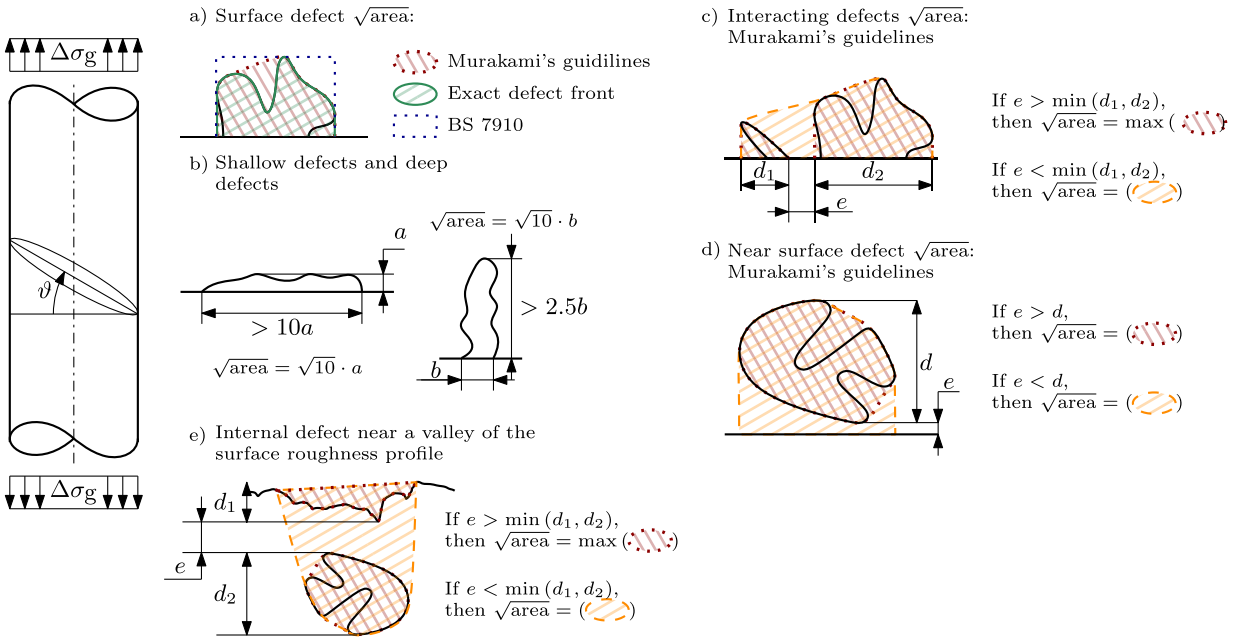

Fig. 13. Guidelines for measuring the crack size of an arbitrarily shaped defect: a) Murakami's guidelines vs. exact defect front vs. BS 7910 guidelines; b) shallow defects and deep defects; c) interacting defects; d) internal vs. near surface defects; e) internal vs. near surface defects considering surface roughness profile.

AMed materials – or deep cracks – characteristic of near-surface voids – see Fig. 13 b).

Lastly, the standard BS 7910 [198] suggests considering a containment rectangle as the effective crack (black dashed line in Fig. 13 a)).

3.3.2. Defects interaction

If two or more defects are close, they may interact with one another and, therefore, have a definite effect on the fatigue limit. Based on the experimental and numerical results for artificial defects and cracks, [169,199–205], Murakami [173] suggested to consider a unique defect when their distance is smaller than the size of the smaller defect, else to consider them separately (Fig. 13 c)). The standard BS 7910 [198] provides similar guidelines, with the only difference being the definition of a rectangular effective defect.

3.3.3. Near-surface defects

For near-surface defects, it may be ambiguous to establish whether a defect is to be considered internal or not due to the presence of the NPCs that could connect it to the outer surface. Murakami [173] suggested considering a single defect connected to the surface when the distance of the defect to the surface is larger than the size of the defect itself, otherwise internal (Fig. 13 d), and for defects near valleys of the surface roughness Fig. 13 e)).

3.3.4. Orientation of defects with respect to the loading direction

Considering that LOFs and crack-like surface defects, typically associated with fatigue crack initiation, are well aligned with the building plane, when the first principal stress is not perpendicular to such plane, the stress field ahead of the tip of the defect is multiaxial. Thus, proper fatigue models should be employed to account for such multiaxiality. Nevertheless, several researchers showed that Murakami's model leads to satisfactory results, provided that the $\sqrt{\text{area}}$ of the defect is projected onto the first principal stress plane (e.g., [93,94] for AMed materials). Note that AM defects may be immersed in a multiaxial stress field for lattice structures, especially near the nodes, due to their inherently notched nature. In these conditions projecting the area of the defect on the plane is no longer sufficient, and proper material models must be adopted (e.g., [173,206]).

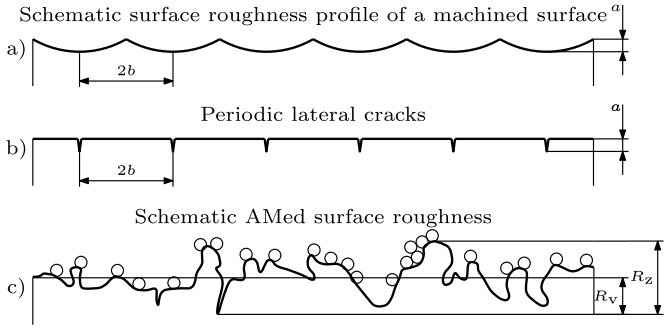

Fig. 14. Schematic surface roughness profile of: a) machined materials and b) corresponding periodic cracks, adapted from [207]; c) AMed surfaces in AB conditions, adapted from [208].

3.3.5. Shielding effect for the surface roughness

Concerning Fig. 14, it may be ambiguous to define the effective crack size of a surface defect because adjacent peaks and valleys of the surface roughness introduce a shielding effect. Similar observations hold for internal voids, especially LOFs; however, LOFs lying on different planes rarely are aligned in the vertical direction, and thus, the shielding effect is minimal.

Murakami et al. 1997 [207] investigated the shielding effect for the periodic surface roughness profile depicted in Fig. 14 a), characteristic of wrought materials. By comparing it to the schematic cascade of periodic lateral cracks illustrated in Fig. 14 b), they proposed the following relationship to account for the shielding effect:

$$a_{\text{eff}} = \begin{cases} 0.65^2 \cdot 2b \left(2.97 \dfrac{a}{2b} - 3.51 \left(\dfrac{a}{2b} \right)^2 \right. \\ \quad \left. -9.74 \left(\dfrac{a}{2b} \right)^3 \right), \quad \left(\dfrac{a}{2b} \right) < 0.195 \\ 0.65^2 \cdot 2b \cdot 0.38, \quad \left(\dfrac{a}{2b} \right) > 0.195 \end{cases} \tag{7}$$

However, real surface roughness profiles of AMed surfaces are not periodic; instead, they are characterized by deep valleys and high peaks as depicted in Fig. 14 c). Starting from the preliminary study of Gre-

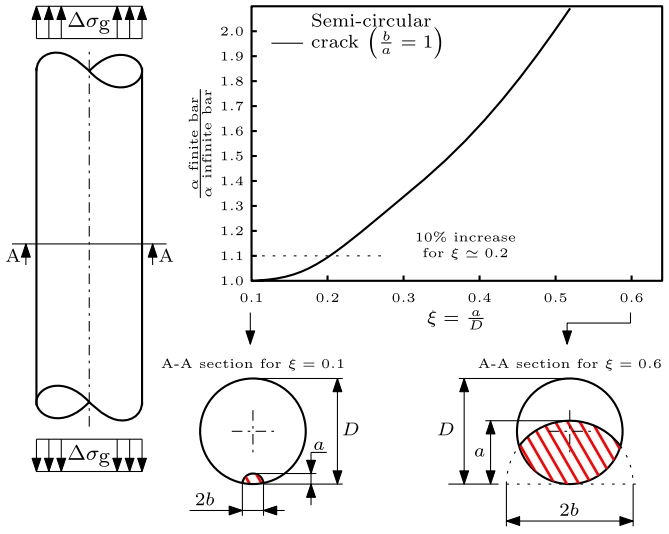

Fig. 15. Influence of the relative size between the crack size and the diameter of the bar for a lateral crack in a finite bar. Shape factors for the elliptical crack from [210], shape factors for elliptical cracks in infinite plates from [211].

itemeier et al. 2017 [209], several authors (e.g., [193,208]) suggested accounting for the surface roughness profile of AMed materials in AB conditions by substituting $a = R_v$ in Equation (7) and $b = R_{sm}$, while $a = R_z$ for hand polished surfaces. Interestingly, while in [193] accounting for the shielding effect provided accurate results, in [189], more accurate predictions were obtained by considering a semicircular crack of size $a = R_v$ and neglecting the shielding effect.

3.3.6. Influence of the crack size to cross-section ratio

Note that the estimation of the SIF with Equation (5) implicitly assumes that the defects are substantially smaller than the cross-section they affect. Therefore, the influence of the remaining ligament of the material is negligible. This assumption may not hold for lattice structures, where the size of individual features of the UCs is so tiny that they can be comparable to that of the manufacturing defects, potentially causing significant underestimations of the SIF. For instance, considering a cylindrical bar weakened by semicircular defects, when the defect size reaches about 10% of the cross-section, the impact of the remaining ligament of material becomes increasingly significant, as depicted in Fig. 15.

3.4. Summary

According to the authors, considering the inherently notched nature of lattice structures and the defectiveness of the AM process, the fatigue assessment should be performed with a defect-tolerant approach based on non-conventional extensions of the LEFM to properly account for: (i) the singularity in the stress field due to the defects, notches, and NPCs, quantified by the SIF; (ii) the defect-sensitivity phenomenon using the ALM model, Equation (4).

Given the complexity of the shape of AMed defects, the SIF of the NPCs propagating from such defects should be estimated using Murakami's $\sqrt{area}$ model, Equation (5), accounting for: (i) the potential interaction between defects; (ii) the potential presence of multiaxial stress fields ahead of defects; (iii) the influence of the notch-defect interaction; (iv) the influence of the relative size between the crack and the geometry weakened by the crack.

Lastly, in a potential future where AM is capable of producing defect-free materials, the fatigue assessment should be performed with an N-SIF approach to account for the notch sensitivity phenomenon as described in the ALM diagram, Fig. 12.

4. State-of-the-art review of the experimental assessment of the fatigue behavior of AMed lattice structures

The unreliability of AMed lattice structures when subjected to fatigue loading and the difficulties in their fatigue assessment have significantly hindered their application in critically loaded components. As a result, extensive research has been conducted to investigate their fatigue strength, as highlighted by the numerous publications in this field. Given the lack of standards regulating the experimental analysis and the assessment of lattice structures subjected to fatigue loading, several testing procedures and design approaches have been proposed to address different research questions. Despite the effort, the complexity of their geometry and manufacturing defects continue to pose challenges, preventing a complete understanding of their fatigue behavior.

This Section offers a comprehensive review of the experimental analysis of the fatigue behavior of lattice structures, providing an overview of the key findings reported in the literature. The discussion begins by focusing on the phenomenology of the fatigue-damaging mechanisms of AMed lattice structures, with a detailed analysis of the Fatigue Crack Initiation Site (FCIS). Then, the influencing parameters, such as the architecture of the UC or the loading conditions, are analyzed. Lastly, it addresses the challenges of the experimental fatigue analysis of lattice structures.

4.1. Phenomenology of fatigue damaging for AMed lattice structures

When subjected to cyclic loading, lattice structures show a significant reduction in stiffness before reaching catastrophic failure of the component as depicted in Fig. 16 a). This behavior, observed in various studies (e.g., [4,36,212,213]), is attributed to the progressive failure of individual features throughout the lattice structure[3] (Fig. 16 b-c)). When the resistant section is no longer sufficient to withstand the external forces, the component undergoes catastrophic failure, which can occur in two different forms depending on the loading conditions: either (i) separation of the component into two halves by static failure[4] (Fig. 16 d)), or (ii) buckling of the UCs, which could be observed when compression is involved (Fig. 16 e)).

Interestingly, the propagation pattern of failing UCs follows a precise path, especially in HCF, dependent on (i) the UC topology and (ii) the loading direction with respect to the UC as shown in Fig. 17. This is attributed to a weak link inside each UC, which will be the most likely site of failure, as suggested by Brailovski et al. [217].

4.1.1. FCIS in the UC

Considering the notched nature of lattice structures, the Fatigue Crack Initiation Site (FCIS) is expected at the location of maximum stress concentration, typically at nodes where two or more adjacent struts meet. However, due to the defectiveness of AMed materials, this is not always the case, and several researchers [36,113,218] observed that fatigue failures may also initiate along the struts, where the stress field should be very homogeneous. This is attributed to the following reasons:

- the Down-Skin (DS) of inclined struts may be characterized by larger surface defects than those at the nodes [19], resulting in more severe stress concentrations;

[3] Note that after the failure of each feature, the loads are redistributed in the surrounding UCs, leading to a variation in the stress amplitude and, potentially, in the force ratio R, and in the local stress field. Therefore, even when subjected to a macroscopic Constant Amplitude (CA) fatigue loading, a large portion of the lattice structure experiences Variable Amplitude (VA) fatigue loading as observed by several researchers [214–216].

[4] Unlike conventional fully dense metallic materials, where uncontrolled crack propagation occurs.

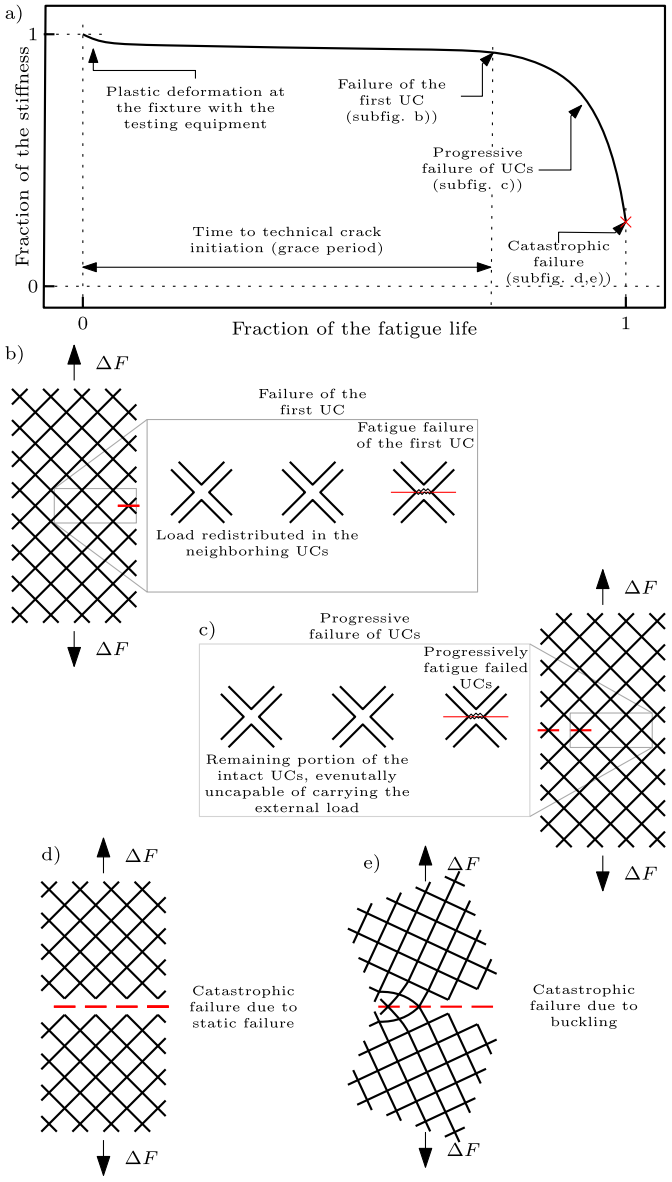

Fig. 16. Schematic representation of the stiffness loss due to the progressive failure of UCs.

- lattice structures can be designed to obtain elastic peak stresses at the notch root very similar to that along the struts (e.g., Dallago et al. [113] observed a stress concentration factor $K_{t,n} \simeq 1.3$ for cubic UCs), thus mitigating the effect of the notch.

In more detail, concerning the schematic Fig. 18 a, b), Dallago et al. [113] studied the fatigue strength and fatigue fracture location of lattice structures with cubic UC with surfaces in AB conditions to changes of the fillet radius at nodes while keeping the rest of the UC geometry fixed, and observed that for blunt notches fatigue crack initiation may occur at nodes and along struts simultaneously, while it is closer to the nodes for shaper notches. Furthermore, they observed that the FCIS tends to be located at the DS side of nodes due to the more pronounced surface roughness and porosity. Similar results are reported for lattice structures with sharp (e.g., [36,221]) and blunt (e.g., [222,223]) notches. Note that these findings highlights that for the tested UCs, the fatigue strength is controlled by defects rather than notches, and thus, fatigue limit predictions based on the N-SIFs or the elastic peak stress would be inaccurate. These observations are consistent with the results obtained for notched defective materials or inhomogeneous materials

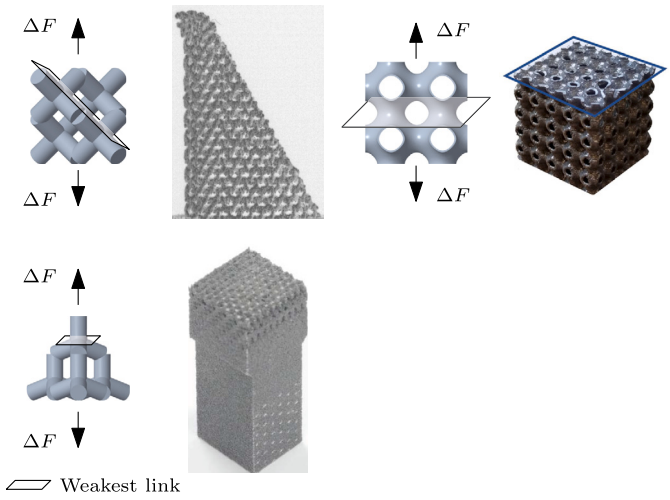

Fig. 17. Favorable fracture planes for different UC geometries: a) and b) diamond UC with [001] and [011] orientations, respectively, from [20,217], with permission from ELSEVIER; c) TPSM Schwartz from [37], with permission from ELSEVIER.

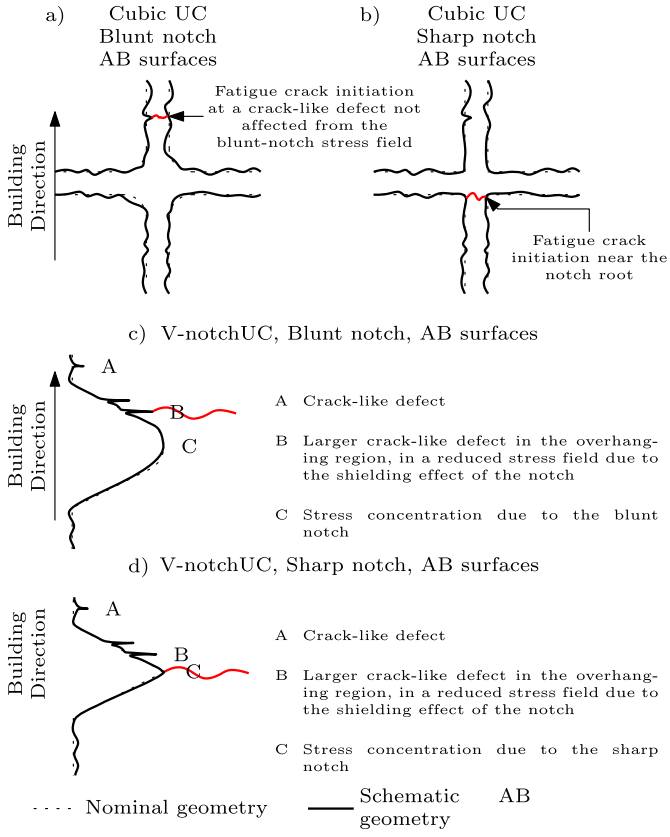

Fig. 18. Schematic representation of the notch-defect interaction; a, b) influence of the notch acuity on lattice structures with cubic UC adapted from the results of [113]; c, d) influence of the notch acuity on V-notched cylindrical specimens, adapted from the results of [219,220].

(e.g., for cast irons [224], or short fiber reinforced composites [225]) where the FCIS is not necessarily at the notch root. Concerning AMed materials, Solberg, Berto, and coworkers [219,220,226] analyzed the Fatigue Crack Initiation Site (FCIS) of vertically built U- and V-notched specimens with surfaces in AB conditions to changes in the severity of the notch and observed that: (i) the FCIS is not at the notch root, due to the pronounced surface roughness of the overhanging surface of the

notch, and (ii) the failure location approaches the notch root for sharper notches (Fig. 18 c, d)) – similar results in [227].

These observations highlight the complex interaction and competition between the stress concentration inherent to the notched nature of lattice structures (e.g., the nodes for strut-based UCs) and the characteristic defects of the AM process (e.g., the pronounced surface roughness or LOF defects).

4.1.2. Fracture surface analysis and FCIS

Given the scarcity of data for AMed lattice structures, the following discussion also includes conventional materials to depict a more complete picture of the fracture surface analysis. For materials with As-Built (AB) surfaces, the FCIS is typically at deep and sharp valleys of the surface roughness profile [26,28,29,31,32,96,121,188,208,229–231] as shown in Fig. 19 a); however, several researchers (e.g., [26,28,29,121,188,230–236]) reported the FCIS at LOFs connected to valleys of the surface roughness profile, Fig. 19 b). Mechanical machining or chemical etching can significantly reduce the severity of the surface roughness; in these conditions, fatigue cracks initiate from internal defects, typically LOFs, that emerge becoming surface or near-surface defects [24,31,54,79,121,234,237–241], as shown in 19 c). Note that for more recent works, the FCIS can be at smaller gas pores, Fig. 19 d), since LOFs are significantly reduced in size and number, if not removed, by proper adjustments of the process parameters [186,228,242]. Combining the HIPing process with the machining of the surfaces allows to obtain almost defect-free materials, and fatigue cracks typically initiate at weak microstructural features (e.g., α facets for Ti-6Al-4V [68,87,92]) as shown in Fig. 19 e).

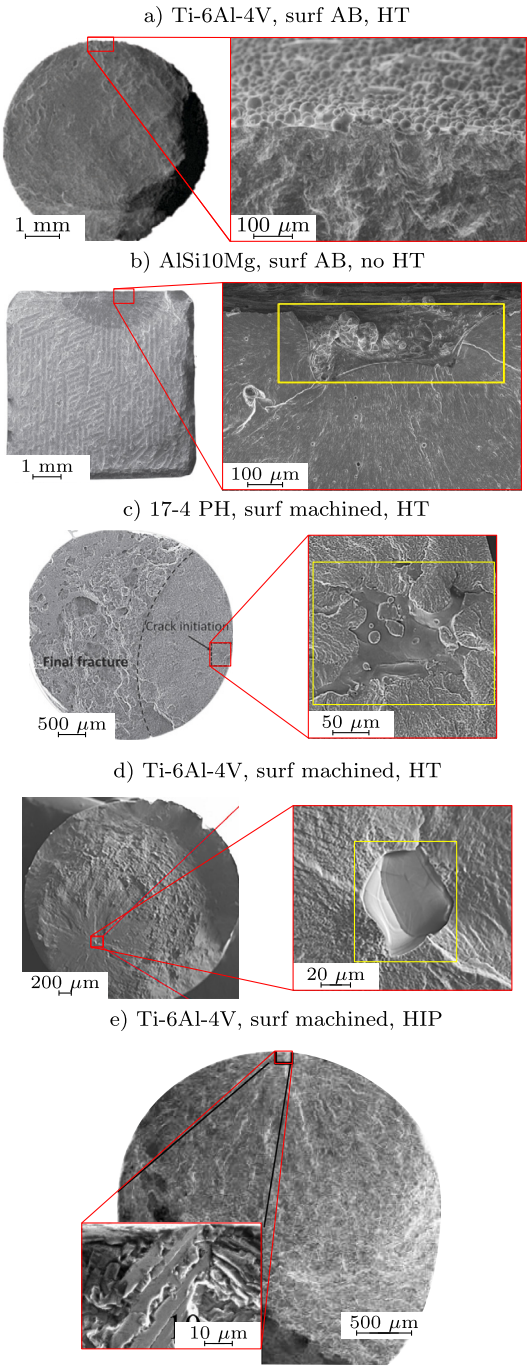

Fig. 19. Crack initiation site for AMed fully dense materials: a) deep and sharp valley of the surface roughness for AB surfaces, from [208]; b) LOF connected to a valley of the surface roughness profile for AB surfaces, from [188], with permission from ELSEVIER; c) near-surface LOF for machined surfaces, from [54], with permission from ELSEVIER; d) near-surface gas porosity defect for machined surface, from [228], with permission from WILEY; e) microstructural defect – large α facets for HIPed and machined materials from [87], with permission from ELSEVIER.

4.2. Influencing parameters

4.2.1. Architecture of the UC

Several factors related to the architecture of the UC influence the fatigue strength of lattice structures. Firstly, it determines how the external loads are redistributed among the features of individual UCs. Thus, different UCs are characterized by different fatigue behaviors. Additionally, the absolute and relative size of the individual features of the UC play a crucial role for various reasons; for example, the potential presence of a scale effect, the size of the fillet radius at nodes, and the slenderness of the struts.

To study the influence of the relative size of the features, several works (e.g., [214,243–247]) investigated the role of the relative density, ρ_{rel}, defined as:

$$\rho_{rel} = \frac{\rho_{lattice}}{\rho_0}, \begin{cases} \rho_{lattice}\text{: lattice structure's density} \\ \rho_0\text{: base material's density} \end{cases} \tag{8}$$

The experimental results showed that the lower the relative density, the lower the fatigue strength since less material carries the load. Interestingly, when analyzing the lattice structure as homogeneous materials at the apparent macroscopic scale, several researchers (e.g., [212,217,243]) observed that the fatigue $\Delta\sigma - N_f$ curves tend to collapse when normalized for the yield strength of the lattice structure at the apparent macroscopic scale σ_Y, to changes of ρ_{rel} and the absolute size of the UC. The obtained $\frac{\Delta\sigma}{\sigma_Y} - N_f$ curves depend on the UC architecture (e.g., [248,249]); interestingly those characterized by smaller stress concentrations, such as the TPSM gyroid, typically show higher fatigue strength [4]. However, concerning Fig. 20, the normalized fatigue strength can exhibit significant variations for a given relative density, even if the analysis is limited to the same material. As highlighted by Berto et al. [4], the proposed relationship fails to capture the difference between fatigue and yielding, which are two distinct physical phenomena. In particular, ρ_{rel} neglects the acuity of the notches, the absolute size of the UC, and the presence of manufacturing defects, all of which have distinct impacts on the fatigue and yield strength of metallic materials. Due to limited literature, understanding the impact of these factors on the fatigue strength of lattice structures is challenging; nonetheless, the following observations can be drawn:

- for a given UC architecture, larger fillet radii at the nodes are related to higher fatigue strength, as reported by Dallago et al. [113] where specimens with a cubic UC were tested to changes of the fillet radii while keeping the other dimensions fixed;

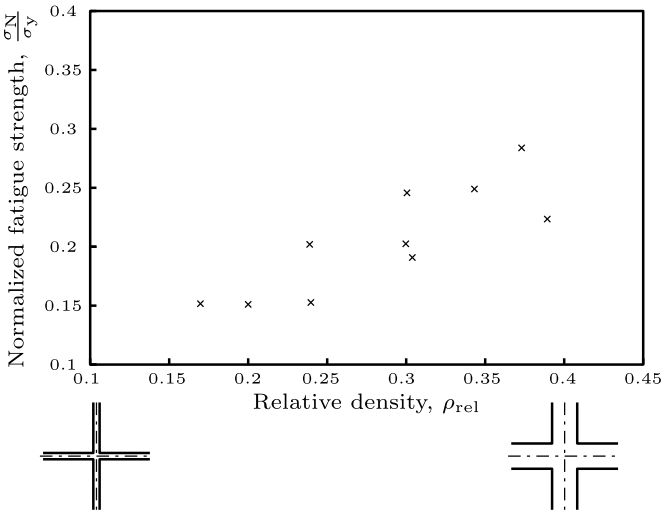

Fig. 20. Review of the data available in the literature for lattice structures AMed from Ti-6Al-4V powders with diamond UCs from [20,243]; data only relevant to $R = 10$, materials tested in air. The fatigue strength reported is the fit of the experimental $\sigma - N$ curves in the HCF regime estimated at $2 \cdot 10^6$ cycles. The interested reader is referred to [4] for a more comprehensive analysis on the influence of ρ_{rel}.

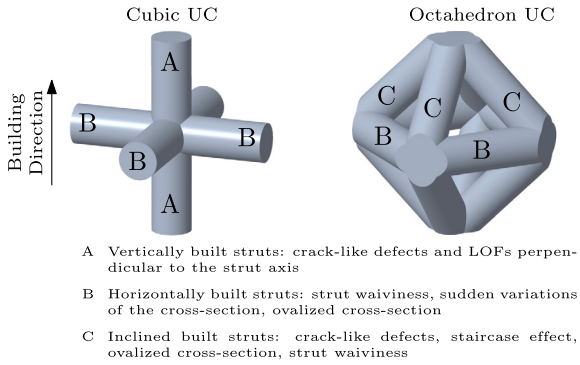

Fig. 21. Schematic representation of the influence of the UC on the defect distribution in each strut: cubic UC vertically built (top); octahedron UC vertically built (bottom).

- for a given UC architecture, the influence of the absolute size of the UC is negligible. In more detail, Dallago et al. [113], who tested specimens with a cubic UC to changes of the absolute size of the UC in geometry similitude, observed that the fatigue strength of the associated homogenized material is almost constant, showing that there is no scale effect;
- reducing the surface roughness by Chemical Etching (CE) leads to a substantial improvement of the fatigue strength (up to 50% according to the results of [20,250] in the HCF regime).

Note that all these observations highlight that, at the current state of the art, the fatigue strength is governed by defects and that fatigue limit predictions based on N-SIFs would be inaccurate with reference to the V-notches at lattice nodes. However, should advancements in AM technology enable the production of near defect-free parts, this situation may change, making N-SIF-based predictions more appropriate.

Lastly, considering the dependency of the defect distribution on the relative orientation between the building direction and the part produced, the UC architecture plays a crucial role in the defect distribution, as schematized in Fig. 21. Interestingly, for plain specimens of sizes comparable to that of the struts of lattice structures, vertically built specimens exhibit higher fatigue strength than horizontally built ones [59,114], contrary to larger specimens (e.g., [52,58,251,252] for sections with diamaters in the range $1 \div 10$ mm). This scale effect is attributed to the relative scale of manufacturing defects and the specimen size: for large specimens, the FCIS is typically at deep valleys of the surface roughness profile or at LOF defects, which tend to be aligned to the building plane; thus, these defects are aligned with horizontally built specimens, leading to reduced stress concentration, while they are perpendicular to the loading direction for vertically built specimens, leading to higher stress concentrations. While these observations also hold for small-sized specimens, the sudden reductions of the cross-section depicted in Fig. 8 characteristic of horizontally built specimens are much more detrimental than the small LOFs of vertically built small-sized specimens.

The lower fatigue strength of inclined and horizontally built struts is reflected in the fatigue strength of lattice structures. For example, vertically built lattice structures with cubic UCs show higher fatigue strength compared to horizontally built cubic lattice structures [113].

4.2.2. Material-microstructure system

There is limited information in the literature regarding the influence of the material-microstructure system on the fatigue strength of lattice structure. Nevertheless, available experimental data suggest that materials with less defect-sensitive microstructures exhibit higher fatigue strength. In more detail, heat-treated lattice structures typically demonstrate improved fatigue strength compared to AB ones [20]. Since heat treatments affect both microstructures, typically reducing the defect sensitivity and the residual stresses with a relieving effect, the improvement cannot be attributed solely to the microstructure's reduced defect sensitivity. However, the works of Zhu et al. [253] and of Popovich et al. [250] showed that longer hold periods and higher temperatures, associated with lower defect sensitivity, lead to higher fatigue strength. Similar conclusions can be drawn from the results of Popovich et al. [245], where lattice structures with diamond UCs AMed from Co-Cr powders, a material known to have a low defect sensitivity, showed exceptionally high fatigue strength in terms of $\frac{\sigma_N}{\sigma_y}$ when compared to Ti-6Al-4V.

The authors believe that at the current state of the art, given the defectiveness of AMed materials, higher fatigue strengths can be achieved with materials with a low defect sensitivity; in a future scenario where AMed materials approach near-defect-free conditions, high-strength materials may become more advantageous, provided that the UCs exhibit reduced stress concentration factors.

4.2.3. Loading conditions

Most of the tests have been performed under compression-compression fatigue with a force ratio[5] $R = 10$ in Constant Amplitude (CA) loading at frequencies ranging from 10 to 50 Hz, in air at room temperature under remote compression-compression loading (e.g., [20,36,60,69,72,221,243,248,249,254–260]). However, real in-service loading conditions for lattice structures are typically pseudo-random in Variable Amplitude (VA). To the best of the author's knowledge, only a few studies were performed at higher frequencies (e.g., [261]), in VA fatigue (e.g., [37,261,262]), under different force ratios including tension–tension or tension-compression (e.g., [113,213,223,261,263–267]), in corrosive environments [268,269], and under remote torsion loading (e.g., [270,271]).

All the studies cited on the influence of the applied force ratio on fatigue strength showed a reduced dependency on the force ratio R. However, these studies were conducted on materials with microstructures in

[5] Note that in the scientific literature relevant to the fatigue strength of lattice structures, the definition of the force ratio R often is $R = \frac{|\sigma_{max}|}{|\sigma_{min}|}$ instead of $R = \frac{\sigma_{min}}{\sigma_{max}}$.

Table 1
Summary of the experimental analysis of lattice structures in corrosive environments.

Ref.	Alloy	UC geometry	Corrosive environment	Fatigue strength variation with respect to test in air
[268]	Pure Fe	Diamond	r-SBF at 37 °C	$-10 \div -5\%$ at $2 \cdot 10^6$ cycles at 15 Hz
[269]	Pure Zn	Diamond	r-SBF at 37 °C	$5 \div 10\%$ at $2 \cdot 10^6$ cycles at 15 Hz
[272]	Pure Zn	TPSM Gyroid	r-SBF at 37 °C	NA, tests in air not conducted
[272]	Mg-Zn alloy	TPSM Gyroid	r-SBF at 37 °C	NA, tests in air not conducted

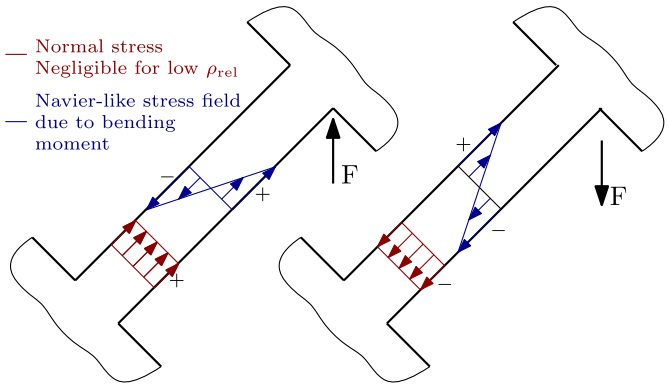

Fig. 22. Schematic representation of the stress field in bending-dominated lattice structures; adapted from [263].

AB conditions and, thus, in the presence of residual stresses that alter the local force ratio. The reduced dependency on R in presence of residual stresses is an already well-known phenomenon for welded joints and fully-dense AMed materials (e.g., Beretta et al. [31,181] showed a negligible dependency of $\Delta K_{th,LC}$ to changes of R, for L-PBFed AlSi10Mg with microstructure in AB conditions). Thus, the experimental evidence in the literature is insufficient to confirm that the reduced dependency on R is a characteristic property of lattice structures. Instead, the authors believe the dependency would be reestablished with a proper stress-relieving HT.

Note that analyzing lattice structures as homogeneous materials at the apparent macroscopic scale may lead to results different from those of their base materials. Consider a generic bending-dominated strut-based lattice structure; as observed by Lietaert et al. [263], the external loads are redistributed in the struts with a stress field characterized by Navier's symmetrical trend due to the bending moments, Fig. 22. Therefore, when the direction of external loads is inverted, the stress field remains mechanically similar, leading to similar results when comparing tension-tension and compression-compression fatigue loading. For example, Lietaert et al. [263], analyzing the fatigue strength of a diamond strut-based lattice structure L-PBFed from Ti-6Al-4V powders, reported similar fatigue strength at $R = 10$ and $R = 0.1$ and slightly higher fatigue strength at $R = -1$. This behavior is expected only when intense bending moments are present: Foletti et al. [37] observed higher fatigue strength for $R = -\infty$ compared to $R = 0$ for a TPSM lattice structure, where bending moments are negligible.

Regarding the influence of corrosive environments and high temperatures, to the best of the author's knowledge, there are only a few preliminary tests on the effect of physiological corrosive environments, [268,269,272]. Table 1 reports the experimental findings; note that lattice structures AMed from Zn-based powders show an increase in fatigue strength that is attributed to the accumulation of corrosion debris at the nodes (similar results for fully dense materials, e.g., [273]). Further research is needed in the field given the significance of corrosion fatigue in several industrial applications such as aviation or biomedical implants. The authors believe that the influence of corrosive environments and high temperature can be accurately analyzed by performing LEFM-based fatigue limit predictions with the precaution of adopting $\Delta K_{th,LC}$ and $\Delta\sigma_0$ for the environment and loading frequency of interest.

4.3. Challenges in fatigue testing of lattice structures

Given the absence of regulations standardizing the experimental fatigue analysis of lattice structures, several testing procedures have been adopted by researchers to tackle specific research questions. The subsequent paragraphs address the most significant challenges related to the experimental fatigue testing of lattice structures.

4.3.1. Geometry of the specimen

The only standard available for the experimental testing of lattice structures is the ISO 13.314 [274] prescribing the static monotonic compression of foams, which gives some guidelines on the geometry of the test specimens; in particular, it requires that the laboratory specimens have at least 10 UCs in all directions to limit edge effects. For cuboid specimens, only 4 UCs can be sufficient to limit edge effects [36,264]; on the other hand, for cylindrical specimens, which are preferred since they allow a more homogeneous number of UCs in all directions, several researchers suggested increasing the number of UCs to 12 (e.g., [20]). A significant concern with cylindrical lattice structure specimens is the partial cutting of the outermost UCs necessary for achieving a cylindrical shape, as illustrated in Fig. 23 a). This practice effectively weakens the structural integrity of the specimen, for example, by: (i) increasing the shape factors for defects in partially cut struts; (ii) reducing the buckling strength of partially cut struts. Consequently, using cylindrical specimens to characterize the strength of the homogeneous material associated with the lattice structure at the macroscopic apparent scale may result in substantial underestimations of its fatigue strength. To address this issue, three different approaches have been proposed in the literature: (i) avoiding the partial cutting of outermost cells, even at the cost of perturbating the cylindrical geometry of the specimen (Fig. 23 b), e.g., [113]), (ii) altering the geometry of the UC, transitioning from cubic UCs to a sector of annulus UCs (Fig. 23 c), e.g., [120]), and (iii) increasing the number of UCs in the radial direction to reduce the ratio between the partially cut UCs on the outer surface of the specimen and those in the core of the specimen (e.g., [20,263]).

Another challenge related to the geometry of laboratory specimens involves the fixture of the specimens to the testing equipment. These portions of the specimens should be designed to guarantee that the fatigue failure occurs in a region not influenced by the clamping system itself, ensuring that the obtained information reflects the fatigue behavior of the lattice structure rather than that of the lattice structure fixed to the testing equipment. For fully-dense materials regulations and good engineering practices, recommend adopting more generous grip sections with respect to the test section, connected by a smooth transition region characterized by low-stress concentration factors (e.g., ASTM E466 [275] suggests specimens with $K_{tn} \leq 1.02$ - Fig. 24 a)). This idea has been applied to lattice structures, and the following design approaches can be identified from a comprehensive analysis of the literature:

- smooth transition in porosity from the gripped region, where higher (potentially up to fully-dense material), to the test section

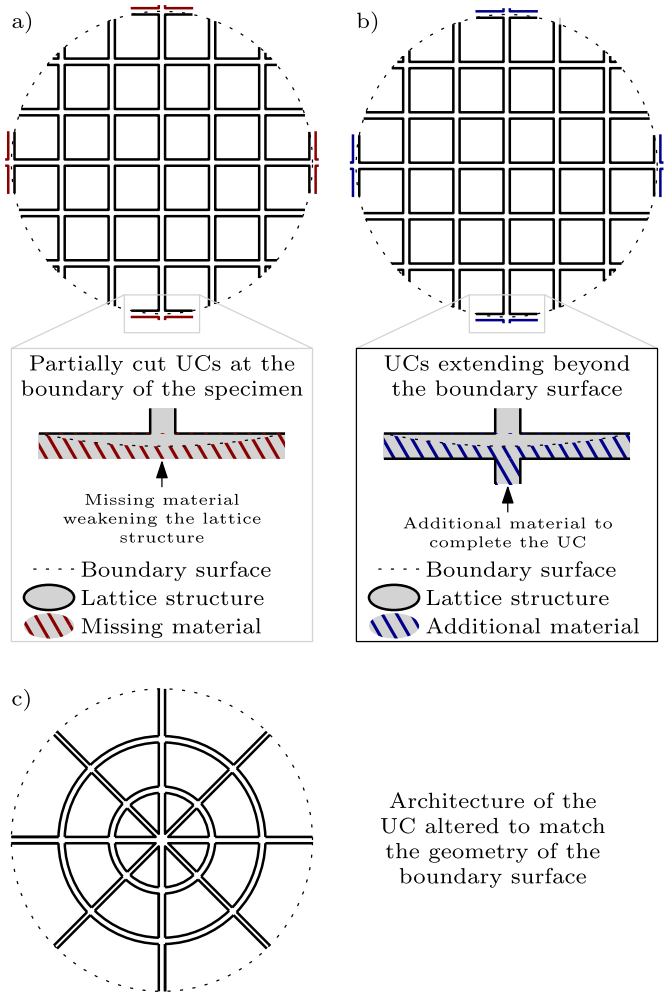

Fig. 23. Schematic representation of the solutions proposed to avoid having partially cut UCs; a) issue statement; b) extended UCs beyond the boundary surface; c) altered UCs as an annulus sector.

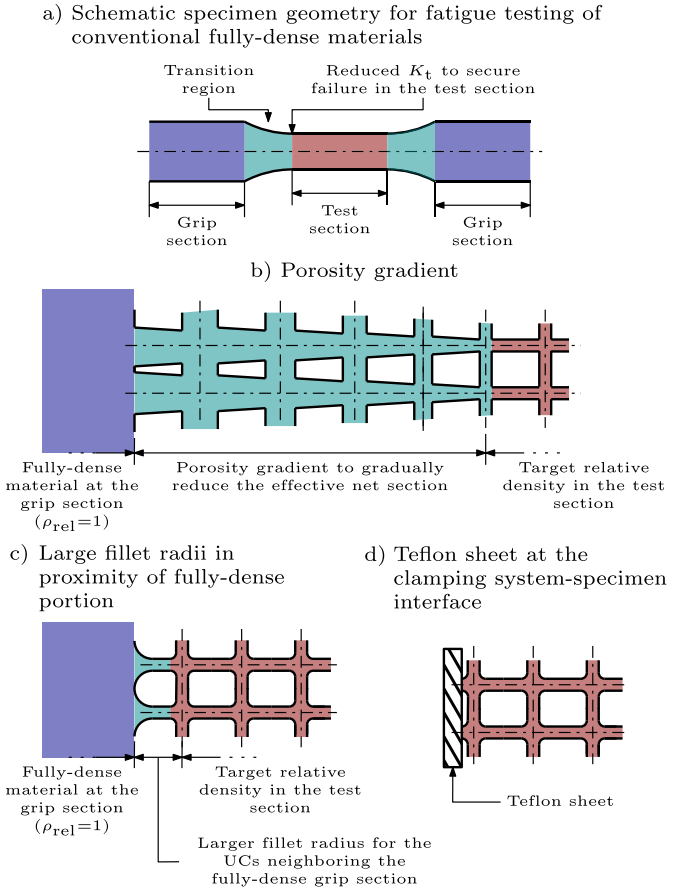

Fig. 24. Schematic representation of proposed solutions for the transition region from the grip region to the test section; a) schematic fully dense specimen with larger grip section; b-d) different approaches proposed in the literature for lattice structures: b) porosity gradient; c) larger fillets near the grip section; d) Teflon sheet at the interface between the clamping system and the specimen.

where the target porosity is tested (e.g., [217,262,263,266,267], Fig. 24 b));
- add large fillets at the transition between the gripped region and the lattice structure (e.g., [113,216]), Fig. 24 c);
- introduce a sheet of Teflon at the interface between the clamping system and the lattice specimen, valid only for compression-compression fatigue loading (e.g., [69]), Fig. 24 d).

An example of the influence of the lack of a properly designed transition region on the fatigue behavior of lattice structures is provided by Coluccia and De Pasquale in [267], where two different batches of specimens are tested: (i) specimens without the transition region, and (ii) specimens with a porosity gradient from fully dense in the grip region to the target porosity of the test section. The results show that two different fatigue $\Delta\sigma - N_f$ curves are obtained and that fatigue failure occurs in the proximity of the fixtures to the test equipment for the specimens without the transition region.

4.3.2. Failure criterion

Considering that the progressive failure of UCs characterizes the fatigue failure of lattice structures, it may be very complex to uniquely identify the failure of each feature before reaching the catastrophic failure. From the fatigue assessment perspective, two distinct moments are of particular interest: the failure of the first UC, which can separate the infinite life regime from the finite life regime, and the failure of the component. Considering that the failure may occur due to buckling of the UCs and generally has a progressive nature, it may be ambiguous to identify the specimen's failure uniquely. Typical failure criteria adopted in the literature monitor the displacement field of the homogenous material associated with the lattice structure. In particular, the specimen is considered broken after a specific stiffness loss (e.g., [37,69]) or after a significant increase of the strain amplitude during force controlled tests (e.g., Foletti et al. [36]).

Identification of the failure of the first UC Due to the inherently notched nature of lattice structures and the defectiveness of the AM process, there is a large number of stress concentrations where fatigue cracks may potentially initiate. Thus, monitoring the health conditions of each feature in each UC is unpracticable, and it is necessary to analyze the behavior of the associated homogeneous material. However, the failure of a single feature of the UC leads to a slight variation in the structural integrity of the entire structure; thus, detecting the failure of the first feature may be challenging. At the current state of the art, several approaches have been proposed to address the identification of the failure of a small portion of UCs, all of which originate from the observation that fatigue damaging phenomenon manifests itself with a progressive failure of UCs. In particular:

- monitoring the stiffness loss of lattice structures during their fatigue life. Although the stiffness loss related to the failure of individual features tends to be smooth, several authors observed that

the failure of a small group of struts can be detected with this approach (e.g., [113]);
- variations of the modal properties, such as the first natural frequency, can indicate for the failure of specific structural elements. Foletti et al. [261] demonstrated that variations below 1% of the first natural frequency could be related to the failure of a single strut.
- monitoring the acoustic emission during the exercise of the specimen tracking the progressive failure of UCs. Note that this approach could also be suitable for real-time health monitoring [276];
- employing the Direct Current Potential Drop (DCPD) technique, Radlof et al. [270] showed that after the failure of a single strut, the measured potential drop exhibits an almost discontinuous trend.

An alternative to monitoring the homogeneous material was recently proposed by Foletti et al. [223], where fatigue tests were conducted inside a micro X-ray Computed Tomography device (μX-CT) to analyze the health condition of the specimen during the fatigue life.

4.4. Summary

The most interesting outcomes from the review of experimental results regarding the fatigue assessment of lattice structures are: (i) the fundamental role of defects and notches in the fatigue strength of lattice structures, as observed by the analysis of the FCIS and the fracture surfaces; (ii) UCs characterized by reduced stress concentrations (e.g., the TPSM gyroid) exhibit higher fatigue strength; (iii) the design of lattice structures should account for the presence of manufacturing defects (e.g., horizontally built struts should be avoided, especially if they are load carrying).

Areas of future research are: (i) the effect of the mean stress, (ii) the effect of high temperature and corrosive environments, and (iii) health monitoring, especially for in-service real components.

Lastly, the Section highlights the necessity of a standard to regulate fatigue testing, with precise guidelines on: (i) the geometry of the specimens to avoid any influence of the loading system, and (ii) the failure criteria to establish the number of cycles to failure and eventually allow cross-comparison between different studies.

5. Validation

This Section validates the models outlined in Section 3 against experimental data from the literature for AMed metallic materials. The data selection adhered to the following criteria, ensuring consistency with the theoretical framework discussed:

- the following data must be available: (i, ii) the fatigue limit of the defect-free material, $\Delta\sigma_0$, and the threshold range of mode I SIF of long cracks ΔK_{thLC}, and (iii) the triplet $\Delta\sigma_g, N_f, a_{\text{eff}}$ for each specimen, where $\Delta\sigma_g$ is the applied nominal gross stress range, N_f is the number of cycles to failure, a_{eff} is the effective crack size;
- all specimens tested must be in stress-relieved conditions. The only exception is the data from [31] because the authors provided all the information necessary to determine the stress field ahead of the defect tip accounting for the residual stresses, and the influence of the force ratio R on ΔK_{thLC} for the same material-microstructure system.

If the material properties $\Delta\sigma_0$, and $\Delta K_{\text{th,LC}}$ are not measured for the same material-microstructure-loading conditions system, they are estimated with the following empirical models:

- $\Delta\sigma_0$ with Murakami's equation $\Delta\sigma_0 = 1.6\text{HV}$, while, if HV is not available, using the following equation $\Delta\sigma_0 = 0.8 \div 1.2\sigma_{\text{UTS}}$. If tests are not conducted under fully reversed loading conditions (i.e., $R \neq -1$), Goodman-Smith's equation is used to account for the force ratio R as [192]:

$$\Delta\sigma_0(R) = 2\left(\frac{1-R}{3-R}\right)\Delta\sigma_0(R=-1) \tag{9}$$

assuming that $\Delta\sigma_0(R=-1) = \sigma_{\text{UTS}}$;
- $\Delta K_{\text{th,LC}}$ with the Rigon-Meneghetti empirical model:

$$\Delta K_{\text{th,LC}} = \alpha \cdot l^{\beta} + \gamma \text{HV}^{\delta} \tag{10}$$

where: l is a characteristic length of the microstructure; $\alpha, \beta, \gamma, \delta$ are empirical constants dependent on R [189,192]. If the microstructural length is not available, then $\Delta K_{\text{th,LC}}$ is estimated with the Atzori-Rigon-Meneghetti model:

$$\Delta K_{\text{th,LC}} = \gamma \text{HV}^{-0.5} \tag{11}$$

where γ is an empirical constant dependent on R [281].

For machined specimens only, the residual stresses due to the machining process alter the local stress field in a thin layer of material. If the original data provide a measure of the residual stresses, σ_{res}, the local stress ratio R can be estimated as:

$$R = \frac{\sigma_{\min} + \sigma_{\text{res}}}{\sigma_{\max} + \sigma_{\text{res}}} \tag{12}$$

Using Equation (9), the $\Delta\sigma_0$ can be adjusted to account for the residual stresses. Otherwise, the remote force ratio is adopted if the residual stresses are not measured.

For specimens with surfaces in AB conditions, the shielding effect is accounted for if the information to input in equations provided in Section 3.3.5 is available.

5.1. Plain specimens and notched specimens

Fig. 25 and Fig. 26 show the comparison between the prediction of Equation (4) against 410+ experimental data of fatigue tests of the plain and notched specimens, respectively, several of which performed in near-threshold conditions. Fig. 27 shows the schematic geometry of the specimens tested, Tables 2,3 report the material properties required for the calibration of the ALM model, and additional information relevant to the estimation of a_{eff} and the residual stress state; for the notched specimens, the estimation of a_{eff} accounts for the notch stress field using the equations provided in [277,278] for the rapid estimation of the SIF of semi-elliptical cracks at the tip of sharp U- and V-notches.

Note that the prediction of the ALM model is consistent with the experimental results since almost all the failed specimens tested lie above the fatigue limit prediction; all the failed specimens below the prediction are from Schimback et al. [33] from data relevant to Scalmalloy powders, and from Liang et al. [252] on AISI 316L. The authors of [33] argued that the inaccurate predictions are due to the overestimation of $\Delta K_{\text{th,LC}}$ inherent to the load decrease experimental measure regulated by ASTM E647, ISO 12108 [287,288] and showed that measures in load increase lead to more accurate results. This is a well-documented topic; the interested reader is referred to [289] for a more detailed discussion.

5.2. Lattice structures and small-sized specimens

The ALM model prediction is compared with the following sets of data: (i) lattice structures with cubic UC from batch A tested by Dallago et al. in [113] and (ii) small-sized specimens tested at $R = -1$ by Benedetti et al. in [114]. Although the second set of data does not pertain to lattice structures, it is included in the discussion because the size of the specimens is comparable to that of struts. Neither of the datasets fully meets the adopted selection criterion. This is due to the lack of information regarding both (i) the range of the gross nominal stress applied and (ii) the number of cycles to failure for the specimen whose fracture surface is reported. Despite that, they allow the comparison of

Table 2
Ti-6Al-4V data.

Ref.	R	$\Delta\sigma_0$, (MPa)	$\Delta K_{th,LC}$, $\left(MPa\sqrt{m}\right)$	Notes
[93,94]	−1	1180[1]	7.0[3]	• geometry a) • L-PBFed and EB-PBFed materials • HT (600 °C - hold NA) for L-PBFed, residual stresses due to AM process relieved [35] • no HT for EB-PBFed, but no residual stresses expected • machined surfaces, residual stresses due to the machining process neglected • $\sqrt{area}$ following Murakami's guidelines, measured from fractographies
[34]	−1	1222[1]	6.9[3]	• HT (670 °C - 300 min), residual stresses due to AM process relieved [35] • machined surfaces, residual stresses due to the machining process neglected • un-notched, geometry a) (from [182]) and notched, geometry c), specimens (from [81]) • $\sqrt{area}$ following Beretta's guidelines, measured from fractography (from [34]) • Shape factor for notched specimens estimated according to [277,278] for semi-elliptical cracks
[77]	−1	1024[1]	7.2[3]	• geometry b) • HT (950 °C - 30 min), residual stresses due to AM process relieved [35] • machined surfaces, residual stresses due to the machining process neglected • $\sqrt{area}$ following Murakami's guidelines, measured from fractographies
[77]	−1	1152[1]	7.0[3]	• same as above, but machining in a cryogenic environment, residual stresses due to the machining process neglected
[251]	0.06	755[1]	4.1[3]	• geometry b) • HT (650 °C - 180 min), residual stresses due to AM process relieved [35] • some specimens with machined surfaces, residual stresses due to machining process neglected • $\sqrt{area}$ following Murakami's guidelines, measured from fractography • shielding effect for AB surfaces neglected • no data in near threshold conditions
[22]	0.1	755[1]	4.1[3]	• geometry b) • HT (650 °C - 180 min), residual stresses due to AM process relieved [35] • some specimens with machined surfaces, residual stresses due to machining process neglected • $\sqrt{area}$ following Murakami's guidelines, measured from fractography • shielding effect for AB surfaces neglected
[191]	0.1	745[1]	4.3[3]	• geometry a) • HT (500 °C - 120 min), residual stresses due to AM process relieved [35] • machined surfaces, residual stresses due to machining process neglected • $\sqrt{area}$ following Murakami's guidelines, measured from fractography • shielding effect for AB surfaces neglected
[114]	−1	1120[1]	7.0[4]	• HT (740 °C - 130 min), residual stresses due to AM process relieved [35] • effects of misalignments neglected due to the reduced stiffness of the specimens • AB surfaces, shielding effect neglected • more details on the estimation of a_{eff} provided in Section 5.2
[279]	−1	1080[2]	8.0[5]	• HT (920 °C - 30 min, FC to 700°- 120 min, air cooling), residual stresses due to AM process relieved [35] • machined surfaces, residual stresses due to the machining process neglected • $\sqrt{area}$ following Murakami's guidelines, measured from fractography (from [279]) • $\Delta K_{th,LC}$ measured in [280] • only 1 data available for the broken specimen in near-threshold conditions
[279]	−1	1080[2]	8.0[5]	• same as above, but different process parameters
[193]	0.1	700[2]	3.6[5]	Ti-6Al-4V • geometry e), under 4 point bending • HT (740 °C - 130 min, cooling to 520° followed by Argon quench), residual stresses due to AM process relieved [35] • results analyzed only for series D of the original work • shielding effect accounted for, as instructed by the authors of the original work

[1] Estimated with Murakami's HV model, Goodman Smith's correction to account for the force ratio R.
[2] Estimated from static UTS, Goodman Smith's correction to account for the force ratio R.
[3] Estimated with Rigon-Meneghetti model [189,192].
[4] Estimated with Atzori-Rigon-Meneghetti model [281].
[5] Measure for the same material-microstructure-environment system provided by the authors.
[6] Goodman Smith's correction to account for residual stresses.
[7] Estimated from stabilized cyclic curve, as suggested in [282].
[8] As suggested by the authors.

the ALM model fatigue limit prediction and the experimental results in near-threshold conditions. In more detail:

- for the cubic UC lattice structure, concerning the $\Delta\sigma - N_f$ curve of Fig. 28 b), note that all specimens are tested in near-threshold conditions;
- for the small-sized specimens, the fracture surface shown in Fig. 29 c) is representative of a specimen tested in HCF.

Table 2 reports the material properties required to calibrate the ALM model (i.e., $\Delta\sigma_0$ and $\Delta K_{th,LC}$) for the two datasets. Fig. 28 c) and Fig. 29 c) show the crack front in near-threshold conditions determined according to the guidelines discussed in Section 3.3; the effective crack size is estimated with the PSM [290,291]. Lastly, the range of the gross nominal stresses to be compared with the ALM prediction is determined as follows:

- by de-homogenization for the cubic UC lattice structure, starting from the homogenized $\sigma_a - N_f$ curve provided by Dallago et al. [113], as:

$$\Delta\sigma_g = \Delta\sigma_{hom} \cdot \frac{4l^2}{\pi d^2} \tag{13}$$

where l is the strut length and d is its diameter. The edge effects are included as instructed by Dallago et al. in [113]. Although the failure occurred near the nodes of the lattice structures, the influ-

Table 3
Other alloys.

Ref.	R	$\Delta\sigma_0$ (MPa)	$\Delta K_{\text{th,LC}}$ $\left(\text{MPa}\sqrt{\text{m}}\right)$	Notes
[31]	0.1	251[2,6]	1.2[5]	AlSi10Mg alloy • geometry a) • no HT, residual stresses due to AM process measured with XRD technique • some surfaces machined surfaces, residual stresses due to machining process measured with XRD technique • $\sqrt{\text{area}}$ following Beretta's guidelines, measured from fractography for machined and AB surfaces; shielding effect neglected
[25]	−1	240[2]	2.0[5]	AlSi10Mg alloy • geometry a) • HT (300 °C - 120 min), residual stresses due to AM process relieved • machined surfaces, residual stresses due to machining process negligible (measured with XRD technique after fatigue testing) • $\sqrt{\text{area}}$ following Murakami's guidelines, measured from fractographies
[283]	0.1	NA	NA	Co-Cr alloy • geometry e), under 4 point bending • Stress relieved, parameters kept confidential • ΔK_{thLC} and $\Delta\sigma_0$ kept confidential, data presented in the form of $\frac{\Delta\sigma_g}{\Delta\sigma_0} - \sqrt{\text{area}}$ • a_0 determined by fitting the EHST model at $\frac{\Delta\sigma_g}{\Delta\sigma_0}\left(\sqrt{\text{area}}\right) = \sqrt{\frac{1}{2}}$ • surfaces in AB conditions, while the original paper discusses the influence of the shielding effect, it is not considered in the present validation
[284]	-1	2300[1]	5.0[4]	18Ni300 alloy • geometry d) • HT (470 °C - 360 min) • specimens with AB surfaces, $\sqrt{\text{area}}$ estimated from fracture surfaces without considering the effect of the surface roughness given the presence of large LOFs
[26]	−1	2130[7]	7.3[4]	17-4 PH alloy • geometry a) • HT (1050 °C - 30 min, air cooling to room temperature + 552 °C - 240 min, air cooling to room temperature) • specimens with AB surfaces, $\sqrt{\text{area}}$ estimated from fracture surfaces, shielding effect neglected
[285]	0.1	487[1]	6.0[4]	Inconel 625 alloy • geometry f), under 4 point bending • HT (1150 °C - 180 min at 1000 bar (HIP) + 1160 °C - 240 min, air cooling to room temperature + 87 °C - 720 min in sulfuric acid solution) • specimens with machined surfaces, residual stresses due to machining neglected • no available data in near-threshold conditions
[286]	−1	1355[1]	6.6[4]	AISI 4140 alloy • geometry a) • HT (1150 °C - 150 min at 1100 bar + 850 °C - NA duration, water quench to room temperature + 450 °C - 120 min) • surfaces machined, residual stresses due to machining neglected
[252]	−1	720[1]	9.0[4]	316L alloy • geometry g) • HT (620 °C - 90 min) • surfaces polished • unusually low fatigue strength when compared to LEFM prediction
[33]	0.1	360[8]	2.0[5]	Scalmalloy • geometry b) • HIP (325 °C - 240 min at 2000 bar (HIP)) • specimens with AB surfaces, $\sqrt{\text{area}}$ estimated from fracture surfaces, shielding effect neglected several data related to unpublished work

[1] Estimated with Murakami's HV model, Goodman Smith's correction to account for the force ratio R.
[2] Estimated from static UTS, Goodman Smith's correction to account for the force ratio R.
[3] Estimated with Rigon-Meneghetti model [189,192].
[4] Estimated with Atzori-Rigon-Meneghetti model [281].
[5] Measure for the same material-microstructure-environment system provided by the authors.
[6] Goodman Smith's correction to account for residual stresses.
[7] Estimated from stabilized cyclic curve, as suggested in [282].
[8] As suggested by the authors.

ence of the stress concentration is neglected given the low K_{tg} of the nominal geometry;
- by considering the net area of the cross-section schematized in Fig. 29 c) for the small-sized specimens, starting from the $\sigma_a - N_f$ curve provided by Benedetti et al. [114].

Fig. 28 a, b) and Fig. 29 a, b) compare the ALM prediction with the experimental data, showing satisfactory results. For both cases analyzed, the effective crack size of the defects is in the long crack regime. Note that the small scale of the cross-section of the analyzed specimens plays a major role: concerning Fig. 29 c), considering the same defects in an infinite body (or, more realistically, in a conventional engineering component) would be considered as a shallow surface defect with shape factor $\alpha = 0.65$ and size $\sqrt{\text{area}} = \sqrt{10}a$ (Fig. 13 b)) where $a \simeq 100$ μm giving $a_{\text{eff}} \simeq 130$ μm, significantly lower than the $a_{\text{eff}} \simeq 300$ μm obtained in the small-sized specimen; similarly, concerning Fig. 28 c), the same defect in an infinite body would be considered as a surface defect with shape factor $\alpha = 0.65$ and defect size $\sqrt{\text{area}} \simeq 350$ μm (Fig. 13 a)), giving $a_{\text{eff}} \simeq 150$ μm.

6. Conclusions and outlook for future research

The article discusses the fatigue behavior of Additively Manufactured (AMed) lattice structures. It proposes an approach based on the Linear Elastic Fracture Mechanics (LEFM) alternative to the well-established nominal models for their fatigue assessment. The key idea is to consider AMed lattice structures as notched and defective materi-

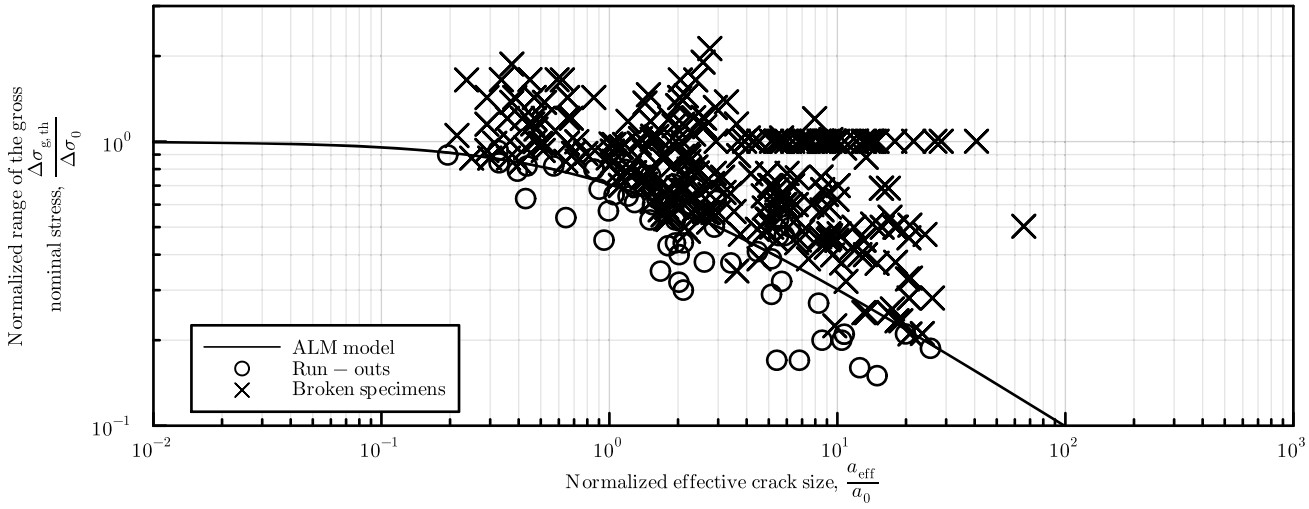

Fig. 25. Validation of the ALM model against experimental data from the literature for plain specimens. Tables 2,3 for more details on the tests conducted.

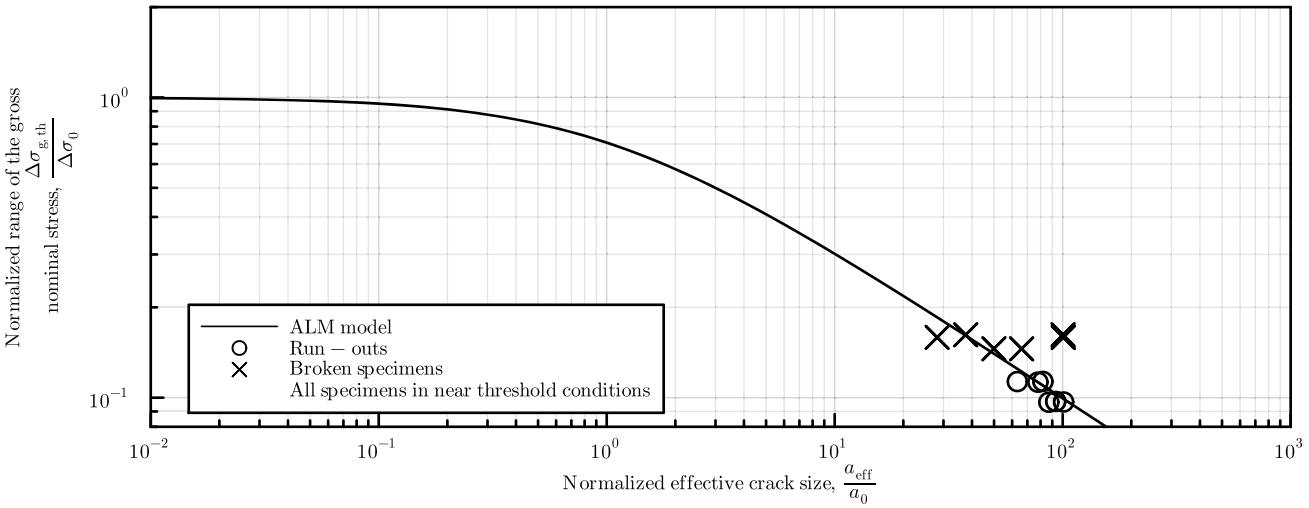

Fig. 26. Validation of the ALM model against experimental data from the literature for notched specimens. Tables 2,3 for more details on the tests conducted.

als and, consequently, to perform the fatigue assessment on the scale of individual struts, AM defects, or notches. Considering that fatigue crack initiation and propagation is a local phenomenon favored by the presence of stress raisers, this study emphasizes the influence of the notched nature of lattice structures and the defectiveness of AMed materials.

The work starts with a descriptive analysis of AM defects, focusing on their detrimental effect on the fatigue strength. It then discusses the fatigue assessment of metallic materials weakened by notches and defects, introducing the LEFM and its non-conventional extensions to assess the presence of defects and notches based on the Atzori-Lazzarin-Meneghetti (ALM) diagram. It then reviews the state-of-the-art experimental fatigue analysis of AMed lattice structures, reporting experimental evidence stressing:

- the role of AM defects on the fatigue strength;
- the similarities and differences between lattice structures and homogeneous materials;
- the need for performing the fatigue assessment with a defect-tolerant approach.
- that in a future scenario where AM approaches the defect-free condition, the fatigue assessment should be performed with an N-SIF-based approach, rather than a defect-tolerant approach.

Furthermore, it addresses ongoing areas of interest that require additional research and the challenges encountered in fatigue testing of lattice structures.

In conclusion, the ALM model is compared to experimental data from the literature for different AMed materials and specimen geometries, including notched and small-sized specimens and lattice structures. Due to the limited data available, the comparison between the experimental data relevant to lattice structures and the ALM model proposed in this paper is not to be considered as a validation. However, it quantifies the qualitative observations drawn from the literature analysis of the fatigue strength of lattice structures and highlights the necessity for further experimental investigation to validate the defect-tolerant approach.

The authors believe that future research should prioritize investigating the following topics:

1. process optimization, with the following objectives: (i) reduce the defectiveness of AMed materials (possibly to sizes below a_0), by tailoring process parameters and printing strategies to lattice structures (e.g., [72]), real-time monitoring of pore formation and healing (e.g., employing in-situ laser remelting [73–75]) and post-processing processes (e.g., chemical etching, sandblasting, and HIPing [20,49]), and (ii) reduce the minimum size of individual fea-

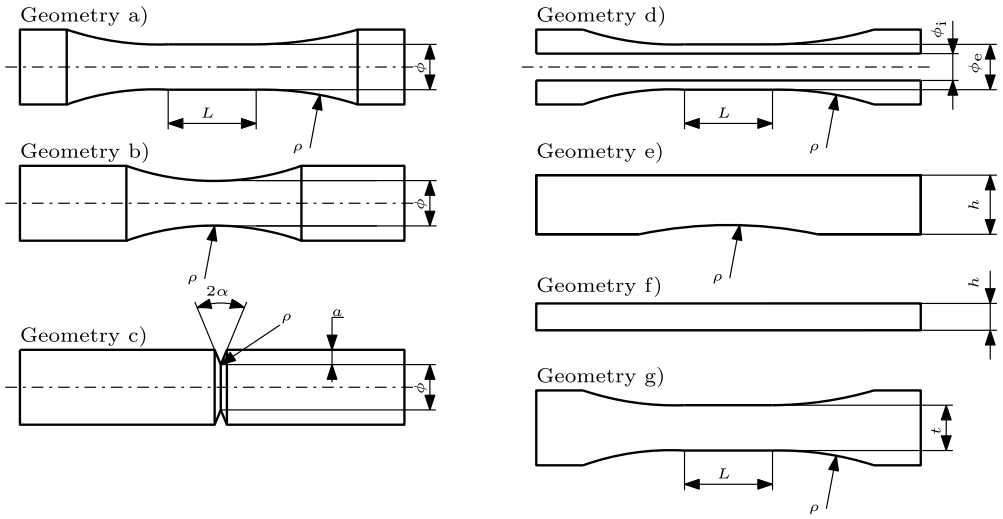

Fig. 27. Geometry of the specimens analyzed in Figs. 25 and 26 and Tables 2,3; a) specimen with tangentially blending fillets between the test section and the grip section and circular cross-section; b) specimen with a continuous radius between the grip section and circular cross-section; c) sharply V-notched cylindrical specimens; d) specimen with tangentially blending fillets between the test section and the grip section and tubular cross-section; e) beams with blunt notch subjected to 4 point bending and rectangular cross-section; f) beams subjected to 4 point bending; g) specimen with a continuous radius between the grip section and rectangular cross-section.

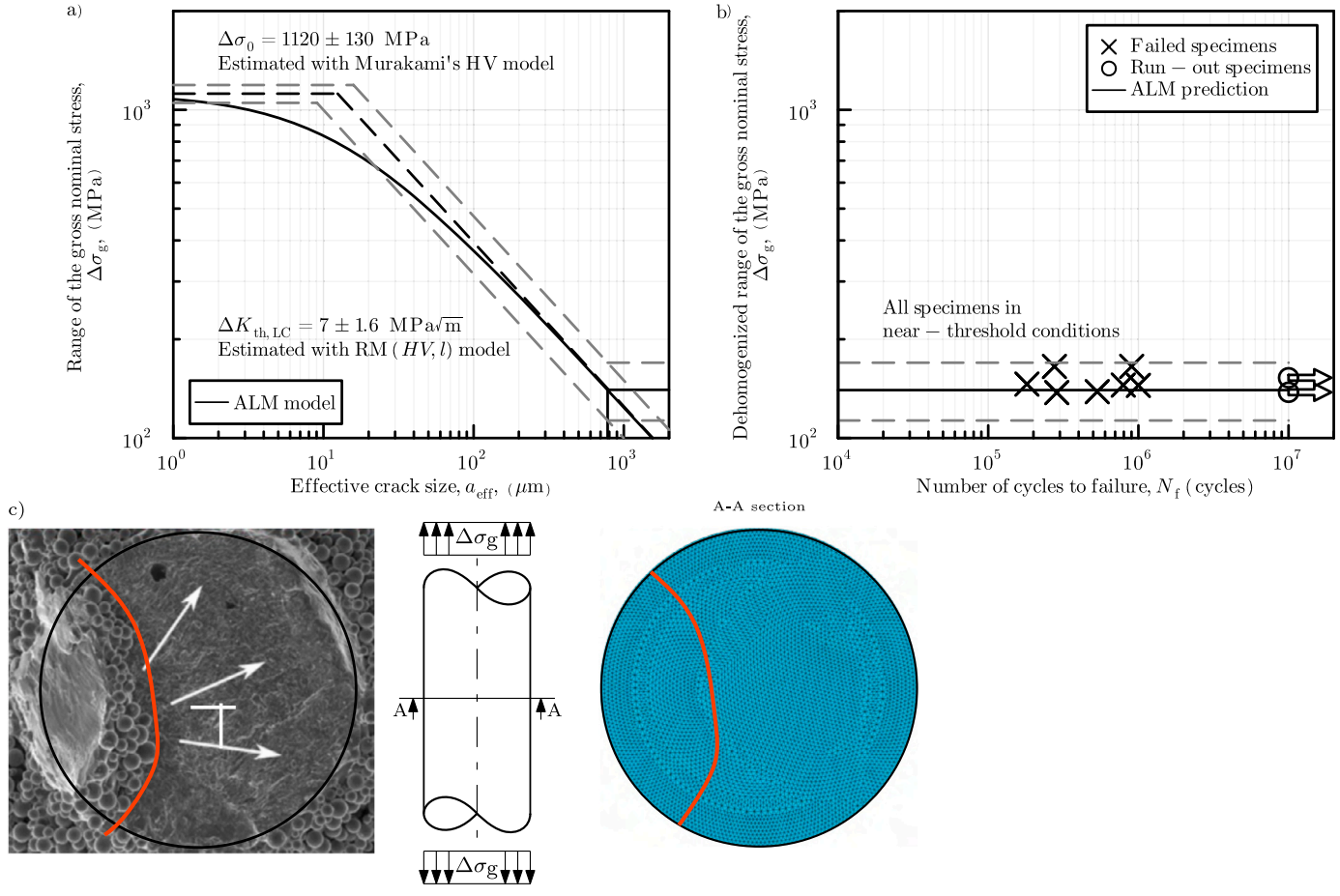

Fig. 28. Comparison of the ALM model against experimental data from tests conducted on lattice structures [113]; lattice structures with cubic UC, AMed from Ti-6Al-4V powders; surfaces in AB conditions; HT microstructure; part of subfigure c adapted from [113] with permission from ELSEVIER.

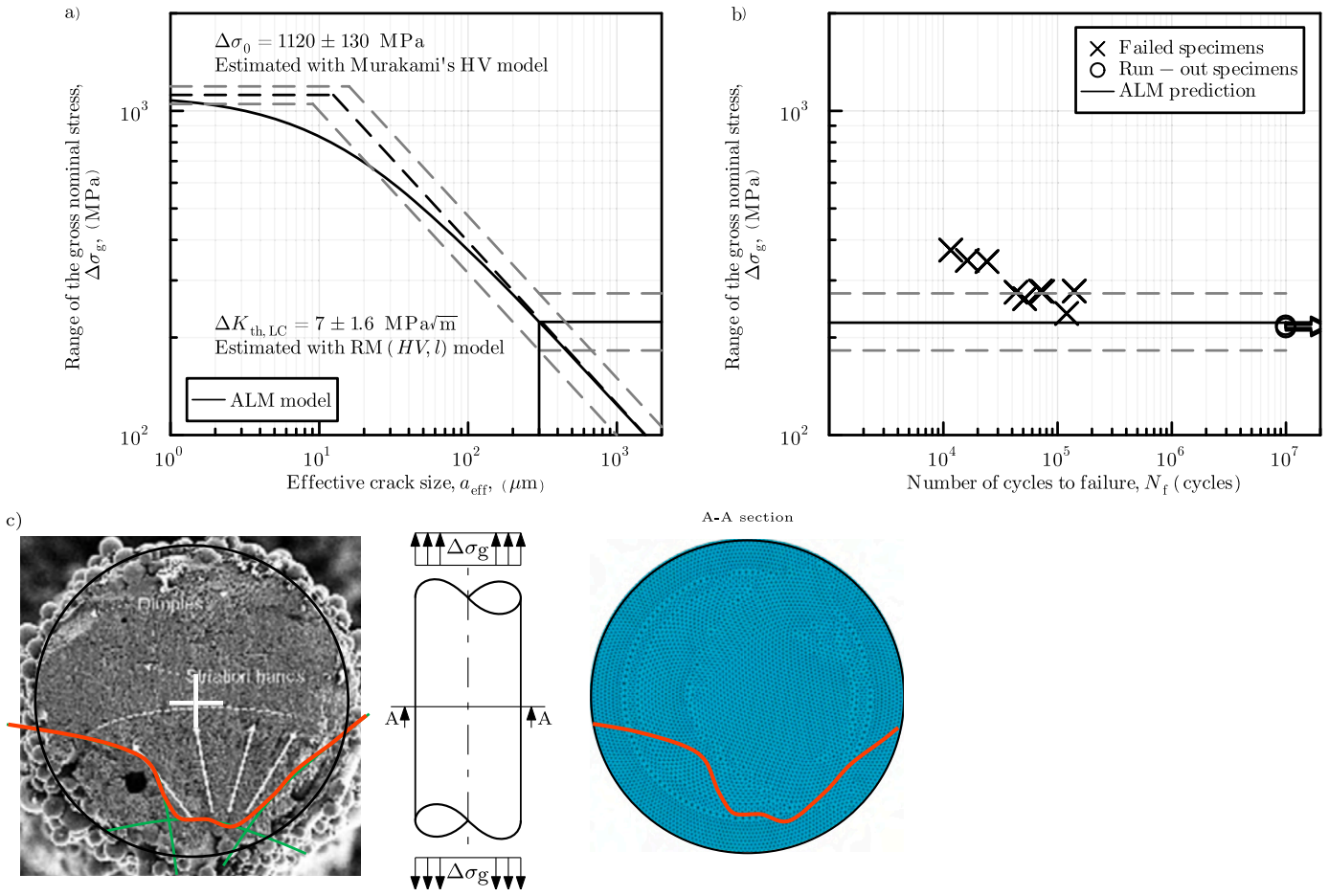

Fig. 29. Comparison of the ALM model against experimental data from tests conducted on small-sized specimens [114]. Cylindrical specimens, AMed from Ti-6Al-4V powders; surfaces in AB conditions; HT microstructure.

tures to reduce the relative density of lattice structures for a given UC size;

2. further experimental fatigue analysis, in particular: (i) validation of the ALM model applied to lattice structures as suggested in this work; (ii) extension of the ALM model to multiaxial loading conditions (some preliminary analyses are reported in [180,292]); (iii) experimental analysis of the fatigue strength of AMed lattice structures under high temperature and corrosive environments;
3. building on the knowledge of the two previous points, developing design optimization procedures where the fatigue strength criterion (which should be defect-tolerant, and material-microstructure-environment system dependent) and the technological limitations of metal AM (e.g., the building direction, minimal size of individual features) are included as constraints.

Given the stochastic nature of the defects distribution of AMed materials, it is impractical to characterize defects in each component deterministically for the fatigue assessment; for real engineering applications, a statistical approach is necessary to determine the crack size a_{eff} to be used in Equation (4). There are several successful applications in the literature of stochastic models for the fatigue limit prediction of fully-dense AMed materials and defective materials using the statistics of extremes (e.g., [31,173,208,293–296]). The authors believe that a similar approach should be adopted to use lattice structures in the industry.

Lastly, in a potential future where the AM process (not necessarily PBF or DED) allows producing features of sizes comparable to that of individual grains of the crystal lattice, dedicated analysis would be required [4].

CRediT authorship contribution statement

Francesco Collini: Writing – original draft, Validation, Methodology, Investigation, Formal analysis, Conceptualization. **Giovanni Meneghetti:** Writing – review & editing, Validation, Supervision, Methodology, Funding acquisition, Conceptualization.

Declaration of competing interest

The authors declare that they have no known competing financial interests or personal relationships that could have appeared to influence the work reported in this paper.

Data availability

Data will be made available on request.

References

[1] Department of Materials Science and Metallurgy - University of Cambridge. (n.d.). Structure of bone and implant materials, https://www.doitpoms.ac.uk/tlplib/bones/index.php.
[2] M.F. Ashby, The properties of foams and lattices, Philos. Trans. R. Soc. A, Math. Phys. Eng. Sci. 364 (2005) 15–30, https://doi.org/10.1098/RSTA.2005.1678.
[3] T. Maconachie, M. Leary, B. Lozanovski, X. Zhang, M. Qian, O. Faruque, M. Brandt, SLM lattice structures: properties, performance, applications and challenges, Mater. Des. 183 (2019) 108137, https://doi.org/10.1016/J.MATDES.2019.108137.

[4] M. Benedetti, A. du Plessis, R.O. Ritchie, M. Dallago, S.M. Razavi, F. Berto, Architected cellular materials: a review on their mechanical properties towards fatigue-tolerant design and fabrication, Mater. Sci. Eng., R Rep. 144 (2021) 100606, https://doi.org/10.1016/J.MSER.2021.100606.
[5] T.A. Schaedler, A.J. Jacobsen, A. Torrents, A.E. Sorensen, J. Lian, J.R. Greer, L. Valdevit, W.B. Carter, Ultralight metallic microlattices, Science 334 (2011) 962–965, https://doi.org/10.1126/science.1211649.
[6] L.R. Meza, S. Das, J.R. Greer, Strong, lightweight, and recoverable three-dimensional ceramic nanolattices, Science 345 (2014) 1322–1326, https://doi.org/10.1126/science.1255908.
[7] X.P. Tan, Y.J. Tan, C.S. Chow, S.B. Tor, W.Y. Yeong, Metallic powder-bed based 3D printing of cellular scaffolds for orthopaedic implants: a state-of-the-art review on manufacturing, topological design, mechanical properties and biocompatibility, Mater. Sci. Eng. C 76 (2017) 1328–1343, https://doi.org/10.1016/J.MSEC.2017.02.094.
[8] S. Arabnejad, B. Johnston, M. Tanzer, D. Pasini, Fully porous 3D printed titanium femoral stem to reduce stress-shielding following total hip arthroplasty, J. Orthop. Res. 35 (2017) 1774–1783, https://doi.org/10.1002/JOR.23445.
[9] M. Shirzad, A. Zolfagharian, M. Bodaghi, S.Y. Nam, Auxetic metamaterials for bone-implanted medical devices: recent advances and new perspectives, Eur. J. Mech. A, Solids 98 (2023) 104905, https://doi.org/10.1016/J.EUROMECHSOL.2022.104905.
[10] D. Jafari, W.W. Wits, The utilization of selective laser melting technology on heat transfer devices for thermal energy conversion applications: a review, Renew. Sustain. Energy Rev. 91 (2018) 420–442, https://doi.org/10.1016/J.RSER.2018.03.109.
[11] H.E. Burton, N.M. Eisenstein, B.M. Lawless, P. Jamshidi, M.A. Segarra, O. Addison, D.E. Shepherd, M.M. Attallah, L.M. Grover, S.C. Cox, The design of additively manufactured lattices to increase the functionality of medical implants, Mater. Sci. Eng. C 94 (2019) 901–908, https://doi.org/10.1016/J.MSEC.2018.10.052.
[12] M. Bici, S. Brischetto, F. Campana, C.G. Ferro, C. Seclì, S. Varetti, P. Maggiore, A. Mazza, Development of a multifunctional panel for aerospace use through SLM additive manufacturing, Proc. CIRP 67 (2018) 215–220, https://doi.org/10.1016/j.procir.2017.12.202.
[13] A. du Plessis, S.M.J. Razavi, M. Benedetti, S. Murchio, M. Leary, M. Watson, D. Bhate, F. Berto, Properties and applications of additively manufactured metallic cellular materials: a review, Prog. Mater. Sci. 125 (2022) 100918, https://doi.org/10.1016/j.pmatsci.2021.100918.
[14] T. Ghidini, M. Grasso, J. Gumpinger, A. Makaya, B. Colosimo, Additive manufacturing in the new space economy: current achievements and future perspectives, Prog. Aerosp. Sci. 142 (2023) 100959, https://doi.org/10.1016/j.paerosci.2023.100959.
[15] Z.S. Bagheri, D. Melancon, L. Liu, R.B. Johnston, D. Pasini, Compensation strategy to reduce geometry and mechanics mismatches in porous biomaterials built with Selective Laser Melting, J. Mech. Behav. Biomed. Mater. 70 (2017) 17–27, https://doi.org/10.1016/J.JMBBM.2016.04.041.
[16] M. Dallago, V. Fontanari, E. Torresani, M. Leoni, C. Pederzolli, C. Potrich, M. Benedetti, Fatigue and biological properties of Ti-6Al-4V ELI cellular structures with variously arranged cubic cells made by selective laser melting, J. Mech. Behav. Biomed. Mater. 78 (2018) 381–394, https://doi.org/10.1016/J.JMBBM.2017.11.044.
[17] M. Dallago, B. Winiarski, F. Zanini, S. Carmignato, M. Benedetti, On the effect of geometrical imperfections and defects on the fatigue strength of cellular lattice structures additively manufactured via Selective Laser Melting, Int. J. Fatigue 124 (2019) 348–360, https://doi.org/10.1016/J.IJFATIGUE.2019.03.019.
[18] M. Alaña, A. Cutolo, G. Probst, S.R. de Galarreta, B.V. Hooreweder, Understanding elastic anisotropy in diamond based lattice structures produced by laser powder bed fusion: effect of manufacturing deviations, Mater. Des. 195 (2020) 108971, https://doi.org/10.1016/J.MATDES.2020.108971.
[19] T. Fritsch, L. Farahbod-Sternahl, I. Serrano-Muñoz, F. Léonard, C. Haberland, G. Bruno, 3D computed tomography quantifies the dependence of bulk porosity, surface roughness, and re-entrant features on build angle in additively manufactured IN625 lattice struts, Adv. Eng. Mater. 24 (2022) 2100689, https://doi.org/10.1002/ADEM.202100689.
[20] B.V. Hooreweder, Y. Apers, K. Lietaert, J.P. Kruth, Improving the fatigue performance of porous metallic biomaterials produced by Selective Laser Melting, Acta Biomater. 47 (2017) 193–202, https://doi.org/10.1016/J.ACTBIO.2016.10.005.
[21] A. Cutolo, B. Engelen, W. Desmet, B.V. Hooreweder, Mechanical properties of diamond lattice Ti-6Al-4V structures produced by laser powder bed fusion: on the effect of the load direction, J. Mech. Behav. Biomed. Mater. 104 (2020) 103656, https://doi.org/10.1016/J.JMBBM.2020.103656.
[22] E. Wycisk, A. Solbach, S. Siddique, D. Herzog, F. Walther, C. Emmelmann, Effects of defects in laser additive manufactured Ti-6Al-4V on fatigue properties, Phys. Proc. 56 (2014) 371–378, https://doi.org/10.1016/J.PHPRO.2014.08.120.
[23] S. Beretta, S. Romano, A comparison of fatigue strength sensitivity to defects for materials manufactured by AM or traditional processes, Int. J. Fatigue 94 (2017) 178–191, https://doi.org/10.1016/J.IJFATIGUE.2016.06.020.
[24] S. Romano, S. Beretta, A. Brandão, J. Gumpinger, T. Ghidini, HCF resistance of AlSi10Mg produced by SLM in relation to the presence of defects, Proc. Struct. Integr. 7 (2017) 101–108, https://doi.org/10.1016/J.PROSTR.2017.11.066.
[25] J.N.D. Ngnekou, Y. Nadot, G. Henaff, J. Nicolai, W.H. Kan, J.M. Cairney, L. Ridosz, Fatigue properties of AlSi10Mg produced by Additive Layer Manufacturing, Int. J. Fatigue 119 (2019) 160–172, https://doi.org/10.1016/J.IJFATIGUE.2018.09.029.
[26] S. Romano, P.D. Nezhadfar, N. Shamsaei, M. Seifi, S. Beretta, High cycle fatigue behavior and life prediction for additively manufactured 17-4 PH stainless steel: effect of sub-surface porosity and surface roughness, Theor. Appl. Fract. Mech. 106 (2020) 102477, https://doi.org/10.1016/J.TAFMEC.2020.102477.
[27] W. Radlof, C. Benz, H. Heyer, M. Sander, Monotonic and fatigue behavior of EBM manufactured Ti-6Al-4V solid samples: experimental, analytical and numerical investigations, Materials 13 (2020) 1–18, https://doi.org/10.3390/MA13204642.
[28] M.H. Nasab, S. Romano, D. Gastaldi, S. Beretta, M. Vedani, Combined effect of surface anomalies and volumetric defects on fatigue assessment of AlSi7Mg fabricated via laser powder bed fusion, Addit. Manuf. 34 (2020) 100918, https://doi.org/10.1016/j.addma.2019.100918.
[29] P. Ferro, A. Fabrizi, F. Berto, G. Savio, R. Meneghello, S. Rosso, Defects as a root cause of fatigue weakening of additively manufactured AlSi10Mg components, Theor. Appl. Fract. Mech. 108 (8 2020), https://doi.org/10.1016/J.TAFMEC.2020.102611.
[30] T.H. Becker, P. Kumar, U. Ramamurty, Fracture and fatigue in additively manufactured metals, Acta Mater. 219 (10 2021), https://doi.org/10.1016/J.ACTAMAT.2021.117240.
[31] S. Beretta, L. Patriarca, M. Gargourimotlagh, A. Hardaker, D. Brackett, M. Salimian, J. Gumpinger, T. Ghidini, A benchmark activity on the fatigue life assessment of AlSi10Mg components manufactured by L-PBF, Mater. Des. 218 (2022) 110713, https://doi.org/10.1016/J.MATDES.2022.110713.
[32] M. Nakamura, K. Takahashi, Y. Saito, Effect of shot and laser peening on fatigue strength of additively manufactured aluminum alloy with rough surfaces, J. Mater. Eng. Perform. 32 (2023) 1589–1600, https://doi.org/10.1007/S11665-022-07225-1/FIGURES/13.
[33] D. Schimbäck, L. Kaserer, P. Mair, F. Palm, G. Leichtfried, S. Pogatscher, A. Hohenwarter, Deformation and fatigue behaviour of additively manufactured Scalmalloy® with bimodal microstructure, Int. J. Fatigue 172 (2023) 107592, https://doi.org/10.1016/J.IJFATIGUE.2023.107592.
[34] M. Benedetti, C. Santus, Building the Kitagawa-Takahashi diagram of flawed materials and components using an optimized V-notched cylindrical specimen, Eng. Fract. Mech. 224 (2020) 106810, https://doi.org/10.1016/J.ENGFRACMECH.2019.106810.
[35] L. Emanuelli, A. Molinari, L. Facchini, E. Sbettega, S. Carmignato, M. Bandini, M. Benedetti, Effect of heat treatment temperature and turning residual stresses on the plain and notch fatigue strength of Ti-6Al-4V additively manufactured via laser powder bed fusion, Int. J. Fatigue 162 (2022) 107009, https://doi.org/10.1016/J.IJFATIGUE.2022.107009.
[36] L. Boniotti, S. Beretta, L. Patriarca, L. Rigoni, S. Foletti, Experimental and numerical investigation on compressive fatigue strength of lattice structures of AlSi7Mg manufactured by SLM, Int. J. Fatigue 128 (2019) 105181, https://doi.org/10.1016/J.IJFATIGUE.2019.06.041.
[37] M. Gavazzoni, S. Beretta, S. Foletti, Response of an aluminium Schwarz triply periodic minimal surface lattice structure under constant amplitude and random fatigue, Int. J. Fatigue 163 (2022) 107020, https://doi.org/10.1016/j.ijfatigue.2022.107020.
[38] S. Raghavendra, M. Dallago, F. Zanini, S. Carmignato, F. Berto, M. Benedetti, A probabilistic average strain energy density approach to assess the fatigue strength of additively manufactured cellular lattice materials, Int. J. Fatigue 172 (2023) 107601, https://doi.org/10.1016/J.IJFATIGUE.2023.107601.
[39] Y. Liu, D. Ren, S. Li, H. Wang, L. Zhang, T. Sercombe, Enhanced fatigue characteristics of a topology-optimized porous titanium structure produced by selective laser melting, Addit. Manuf. 32 (2020) 101060, https://doi.org/10.1016/j.addma.2020.101060.
[40] J. Song, Q. Tang, Q. Feng, S. Ma, F. Guo, Q. Han, Investigation on the modelling approach for variable-density lattice structures fabricated using selective laser melting, Mater. Des. 212 (2021) 110236.
[41] A. Viswanath, K.A. Khan, I. Barsoum, Design of novel isosurface strut-based lattice structures: effective stiffness, strength, anisotropy and fatigue properties, Mater. Des. 224 (2022) 111293.
[42] X. Chen, W. Ren, Y. Sun, J. Zhang, J. Yang, K. Wang, Y. Gong, Z. Zhang, L. Bai, Adjusting unit cell three-dimensional posture and mirror array: a novel lattice structure design approach, Mater. Des. 221 (2022) 110852.
[43] J.-H. Bastek, S. Kumar, B. Telgen, R.N. Glaesener, D.M. Kochmann, Inverting the structure-property map of truss metamaterials by deep learning, Proc. Natl. Acad. Sci. 119 (1 2022), https://doi.org/10.1073/pnas.2111505119.
[44] A. Cutolo, E. Beevers, B.V. Hooreweder, A design strategy to enhance the mechanical response of diamond-based lattice structures produced by laser powder bed fusion, Mater. Sci. Eng. A 876 (2023) 145120, https://doi.org/10.1016/j.msea.2023.145120.
[45] R. De Biasi, S. Murchio, E. Sbettega, S. Carmignato, V. Luchin, M. Benedetti, Efficient optimization framework for L-PBF fatigue enhanced Ti6Al4V lattice component, Mater. Des. 230 (2023) 111975.
[46] I. Gibson, D.W. Rosen, B. Stucker, M. Khorasani, D. Rosen, B. Stucker, M. Khorasani, Additive Manufacturing Technologies, vol. 17, Springer, 2021.

[47] L. Yang, K. Hsu, B. Baughman, D. Godfrey, F. Medina, M. Menon, S. Wiener, Additive Manufacturing of Metals: the Technology, Materials, Design and Production, 2017.
[48] M.M. Shalabi, A. Gortemaker, M.A.V. Hof, J.A. Jansen, N.H. Creugers, Implant surface roughness and bone healing: a systematic review, 85 (2006) 496–500, https://doi.org/10.1177/154405910608500603.
[49] T. Persenot, A. Burr, R. Dendievel, J.Y. Buffière, E. Maire, J. Lachambre, G. Martin, Fatigue performances of chemically etched thin struts built by selective electron beam melting: experiments and predictions, Materialia 9 (2020) 100589, https://doi.org/10.1016/J.MTLA.2020.100589.
[50] L. Thijs, K. Kempen, J.-P. Kruth, J.V. Humbeeck, Fine-structured aluminium products with controllable texture by selective laser melting of pre-alloyed AlSi10Mg powder, Acta Mater. 61 (2013) 1809–1819, https://doi.org/10.1016/j.actamat.2012.11.052.
[51] S. Zhao, S.J. Li, W.T. Hou, Y.L. Hao, R. Yang, R.D. Misra, The influence of cell morphology on the compressive fatigue behavior of Ti-6Al-4V meshes fabricated by electron beam melting, J. Mech. Behav. Biomed. Mater. 59 (2016) 251–264, https://doi.org/10.1016/J.JMBBM.2016.01.034.
[52] G. Meneghetti, D. Rigon, C. Gennari, An analysis of defects influence on axial fatigue strength of maraging steel specimens produced by additive manufacturing, Int. J. Fatigue 118 (2019) 54–64, https://doi.org/10.1016/J.IJFATIGUE.2018.08.034.
[53] EOS Aluminium AlSi10Mg Material Data Sheet Metal Solutions.
[54] A. Yadollahi, N. Shamsaei, S.M. Thompson, A. Elwany, L. Bian, Effects of building orientation and heat treatment on fatigue behavior of selective laser melted 17-4 PH stainless steel, Int. J. Fatigue 94 (2017) 218–235, https://doi.org/10.1016/J.IJFATIGUE.2016.03.014.
[55] Z. Qu, Z. Zhang, R. Liu, L. Xu, Y. Zhang, X. Li, Z. Zhao, Q. Duan, S. Wang, S. Li, et al., High fatigue resistance in a titanium alloy via near-void-free 3d printing, Nature 626 (8001) (2024) 999–1004.
[56] J.C. Fox, S.P. Moylan, B.M. Lane, Effect of process parameters on the surface roughness of overhanging structures in laser powder bed fusion additive manufacturing, in: 3rd CIRP Conference on Surface Integrity, Proc. CIRP 45 (2016) 131–134, https://doi.org/10.1016/j.procir.2016.02.347.
[57] J. Pegues, M. Roach, R.S. Williamson, N. Shamsaei, Surface roughness effects on the fatigue strength of additively manufactured Ti-6Al-4V, Int. J. Fatigue 116 (2018) 543–552, https://doi.org/10.1016/j.ijfatigue.2018.07.013.
[58] T. Persenot, A. Burr, G. Martin, J.Y. Buffiere, R. Dendievel, E. Maire, Effect of build orientation on the fatigue properties of as-built Electron Beam Melted Ti-6Al-4V alloy, Int. J. Fatigue 118 (2019) 65–76, https://doi.org/10.1016/J.IJFATIGUE.2018.08.006.
[59] S. Murchio, M. Dallago, F. Zanini, S. Carmignato, G. Zappini, F. Berto, D. Maniglio, M. Benedetti, Additively manufactured Ti-6Al-4V thin struts via laser powder bed fusion: effect of building orientation on geometrical accuracy and mechanical properties, J. Mech. Behav. Biomed. Mater. 119 (2021) 104495, https://doi.org/10.1016/j.jmbbm.2021.104495.
[60] A. Cutolo, C. Elangeswaran, G.K. Muralidharan, B.V. Hooreweder, On the role of building orientation and surface post-processes on the fatigue life of Ti-6Al-4V coupons manufactured by laser powder bed fusion, Mater. Sci. Eng. A 840 (2022) 142747, https://doi.org/10.1016/j.msea.2022.142747.
[61] B. Vandenbroucke, J.P. Kruth, Selective laser melting of biocompatible metals for rapid manufacturing of medical parts, Rapid Prototyping J. 13 (2007) 196–203, https://doi.org/10.1108/13552540710776142.
[62] C. Qiu, N.J. Adkins, M.M. Attallah, Microstructure and tensile properties of selectively laser-melted and of HIPed laser-melted Ti-6Al-4V, Mater. Sci. Eng. A 578 (2013) 230–239, https://doi.org/10.1016/J.MSEA.2013.04.099.
[63] K. Kempen, L. Thijs, J.V. Humbeeck, J.P. Kruth, Processing AlSi10Mg by selective laser melting: parameter optimisation and material characterisation 31 (2014) 917–923, https://doi.org/10.1179/1743284714Y.0000000702.
[64] H. Gong, K. Rafi, H. Gu, T. Starr, B. Stucker, Analysis of defect generation in Ti-6Al-4V parts made using powder bed fusion additive manufacturing processes, Addit. Manuf. 1–4 (2014) 87–98, https://doi.org/10.1016/J.ADDMA.2014.08.002.
[65] H. Gong, K. Rafi, H. Gu, G.D.J. Ram, T. Starr, B. Stucker, Influence of defects on mechanical properties of Ti-6Al-4 V components produced by selective laser melting and electron beam melting, Mater. Des. 86 (2015) 545–554, https://doi.org/10.1016/J.MATDES.2015.07.147.
[66] W. Xu, M. Brandt, S. Sun, J. Elambasseril, Q. Liu, K. Latham, K. Xia, M. Qian, Additive manufacturing of strong and ductile Ti-6Al-4V by selective laser melting via in situ martensite decomposition, Acta Mater. 85 (2015) 74–84, https://doi.org/10.1016/J.ACTAMAT.2014.11.028.
[67] M. Elsayed, M. Ghazy, Y. Youssef, K. Essa, Optimization of slm process parameters for ti6al4v medical implants, Rapid Prototyping J. 25 (3) (2019) 433–447.
[68] G. Kasperovich, J. Hausmann, Improvement of fatigue resistance and ductility of TiAl6V4 processed by selective laser melting, J. Mater. Process. Technol. 220 (2015) 202–214, https://doi.org/10.1016/J.JMATPROTEC.2015.01.025.
[69] M. Alaña, A. Cutolo, S.R. de Galarreta, B.V. Hooreweder, Influence of relative density on quasi-static and fatigue failure of lattice structures in Ti6Al4V produced by laser powder bed fusion, Sci. Rep. 11 (2021) 19314, https://doi.org/10.1038/s41598-021-98631-3.
[70] J.W. Pegues, S. Shao, N. Shamsaei, N. Sanaei, A. Fatemi, D.H. Warner, P. Li, N. Phan, Fatigue of additive manufactured Ti-6Al-4V, part I: the effects of powder feedstock, manufacturing, and post-process conditions on the resulting microstructure and defects, Int. J. Fatigue 132 (2020) 105358, https://doi.org/10.1016/J.IJFATIGUE.2019.105358.
[71] P. Wüst, A. Edelmann, R. Hellmann, Areal surface roughness optimization of maraging steel parts produced by hybrid additive manufacturing, Materials 13 (2) (2020) 418.
[72] E. Beevers, A. Cutolo, F. Mertens, B.V. Hooreweder, Unravelling the relation between Laser Powder Bed Fusion processing parameters and the mechanical behaviour of as built lattices in a novel Al-Cu-Mg-Ag-Ti-B alloy, J. Mater. Process. Technol. 315 (2023) 117915, https://doi.org/10.1016/j.jmatprotec.2023.117915.
[73] M. Hamidi Nasab, G. Masinelli, C. de Formanoir, L. Schlenger, S. Van Petegem, R. Esmaeilzadeh, K. Wasmer, A. Ganvir, A. Salminen, F. Aymanns, et al., Harmonizing sound and light: X-ray imaging unveils acoustic signatures of stochastic inter-regime instabilities during laser melting, Nat. Commun. 14 (1) (2023) 8008.
[74] C. de Formanoir, M.H. Nasab, L. Schlenger, S. Van Petegem, G. Masinelli, F. Marone, A. Salminen, A. Ganvir, K. Wasmer, R.E. Logé, Healing of keyhole porosity by means of defocused laser beam remelting: operando observation by x-ray imaging and acoustic emission-based detection, Addit. Manuf. 79 (2024) 103880.
[75] D. Ordnung, T. Mertens, J. Metelkova, B. Van Hooreweder, Novel strategy for automated quality enhancement of up-facing inclined surfaces by incremental dual laser powder bed fusion, Opt. Lasers Eng. 178 (2024) 108172.
[76] D. Ordnung, T. Mertens, J. Tacq, M. Hamidi Nasab, M. Sinico, G. Li, L. Thijs, B. Vrancken, B. Van Hooreweder, Enhancing fatigue life of as-printed martensitic M789 steel produced by laser powder bed fusion via in-process surface integrity improvement and phase change induced compressive residual stresses, SSRN (2024), https://doi.org/10.2139/ssrn.4789956.
[77] R. Bertolini, A. Campagnolo, M. Sorgato, A. Ghiotti, S. Bruschi, G. Meneghetti, Fatigue strength of LPBF Ti6Al4V machined under flood and cryogenic lubricooling conditions, Int. J. Fatigue 162 (2022) 106973, https://doi.org/10.1016/J.IJFATIGUE.2022.106973.
[78] P. Lhuissier, C. de Formanoir, G. Martin, R. Dendievel, S. Godet, Geometrical control of lattice structures produced by EBM through chemical etching: investigations at the scale of individual struts, Mater. Des. 110 (2016) 485–493.
[79] E. Brandl, U. Heckenberger, V. Holzinger, D. Buchbinder, Additive manufactured AlSi10Mg samples using Selective Laser Melting (SLM): microstructure, high cycle fatigue, and fracture behavior, Mater. Des. 34 (2012) 159–169, https://doi.org/10.1016/J.MATDES.2011.07.067.
[80] R. Molaei, A. Fatemi, Crack paths in additive manufactured metallic materials subjected to multiaxial cyclic loads including surface roughness, HIP, and notch effects, Int. J. Fatigue 124 (2019) 558–570, https://doi.org/10.1016/J.IJFATIGUE.2019.03.007.
[81] M. Benedetti, C. Santus, Notch fatigue and crack growth resistance of Ti-6Al-4V ELI additively manufactured via selective laser melting: a critical distance approach to defect sensitivity, Int. J. Fatigue 121 (2019) 281–292, https://doi.org/10.1016/J.IJFATIGUE.2018.12.020.
[82] S. Leuders, T. Lieneke, S. Lammers, T. Tröster, T. Niendorf, On the fatigue properties of metals manufactured by selective laser melting - the role of ductility, J. Mater. Res. 29 (2014) 1911–1919, https://doi.org/10.1557/JMR.2014.157/FIGURES/7.
[83] S.L. Lu, H.P. Tang, Y.P. Ning, N. Liu, D.H. StJohn, M. Qian, Microstructure and mechanical properties of long Ti-6Al-4V rods additively manufactured by selective electron beam melting out of a deep powder bed and the effect of subsequent hot isostatic pressing, Metall. Mater. Trans. A 46 (2015) 3824–3834, https://doi.org/10.1007/s11661-015-2976-3.
[84] S. Leuders, M. Vollmer, F. Brenne, T. Tröster, T. Niendorf, Fatigue strength prediction for titanium alloy TiAl6V4 manufactured by selective laser melting, Metall. Mater. Trans. A, Phys. Metall. Mater. Sci. 46 (2015) 3816–3823, https://doi.org/10.1007/S11661-015-2864-X.
[85] M.-W. Wu, P.-H. Lai, The positive effect of hot isostatic pressing on improving the anisotropies of bending and impact properties in selective laser melted Ti-6Al-4V alloy, Mater. Sci. Eng. A 658 (2016) 429–438, https://doi.org/10.1016/j.msea.2016.02.023.
[86] S. Tammas-Williams, P.J. Withers, I. Todd, P.B. Prangnell, Porosity regrowth during heat treatment of hot isostatically pressed additively manufactured titanium components, Scr. Mater. 122 (2016) 72–76, https://doi.org/10.1016/J.SCRIPTAMAT.2016.05.002.
[87] X. Zhao, S. Li, M. Zhang, Y. Liu, T.B. Sercombe, S. Wang, Y. Hao, R. Yang, L.E. Murr, Comparison of the microstructures and mechanical properties of Ti-6Al-4V fabricated by selective laser melting and electron beam melting, Mater. Des. 95 (2016) 21–31, https://doi.org/10.1016/j.matdes.2015.12.135.
[88] S. Tammas-Williams, P.J. Withers, I. Todd, P.B. Prangnell, The influence of porosity on fatigue crack initiation in additively manufactured titanium components, Sci. Rep. 7 (2017) 7308, https://doi.org/10.1038/s41598-017-06504-5.
[89] W. Tillmann, C. Schaak, J. Nellesen, M. Schaper, M.E. Aydinöz, K.P. Hoyer, Hot isostatic pressing of IN718 components manufactured by selective laser melting, Addit. Manuf. 13 (2017) 93–102, https://doi.org/10.1016/J.ADDMA.2016.11.006.
[90] X. Shui, K. Yamanaka, M. Mori, Y. Nagata, K. Kurita, A. Chiba, Effects of post-processing on cyclic fatigue response of a titanium alloy additively manufactured by electron beam melting, Mater. Sci. Eng. A 680 (2017) 239–248, https://doi.org/10.1016/j.msea.2016.10.059.

[91] M. Seifi, A. Salem, D. Satko, J. Shaffer, J.J. Lewandowski, Defect distribution and microstructure heterogeneity effects on fracture resistance and fatigue behavior of EBM Ti-6Al-4V, Int. J. Fatigue 94 (2017) 263–287, https://doi.org/10.1016/J.IJFATIGUE.2016.06.001.
[92] J. Günther, D. Krewerth, T. Lippmann, S. Leuders, T. Tröster, A. Weidner, H. Biermann, T. Niendorf, Fatigue life of additively manufactured Ti-6Al-4V in the very high cycle fatigue regime, Int. J. Fatigue 94 (2017) 236–245, https://doi.org/10.1016/J.IJFATIGUE.2016.05.018.
[93] H. Masuo, Y. Tanaka, S. Morokoshi, H. Yagura, T. Uchida, Y. Yamamoto, Y. Murakami, Effects of defects, surface roughness and HIP on fatigue strength of Ti-6Al-4V manufactured by additive manufacturing, Proc. Struct. Integr. 7 (2017) 19–26, https://doi.org/10.1016/J.PROSTR.2017.11.055.
[94] H. Masuo, Y. Tanaka, S. Morokoshi, H. Yagura, T. Uchida, Y. Yamamoto, Y. Murakami, Influence of defects, surface roughness and HIP on the fatigue strength of Ti-6Al-4V manufactured by additive manufacturing, Int. J. Fatigue 117 (2018) 163–179, https://doi.org/10.1016/j.ijfatigue.2018.07.020.
[95] P. Li, D.H. Warner, J.W. Pegues, M.D. Roach, N. Shamsaei, N. Phan, Investigation of the mechanisms by which hot isostatic pressing improves the fatigue performance of powder bed fused Ti-6Al-4V, Int. J. Fatigue 120 (2019) 342–352, https://doi.org/10.1016/J.IJFATIGUE.2018.10.015.
[96] R. Molaei, A. Fatemi, N. Phan, Significance of hot isostatic pressing (HIP) on multiaxial deformation and fatigue behaviors of additive manufactured Ti-6Al-4V including build orientation and surface roughness effects, Int. J. Fatigue 117 (2018) 352–370, https://doi.org/10.1016/j.ijfatigue.2018.07.035.
[97] H.V. Atkinson, S. Davies, Fundamental aspects of hot isostatic pressing: an overview, Metall. Mater. Trans. A, Phys. Metall. Mater. Sci. 31 (2000) 2981–3000, https://doi.org/10.1007/S11661-000-0078-2/METRICS.
[98] N. Shamsaei, J. Simsiriwong, Fatigue behaviour of additively-manufactured metallic parts, Proc. Struct. Integr. 7 (2017) 3–10, https://doi.org/10.1016/J.PROSTR.2017.11.053.
[99] U. Tradowsky, J. White, R.M. Ward, N. Read, W. Reimers, M.M. Attallah, Selective laser melting of AlSi10Mg: influence of post-processing on the microstructural and tensile properties development, Mater. Des. 105 (2016) 212–222, https://doi.org/10.1016/J.MATDES.2016.05.066.
[100] N.O. Larrosa, W. Wang, N. Read, M.H. Loretto, C. Evans, J. Carr, U. Tradowsky, M.M. Attallah, P.J. Withers, Linking microstructure and processing defects to mechanical properties of selectively laser melted AlSi10Mg alloy, Theor. Appl. Fract. Mech. 98 (2018) 123–133, https://doi.org/10.1016/J.TAFMEC.2018.09.011.
[101] J.G.S. Macías, L. Zhao, D. Tingaud, B. Bacroix, G. Pyka, C. van der Rest, L. Ryelandt, A. Simar, Hot isostatic pressing of laser powder bed fusion AlSi10Mg: parameter identification and mechanical properties, J. Mater. Sci. 57 (2022) 9726–9740, https://doi.org/10.1007/S10853-022-07027-9/FIGURES/11.
[102] S.V. Bael, G. Kerckhofs, M. Moesen, G. Pyka, J. Schrooten, J. Kruth, Micro-CT-based improvement of geometrical and mechanical controllability of selective laser melted Ti6Al4V porous structures, Mater. Sci. Eng. A 528 (2011) 7423–7431, https://doi.org/10.1016/j.msea.2011.06.045.
[103] C. Qiu, S. Yue, N.J. Adkins, M. Ward, H. Hassanin, P.D. Lee, P.J. Withers, M.M. Attallah, Influence of processing conditions on strut structure and compressive properties of cellular lattice structures fabricated by selective laser melting, Mater. Sci. Eng. A 628 (2015) 188–197, https://doi.org/10.1016/J.MSEA.2015.01.031.
[104] L. Liu, P. Kamm, F. García-Moreno, J. Banhart, D. Pasini, Elastic and failure response of imperfect three-dimensional metallic lattices: the role of geometric defects induced by Selective Laser Melting, J. Mech. Phys. Solids 107 (2017) 160–184, https://doi.org/10.1016/j.jmps.2017.07.003.
[105] C. Tan, S. Li, K. Essa, P. Jamshidi, K. Zhou, W. Ma, M.M. Attallah, Laser Powder Bed Fusion of Ti-rich TiNi lattice structures: process optimisation, geometrical integrity, and phase transformations, Int. J. Mach. Tools Manuf. 141 (2019) 19–29, https://doi.org/10.1016/j.ijmachtools.2019.04.002.
[106] H. Lei, C. Li, J. Meng, H. Zhou, Y. Liu, X. Zhang, P. Wang, D. Fang, Evaluation of compressive properties of SLM-fabricated multi-layer lattice structures by experimental test and μ-CT-based finite element analysis, Mater. Des. 169 (2019) 107685, https://doi.org/10.1016/j.matdes.2019.107685.
[107] B. Lozanovski, M. Leary, P. Tran, D. Shidid, M. Qian, P. Choong, M. Brandt, Computational modelling of strut defects in SLM manufactured lattice structures, Mater. Des. 171 (2019) 107671, https://doi.org/10.1016/j.matdes.2019.107671.
[108] H. Hassanin, Y. Alkendi, M. Elsayed, K. Essa, Y. Zweiri, Controlling the properties of additively manufactured cellular structures using machine learning approaches, Adv. Eng. Mater. 22 (2020) 1901338, https://doi.org/10.1002/adem.201901338.
[109] L. Xiao, S. Li, W. Song, X. Xu, S. Gao, Process-induced geometric defect sensitivity of Ti–6Al–4V lattice structures with different mesoscopic topologies fabricated by electron beam melting, Mater. Sci. Eng. A 778 (2020) 139092, https://doi.org/10.1016/j.msea.2020.139092.
[110] F. Günther, F. Hirsch, S. Pilz, M. Wagner, A. Gebert, M. Kästner, M. Zimmermann, Structure-property relationships of imperfect additively manufactured lattices based on triply periodic minimal surfaces, Mater. Des. 222 (2022) 111036.
[111] U. Gebhardt, T. Gustmann, L. Giebeler, F. Hirsch, J.K. Hufenbach, M. Kästner, Additively manufactured AlSi10Mg lattices–potential and limits of modelling as-designed structures, Mater. Des. 220 (2022) 110796.
[112] H. Jia, B. Liu, Z. Zhao, S. Duan, P. Wang, H. Lei, Experimental investigation and numerical modeling of laser powder bed fusion process-induced angle-dependent defects in strut-based lattice structure, Mater. Des. 224 (2022) 111354.
[113] M. Dallago, S. Raghavendra, V. Luchin, G. Zappini, D. Pasini, M. Benedetti, The role of node fillet, unit-cell size and strut orientation on the fatigue strength of Ti-6Al-4V lattice materials additively manufactured via laser powder bed fusion, Int. J. Fatigue 142 (2021) 105946, https://doi.org/10.1016/J.IJFATIGUE.2020.105946.
[114] S. Murchio, A.D. Plessis, V. Luchin, D. Maniglio, M. Benedetti, Influence of mean stress and building orientation on the fatigue properties of sub-unital thin-strut miniaturized Ti6Al4V specimens additively manufactured via Laser-Powder Bed Fusion, Int. J. Fatigue 180 (2024) 108102, https://doi.org/10.1016/j.ijfatigue.2023.108102.
[115] C. Zhang, H. Zheng, L. Yang, Y. Li, J. Jin, W. Cao, C. Yan, Y. Shi, Mechanical responses of sheet-based gyroid-type triply periodic minimal surface lattice structures fabricated using selective laser melting, Mater. Des. 214 (2022) 110407.
[116] S. Ahmadi, S. Yavari, R. Wauthle, B. Pouran, J. Schrooten, H. Weinans, A. Zadpoor, Additively manufactured open-cell porous biomaterials made from six different space-filling unit cells: the mechanical and morphological properties, Materials 8 (2015) 1871–1896, https://doi.org/10.3390/ma8041871.
[117] J. Kessler, N. Balc, A. Gebhardt, K. Abbas, Basic design rules of unit cells for additive manufactured lattice structures, MATEC Web Conf. 137 (2017) 02005, https://doi.org/10.1051/matecconf/201713702005.
[118] S. Leuders, M. Thöne, A. Riemer, T. Niendorf, T. Tröster, H.A. Richard, H.J. Maier, On the mechanical behaviour of titanium alloy TiAl6V4 manufactured by selective laser melting: fatigue resistance and crack growth performance, Int. J. Fatigue 48 (2013) 300–307, https://doi.org/10.1016/J.IJFATIGUE.2012.11.011.
[119] P. Edwards, M. Ramulu, Fatigue performance evaluation of selective laser melted Ti-6Al-4V, Mater. Sci. Eng. A 598 (2014) 327–337, https://doi.org/10.1016/J.MSEA.2014.01.041.
[120] M. Dallago, V. Fontanari, B. Winiarski, F. Zanini, S. Carmignato, M. Benedetti, Fatigue properties of Ti6Al4V cellular specimens fabricated via SLM: CAD vs real geometry, Proc. Struct. Integr. 7 (2017) 116–123, https://doi.org/10.1016/J.PROSTR.2017.11.068.
[121] F. Sausto, C. Tezzele, S. Beretta, Analysis of fatigue strength of L-PBF AlSi10Mg with different surface post-processes: effect of residual stresses, Metals 12 (6) (2022) 898, https://doi.org/10.3390/MET12060898.
[122] M.M.H. Tusher, A. Ince, Effect of stress-relieved heat treatment on very high cycle fatigue performance of additive manufactured ti-6al-4v alloy, Fatigue Fract. Eng. Mater. Struct. 46 (10) (2023) 3982–4000, https://doi.org/10.1111/ffe.14119.
[123] J.G.S. Macías, C. Elangeswaran, L. Zhao, J.Y. Buffière, B.V. Hooreweder, A. Simar, Fatigue crack nucleation and growth in laser powder bed fusion AlSi10Mg under as built and post-treated conditions, Mater. Des. 210 (2021) 110084, https://doi.org/10.1016/J.MATDES.2021.110084.
[124] M.D. Sangid, The physics of fatigue crack initiation, Int. J. Fatigue 57 (2013) 58–72, https://doi.org/10.1016/J.IJFATIGUE.2012.10.009.
[125] Y. Li, M. Pavier, H. Coules, Experimental study on fatigue crack propagation of octet-truss lattice, in: iCSI 2021 the 4th International Conference on Structural Integrity, Proc. Struct. Integr. 37 (2022) 41–48, https://doi.org/10.1016/j.prostr.2022.01.057.
[126] Y. Li, M.M. Attallah, H. Coules, R. Martinez, M. Pavier, Fatigue of octet-truss lattices manufactured by laser powder bed fusion, Int. J. Fatigue 170 (2023) 107524.
[127] J. Huang, J. Lin, Fatigue of cellular materials, Acta Mater. 44 (1) (1996) 289–296, https://doi.org/10.1016/1359-6454(95)00170-4.
[128] O. Olurin, K. McCullough, N. Fleck, M. Ashby, Fatigue crack propagation in aluminium alloy foams, Int. J. Fatigue 23 (5) (2001) 375–382.
[129] C. Motz, O. Friedl, R. Pippan, Fatigue crack propagation in cellular metals, Int. J. Fatigue 27 (10–12) (2005) 1571–1581.
[130] G.R. Irwin, Analysis of stresses and strains near the end of a crack traversing a plate, J. Appl. Mech. 24 (1957) 361–364, https://doi.org/10.1115/1.4011547.
[131] S. Suresh, R.O. Ritchie, Propagation of short fatigue cracks, Int. Met. Rev. 29 (1984) 445–473, https://doi.org/10.1179/IMTR.1984.29.1.445.
[132] P.C. Paris, A note on the variables affecting the rate of crack growth due to cyclic loading, The Boeing Company. Document No D-17867, 9 1957.
[133] D. Martin, G.M. Sinclair, Crack propagation under repeated loading, in: Proceedings of the Third U.S. National Congress of Applied Mechanics, 1958, pp. 595–604.
[134] P. Paris, F. Erdogan, A critical analysis of crack propagation laws, J. Basic Eng. 85 (1963) 528–533, https://doi.org/10.1115/1.3656900.
[135] H. Kitagawa, S. Takahashi, Fracture mechanical approach to very small fatigue crack growth and to the threshold condition (in Japanese), Trans. Jpn. Soc. Mech. Eng. Ser. A 45 (1979) 1289–1303, https://doi.org/10.1299/KIKAIA.45.1289.
[136] H. Kitagawa, S. Takahashi, Applicability of fracture mechanics to very small cracks or the cracks in the early stage, in: Proceedings of the 2nd International Conference on Mechanical Behaviour of Materials, 1976, pp. 627–631, https://ci.nii.ac.jp/naid/10025887201/.
[137] N.E. Frost, A relation between the critical alternating propagation stress and crack length for mild steel, 173 (1959) 811–836, https://doi.org/10.1243/PIME_PROC_1959_173_065_02.
[138] N.E. Frost, Notch effects and the critical alternating stress required to propagate a crack in an aluminium alloy subject to fatigue loading, 2 (1960) 109–119, https://doi.org/10.1243/JMES_JOUR_1960_002_020_02.
[139] K. Tanaka, Y. Nakai, M. Yamashita, Fatigue growth threshold of small cracks, Int. J. Fract. 17 (1981) 519–533, https://doi.org/10.1007/BF00033345/METRICS.
[140] R.K. Nalla, B.L. Boyce, J.P. Campbell, J.O. Peters, R.O. Ritchie, Influence of microstructure on high-cycle fatigue of Ti-6Al-4V: bimodal vs. lamellar structures,

Metall. Mater. Trans. A, Phys. Metall. Mater. Sci. 33 (2002) 899–918, https://doi.org/10.1007/S11661-002-1023-3/METRICS.
[141] C. Gaëlle, S.-B. Christine, L. Laurie, H. Zeline, Near-threshold fatigue propagation of physically short and long cracks in Titanium alloy, Proc. Struct. Integr. 2 (2016) 950–957, https://doi.org/10.1016/j.prostr.2016.06.122.
[142] M.H.E. Haddad, T.H. Topper, K.N. Smith, Prediction of non propagating cracks, Eng. Fract. Mech. 11 (1979) 573–584, https://doi.org/10.1016/0013-7944(79)90081-X.
[143] M.H.E. Haddad, K.N. Smith, T.H. Topper, Fatigue crack propagation of short cracks, J. Eng. Mater. Technol. 101 (1979) 42–46, https://doi.org/10.1115/1.3443647.
[144] B. Atzori, P. Lazzarin, G. Meneghetti, Fracture mechanics and notch sensitivity, Fatigue Fract. Eng. Mater. Struct. 26 (2003) 257–267, https://doi.org/10.1046/J.1460-2695.2003.00633.X.
[145] B. Atzori, P. Lazzarin, G. Meneghetti, A unified treatment of the mode I fatigue limit of components containing notches or defects, Int. J. Fract. 133 (2005) 61–87, https://doi.org/10.1007/S10704-005-2183-0.
[146] K. Tanaka, Y. Akiniwa, Resistance-curve method for predicting propagation threshold of short fatigue cracks at notches, Eng. Fract. Mech. 30 (1988) 863–876, https://doi.org/10.1016/0013-7944(88)90146-4.
[147] U. Zerbst, M. Vormwald, R. Pippan, H.-P. Gänser, C. Sarrazin-Baudoux, M. Madia, About the fatigue crack propagation threshold of metals as a design criterion – a review, Eng. Fract. Mech. 153 (2016) 190–243, https://doi.org/10.1016/j.engfracmech.2015.12.002.
[148] M. Madia, U. Zerbst, T. Werner, Estimation of the Kitagawa-Takahashi diagram by cyclic R curve analysis, Proc. Struct. Integr. 38 (2022) 309–316, https://doi.org/10.1016/j.prostr.2022.03.032.
[149] J.C. Newman, A crack opening stress equation for fatigue crack growth, Int. J. Fract. 24 (1984) R131–R135, https://doi.org/10.1007/BF00020751/METRICS.
[150] J.C. Newman, A Crack-Closure Model for Predicting Fatigue-Crack Growth Under Aircraft Spectrum Loading, 1981.
[151] J.C. Newman, FASTRAN-2: A Fatigue Crack Growth Structural Analysis Program, 1992.
[152] A. Yadollahi, M.J. Mahtabi, H.R. Doude, J.C.J. Newman, Prediction of Fatigue Lives in Additively Manufactured Alloys Based on the Crack-Growth Concept, 2017.
[153] A. Yadollahi, M. Mahmoudi, A. Elwany, H. Doude, L. Bian, J.C. Newman, Fatigue-life prediction of additively manufactured material: effects of heat treatment and build orientation, Fatigue Fract. Eng. Mater. Struct. 43 (2020) 831–844, https://doi.org/10.1111/FFE.13200.
[154] U. Zerbst, G. Bruno, J.Y. Buffière, T. Wegener, T. Niendorf, T. Wu, X. Zhang, N. Kashaev, G. Meneghetti, N. Hrabe, M. Madia, T. Werner, K. Hilgenberg, M. Koukolíková, R. Procházka, J. Džugan, B. Möller, S. Beretta, A. Evans, R. Wagener, K. Schnabel, Damage tolerant design of additively manufactured metallic components subjected to cyclic loading: state of the art and challenges, Prog. Mater. Sci. 121 (2021) 100786, https://doi.org/10.1016/J.PMATSCI.2021.100786.
[155] M. Bergant, T. Werner, M. Madia, A. Yawny, U. Zerbst, Short crack propagation analysis and fatigue strength assessment of additively manufactured materials: an application to AISI 316L, Int. J. Fatigue 151 (2021) 106396, https://doi.org/10.1016/J.IJFATIGUE.2021.106396.
[156] N. Macallister, T.H. Becker, Fatigue life estimation of additively manufactured Ti-6Al-4V: sensitivity, scatter and defect description in Damage-tolerant models, Acta Mater. 237 (2022) 118189, https://doi.org/10.1016/J.ACTAMAT.2022.118189.
[157] M. Bergant, N.O. Larrosa, A. Yawny, M. Madia, Short crack growth model for the evaluation of the fatigue strength of WAAM Ti-6Al-4V alloy containing pore-type defects, Eng. Fract. Mech. 289 (2023) 109467, https://doi.org/10.1016/j.engfracmech.2023.109467.
[158] Y. Murakami, Analysis of stress intensity factors of modes I, II and III for inclined surface cracks of arbitrary shape, Eng. Fract. Mech. 22 (1985) 101–114, https://doi.org/10.1016/0013-7944(85)90163-8.
[159] C.E. Phillips, Proc. Colloq on Fatigue IUTUM Stockholm 1955, 1956.
[160] D. Eylon, C.M. Pierce, Effect of microstructure on notch fatigue properties of Ti-6Al-4V, Metall. Trans. A 7 (1976) 111–121, https://doi.org/10.1007/BF02644046/METRICS.
[161] Y. Murakami, S. Fukuda, T. Endo, Effect of micro-hole on fatigue strength 1st report, effect of micro-hole (dia.: 40, 50, 80, 100 and 200 μm) on the fatigue strength of 0.13% and 0.46% carbon steel (in Japanese), Trans. Jpn. Soc. Mech. Eng. Ser. 44 (1978) 4003–4013, https://doi.org/10.1299/KIKAI1938.44.4003.
[162] Y. Murakami, H. Kawano, T. Endo, Effect of micro-hole on fatigue strength (2nd report, effect of micro-hole of 40-200 μm in diameter on the fatigue strength of quenched or quenched and tempered 0.46 Japanese), Trans. Jpn. Soc. Mech. Eng. A 45 (1979) 1479–1486, https://doi.org/10.1299/KIKAIA.45.1479.
[163] Y. Murakami, T. Endo, Effects of small defects on fatigue strength of metals, Int. J. Fatigue 2 (1980) 23–30, https://doi.org/10.1016/0142-1123(80)90024-9.
[164] H. Matsunaga, Y. Murakami, M. Kubota, J.H. Lee, Fatigue strength of Ti-6Al-4V alloys containing small artificial defects, Mater. Sci. Res. Int. 9 (2003) 263–269, https://doi.org/10.2472/jsms.52.12appendix_263.
[165] K. Shojima, S. Weldle, S. Okazaki, M. Endo, D. Eifler, F. Balle, Notch effects in high cycle fatigue of Ti-6Al-4V, Mater. Sci. Forum 750 (2013) 232–235, https://doi.org/10.4028/WWW.SCIENTIFIC.NET/MSF.750.232.
[166] Y. Murakami, H. Usuki, Prediction of fatigue strength of high-strength steels based on statistical evaluation of inclusion size (in Japanese), Trans. Jpn. Soc. Mech. Eng. A 55 (1989) 213–221, https://doi.org/10.1299/KIKAIA.55.213.
[167] K.J. Miller, The two thresholds of fatigue behaviour, Fatigue Fract. Eng. Mater. Struct. 16 (1993) 931–939, https://doi.org/10.1111/j.1460-2695.1993.tb00129.x.
[168] S. Usami, S. Shida, Elastic-plastic analysis of the fatigue limit for a material with small flaws, Fatigue Fract. Eng. Mater. Struct. 1 (1979) 471–481, https://doi.org/10.1111/J.1460-2695.1979.TB01334.X.
[169] Y. Murakami, S. Nemat-Nasser, Growth and stability of interacting surface flaws of arbitrary shape, Eng. Fract. Mech. 17 (1983) 193–210, https://doi.org/10.1016/0013-7944(83)90027-9.
[170] Y. Murakami, M. Isida, Analysis of an arbitrarily shaped surface crack and stress field at crack front near surface (in Japanese), Trans. Jpn. Soc. Mech. Eng. Ser. A 51 (1985) 1050–1056, https://doi.org/10.1299/kikaia.51.1050.
[171] Y. Murakami, M. Endo, Effects of hardness and crack geometry on ΔKth of small cracks (in Japanese), J. Soc. Mater. Sci. Jpn. 35 (1986) 911–917, https://doi.org/10.2472/JSMS.35.911.
[172] Y. Murakami, M. Endo, Effects of Hardness and Crack Geometry on ΔKth of Small Cracks Emanating from Small Defects, 1986.
[173] Y. Murakami, Metal Fatigue: Effects of Small Defects and Nonmetallic Inclusions, 2019.
[174] B. Atzori, P. Lazzarin, Notch sensitivity and defect sensitivity under fatigue loading: two sides of the same medal, Int. J. Fract. 107 (2001) 1–8, https://doi.org/10.1023/A:1007686727207.
[175] P. Lazzarin, R. Tovo, A unified approach to the evaluation of linear elastic stress fields in the neighborhood of cracks and notches, Int. J. Fract. 78 (1996) 3–19, https://doi.org/10.1007/BF00018497.
[176] M.L. Williams, Stress Singularities Resulting from Various Boundary Conditions in Angular Corners of Plates in Extension, J. Appl. Mech. 19 (1952), https://doi.org/10.1115/1.4010553.
[177] B. Gross, A. Mendelson, Plane elastostatic analysis of V-notched plates, Int. J. Fract. Mech. 8 (1972) 267–276, https://doi.org/10.1007/BF00186126.
[178] B. Atzori, P. Lazzarin, S. Filippi, Cracks and notches: analogies and differences of the relevant stress distributions and practical consequences in fatigue limit predictions, Int. J. Fatigue 23 (4) (2001) 355–362, https://doi.org/10.1016/S0142-1123(00)00107-9.
[179] P. Lazzarin, S. Filippi, A generalized stress intensity factor to be applied to rounded V-shaped notches, Int. J. Solids Struct. 43 (9) (2006) 2461–2478, https://doi.org/10.1016/j.ijsolstr.2005.03.007.
[180] F. Collini, D. Rigon, G. Meneghetti, A unified treatment of the fatigue limit of components weakened by stress raisers, subject to multiaxial mode I, II, and III loading, Proc. Struct. Integr. 53 (2024) 74–80, https://doi.org/10.1016/j.prostr.2024.01.010.
[181] S. Romano, A. Brückner-Foit, A. Brandão, J. Gumpinger, T. Ghidini, S. Beretta, Fatigue properties of AlSi10Mg obtained by additive manufacturing: defect-based modelling and prediction of fatigue strength, Eng. Fract. Mech. 187 (2018) 165–189, https://doi.org/10.1016/J.ENGFRACMECH.2017.11.002.
[182] M. Benedetti, V. Fontanari, M. Bandini, F. Zanini, S. Carmignato, Low- and high-cycle fatigue resistance of Ti-6Al-4V ELI additively manufactured via selective laser melting: mean stress and defect sensitivity, Int. J. Fatigue 107 (2018) 96–109, https://doi.org/10.1016/J.IJFATIGUE.2017.10.021.
[183] Y. Yamashita, T. Murakami, R. Mihara, M. Okada, Y. Murakami, Defect analysis and fatigue design basis for Ni-based superalloy 718 manufactured by selective laser melting, Int. J. Fatigue 117 (2018) 485–495, https://doi.org/10.1016/J.IJFATIGUE.2018.08.002.
[184] V.-D. Le, E. Pessard, F. Morel, F. Edy, Interpretation of the fatigue anisotropy of additively manufactured TA6V alloys via a fracture mechanics approach, Eng. Fract. Mech. 214 (2019) 410–426, https://doi.org/10.1016/j.engfracmech.2019.03.048.
[185] F. Stern, J. Kleinhorst, J. Tenkamp, F. Walther, Investigation of the anisotropic cyclic damage behavior of selective laser melted AISI 316L stainless steel, Fatigue Fract. Eng. Mater. Struct. 42 (2019) 2422–2430, https://doi.org/10.1111/ffe.13029.
[186] R. Biswal, X. Zhang, A.K. Syed, M. Awd, J. Ding, F. Walther, S. Williams, Criticality of porosity defects on the fatigue performance of wire + arc additive manufactured titanium alloy, Int. J. Fatigue 122 (2019) 208–217, https://doi.org/10.1016/j.ijfatigue.2019.01.017.
[187] G. Qian, Y. Li, D.S. Paolino, A. Tridello, F. Berto, Y. Hong, Very-high-cycle fatigue behavior of Ti-6Al-4V manufactured by selective laser melting: effect of build orientation, Int. J. Fatigue 136 (2020) 105628, https://doi.org/10.1016/J.IJFATIGUE.2020.105628.
[188] S. Beretta, M. Gargourimotlagh, S. Foletti, A. du Plessis, M. Riccio, Fatigue strength assessment of “as built” AlSi10Mg manufactured by SLM with different build orientations, Int. J. Fatigue 139 (2020) 105737, https://doi.org/10.1016/J.IJFATIGUE.2020.105737.
[189] D. Rigon, G. Meneghetti, An engineering estimation of fatigue thresholds from a microstructural size and Vickers hardness: application to wrought and additively manufactured metals, Int. J. Fatigue 139 (10 2020), https://doi.org/10.1016/J.IJFATIGUE.2020.105796.
[190] J. Gumpinger, A.D. Brandao, E. Beevers, T. Rohr, T. Ghidini, S. Beretta, S. Romano, Expression of additive manufacturing surface irregularities through a flaw-based

assessment, structural integrity of additive manufactured parts, ASTM Int. (2020) 234–249, https://doi.org/10.1520/STP162020180098.
[191] Y.N. Hu, S.C. Wu, Z.K. Wu, X.L. Zhong, S. Ahmed, S. Karabal, X.H. Xiao, H.O. Zhang, P.J. Withers, A new approach to correlate the defect population with the fatigue life of selective laser melted Ti-6Al-4V alloy, Int. J. Fatigue 136 (2020) 105584, https://doi.org/10.1016/J.IJFATIGUE.2020.105584.
[192] D. Rigon, G. Meneghetti, Engineering estimation of the fatigue limit of wrought and defective additively manufactured metals for different load ratios, Int. J. Fatigue 154 (2022) 106530, https://doi.org/10.1016/J.IJFATIGUE.2021.106530.
[193] L. Barricelli, L. Patriarca, A. du Plessis, S. Beretta, Orientation-dependent fatigue assessment of Ti6Al4V manufactured by L-PBF: size of surface features and shielding effect, Int. J. Fatigue 168 (2023) 107401, https://doi.org/10.1016/J.IJFATIGUE.2022.107401.
[194] A. Tognan, E. Salvati, Probabilistic defect-based modelling of fatigue strength for incomplete datasets assisted by literature data, Int. J. Fatigue 173 (2023) 107665, https://doi.org/10.1016/j.ijfatigue.2023.107665.
[195] K. Morishita, T. Yamaguchi, K. Wada, J. Yamabe, Technique for introducing internal defects with arbitrary sizes and locations in metals via additive manufacturing and evaluation of fatigue properties, Int. J. Autom. Technol. 17 (2023) 378–387, https://doi.org/10.20965/ijat.2023.p0378.
[196] Y. Murakami, S. Nemat-Nasser, Interacting dissimilar semi-elliptical surface flaws under tension and bending, Eng. Fract. Mech. 16 (1982) 373–386, https://doi.org/10.1016/0013-7944(82)90115-1.
[197] K.F. Walker, J.M. Lourenço, S. Sun, M. Brandt, C.H. Wang, Quantitative fractography and modelling of fatigue crack propagation in high strength AerMet®100 steel repaired with a laser cladding process, Int. J. Fatigue 94 (2017) 288–301, https://doi.org/10.1016/J.IJFATIGUE.2016.06.031.
[198] BS 7910 - Guide to methods for assessing the acceptability of flaws in metallic structures.
[199] Y. Murakami, Y. Tazunoki, T. Endo, Existence of coaxing effect and effect of small artificial holes of 40-200 μm diameter on fatigue strength in 2017S-T4 Al alloy and 7:3 brass (in Japanese), Trans. Jpn. Soc. Mech. Eng. 47 (1981) 1293–1300, https://doi.org/10.1299/KIKAIA.47.1293.
[200] W.O. Soboyejo, K. Kishimoto, R.A. Smith, J.F. Knott, A study of the interaction and coalescence of two coplanar fatigue cracks in bending, Fatigue Fract. Eng. Mater. Struct. 12 (1989) 167–174, https://doi.org/10.1111/J.1460-2695.1989.TB00524.X.
[201] N.A. Noda, K. Kobayashi, T. Oohashi, Variation of the stress intensity factor along the crack front of interacting semi-elliptical surface cracks, Arch. Appl. Mech. 71 (2001) 43–52, https://doi.org/10.1007/S004190000113/METRICS.
[202] Y. Wang, K. Hashimoto, K. Terai, Y. Tomita, N. Osawa, Study on setting the conditions of initial cracks for fatigue strength evaluation of welded structures, J. Soc. Nav. Archit. Jpn. 2002 (2002) 545–553, https://doi.org/10.2534/JJASNAOE1968.2002.545.
[203] A. Carpinteri, R. Brighenti, S. Vantadori, A numerical analysis on the interaction of twin coplanar flaws, Eng. Fract. Mech. 71 (2004) 485–499, https://doi.org/10.1016/S0013-7944(03)00040-7.
[204] M. Åman, S. Okazaki, H. Matsunaga, G.B. Marquis, H. Remes, Interaction effect of adjacent small defects on the fatigue limit of a medium carbon steel, Fatigue Fract. Eng. Mater. Struct. 40 (2017) 130–144, https://doi.org/10.1111/FFE.12482.
[205] J. Alegre, I. Cuesta, A. Díaz, Stress-intensity factor solutions for embedded elliptical cracks in round bars subjected to tensile load, Theor. Appl. Fract. Mech. 117 (2022) 103189, https://doi.org/10.1016/j.tafmec.2021.103189.
[206] K. Yanase, M. Endo, Multiaxial high cycle fatigue threshold with small defects and cracks, Eng. Fract. Mech. 123 (2014) 182–196.
[207] Y. Murakami, K. Takahashi, T. Yamashita, Quantitative evaluation of the effect of the surface roughness on fatigue strength (in Japanese), Trans. Jpn. Soc. Mech. Eng. Ser. A 63 (1997) 1612–1619, https://doi.org/10.1299/KIKAIA.63.1612.
[208] D. Rigon, F. Coppola, G. Meneghetti, Fracture mechanics-based analysis of the fatigue limit of Ti6Al4V alloy specimens manufactured by SLM in as-built surface conditions by means of areal measurements, Eng. Fract. Mech. 295 (2024) 109720, https://doi.org/10.1016/j.engfracmech.2023.109720.
[209] D. Greitemeier, F. Palm, F. Syassen, T. Melz, Fatigue performance of additive manufactured TiAl6V4 using electron and laser beam melting, Int. J. Fatigue 94 (2017) 211–217, https://doi.org/10.1016/J.IJFATIGUE.2016.05.001.
[210] A. Carpinteri, Elliptical-arc surface cracks in round bars, Fatigue Fract. Eng. Mater. Struct. 15 (1992) 1141–1153, https://doi.org/10.1111/j.1460-2695.1992.tb00039.x.
[211] J.C. Newman Jr., I.S. Raju, Analysis of Surface Cracks in Finite Plates Under Tension or Bending Loads, 1979.
[212] S.A. Yavari, R. Wauthle, J. van der Stok, A. Riemslag, M. Janssen, M. Mulier, J. Kruth, J. Schrooten, H. Weinans, A. Zadpoor, Fatigue behavior of porous biomaterials manufactured using selective laser melting, Mater. Sci. Eng. C 33 (2013) 4849–4858, https://doi.org/10.1016/j.msec.2013.08.006.
[213] J. de Krijger, C. Rans, B.V. Hooreweder, K. Lietaert, B. Pouran, A.A. Zadpoor, Effects of applied stress ratio on the fatigue behavior of additively manufactured porous biomaterials under compressive loading, J. Mech. Behav. Biomed. Mater. 70 (2017) 7–16, https://doi.org/10.1016/J.JMBBM.2016.11.022.
[214] S.A. Yavari, S.M. Ahmadi, R. Wauthle, B. Pouran, J. Schrooten, H. Weinans, A.A. Zadpoor, Relationship between unit cell type and porosity and the fatigue behavior of selective laser melted meta-biomaterials, J. Mech. Behav. Biomed. Mater. 43 (2015) 91–100, https://doi.org/10.1016/J.JMBBM.2014.12.015.
[215] R. Hedayati, H. Hosseini-Toudeshky, M. Sadighi, M. Mohammadi-Aghdam, A.A. Zadpoor, Computational prediction of the fatigue behavior of additively manufactured porous metallic biomaterials, Int. J. Fatigue 84 (2016) 67–79, https://doi.org/10.1016/J.IJFATIGUE.2015.11.017.
[216] A. Burr, T. Persenot, P.-T. Doutre, J.-Y. Buffiere, P. Lhuissier, G. Martin, R. Dendievel, A numerical framework to predict the fatigue life of lattice structures built by additive manufacturing, Int. J. Fatigue 139 (2020) 105769, https://doi.org/10.1016/J.IJFATIGUE.2020.105769.
[217] H. Soul, P. Terriault, V. Brailovski, The static and fatigue behavior of AlSiMg alloy plain, notched, and diamond lattice specimens fabricated by laser powder bed fusion, J. Manuf. Mater. Process. 2 (2018) 25, https://doi.org/10.3390/jmmp2020025.
[218] A. Yánez, M.P. Fiorucci, A. Cuadrado, O. Martel, D. Monopoli, Surface roughness effects on the fatigue behaviour of gyroid cellular structures obtained by additive manufacturing, Int. J. Fatigue 138 (2020) 105702, https://doi.org/10.1016/j.ijfatigue.2020.105702.
[219] K. Solberg, F. Berto, Notch-defect interaction in additively manufactured Inconel 718, Int. J. Fatigue 122 (2019) 35–45, https://doi.org/10.1016/J.IJFATIGUE.2018.12.021.
[220] K. Solberg, D. Wan, F. Berto, Fatigue assessment of as-built and heat-treated Inconel 718 specimens produced by additive manufacturing including notch effects, Fatigue Fract. Eng. Mater. Struct. 43 (2020) 2326–2336, https://doi.org/10.1111/FFE.13300.
[221] P. Köhnen, C. Haase, J. Bültmann, S. Ziegler, J.H. Schleifenbaum, W. Bleck, Mechanical properties and deformation behavior of additively manufactured lattice structures of stainless steel, Mater. Des. 145 (2018) 205–217, https://doi.org/10.1016/J.MATDES.2018.02.062.
[222] S. Murchio, M. Dallago, A. Rigatti, V. Luchin, F. Berto, D. Maniglio, M. Benedetti, On the effect of the node and building orientation on the fatigue behavior of L-PBF Ti6Al4V lattice structure sub-unital elements, Mater. Des. Process. Commun. 3 (12 2021), https://doi.org/10.1002/mdp2.258.
[223] L. Boniotti, S. Dancette, M. Gavazzoni, J. Lachambre, J.Y. Buffiere, S. Foletti, Experimental and numerical investigation on fatigue damage in micro-lattice materials by Digital Volume Correlation and μCT-based finite element models, Eng. Fract. Mech. 266 (2022) 108370, https://doi.org/10.1016/J.ENGFRACMECH.2022.108370.
[224] M. Pedranz, V. Fontanari, S. Raghavendra, C. Santus, F. Zanini, S. Carmignato, D. Lusuardi, F. Berto, M. Benedetti, A new energy based highly stressed volume concept to investigate the notch-pores interaction in thick-walled ductile cast iron subjected to uniaxial fatigue, Int. J. Fatigue 169 (2023) 107491, https://doi.org/10.1016/j.ijfatigue.2022.107491.
[225] E. Belmonte, M.D. Monte, C.-J. Hoffmann, M. Quaresimin, Damage initiation and evolution in short fiber reinforced polyamide under fatigue loading: influence of fiber volume fraction, Compos., Part B, Eng. 113 (2017) 331–341, https://doi.org/10.1016/j.compositesb.2017.01.023.
[226] K. Solberg, F. Berto, A diagram for capturing and predicting failure locations in notch geometries produced by additive manufacturing, Int. J. Fatigue 134 (2020) 105428, https://doi.org/10.1016/j.ijfatigue.2019.105428.
[227] S. Afkhami, E. Dabiri, K. Lipiäinen, H. Piili, T. Björk, Effects of notch-load interactions on the mechanical performance of 3D printed tool steel 18Ni300, Addit. Manuf. 47 (2021) 102260, https://doi.org/10.1016/j.addma.2021.102260.
[228] A. Fatemi, R. Molaei, J. Simsiriwong, N. Sanaei, J. Pegues, B. Torries, N. Phan, N. Shamsaei, Fatigue behaviour of additive manufactured materials: an overview of some recent experimental studies on Ti-6Al-4V considering various processing and loading direction effects, Fatigue Fract. Eng. Mater. Struct. 42 (2019) 991–1009, https://doi.org/10.1111/FFE.13000.
[229] D. Greitemeier, C.D. Donne, F. Syassen, J. Eufinger, T. Melz, Effect of surface roughness on fatigue performance of additive manufactured Ti–6Al–4V, Mater. Sci. Technol. 32 (2016) 629–634, https://doi.org/10.1179/1743284715Y.0000000053.
[230] S. Bagherifard, N. Beretta, S. Monti, M. Riccio, M. Bandini, M. Guagliano, On the fatigue strength enhancement of additive manufactured AlSi10Mg parts by mechanical and thermal post-processing, Mater. Des. 145 (2018) 28–41, https://doi.org/10.1016/J.MATDES.2018.02.055.
[231] F. Sausto, S. Romano, L. Patriarca, S. Miccoli, S. Beretta, Benchmark of a probabilistic fatigue software based on machined and as-built components manufactured in AlSi10Mg by L-PBF, Int. J. Fatigue 165 (2022) 107171, https://doi.org/10.1016/J.IJFATIGUE.2022.107171.
[232] H.K. Rafi, N.V. Karthik, H. Gong, T.L. Starr, B.E. Stucker, Microstructures and mechanical properties of Ti6Al4V parts fabricated by selective laser melting and electron beam melting, J. Mater. Eng. Perform. 22 (2013) 3872–3883, https://doi.org/10.1007/s11665-013-0658-0.
[233] V. Chastand, A. Tezenas, Y. Cadoret, P. Quaegebeur, W. Maia, E. Charkaluk, Fatigue characterization of titanium Ti-6Al-4V samples produced by additive manufacturing, Proc. Struct. Integr. 2 (2016) 3168–3176, https://doi.org/10.1016/j.prostr.2016.06.395.
[234] F. Sausto, P. Carrion, N. Shamsaei, S. Beretta, Fatigue failure mechanisms for AlSi10Mg manufactured by L-PBF under axial and torsional loads: the role of de-

fects and residual stresses, Int. J. Fatigue 162 (2022) 106903, https://doi.org/10.1016/J.IJFATIGUE.2022.106903.

[235] P. Lehner, B. Blinn, T. Beck, Improving the defect tolerance and fatigue strength of AM AlSi10Mg, Adv. Eng. Mater. 25 (8 2023), https://doi.org/10.1002/adem.202201855.

[236] N. Razavi, S. Bagherifard, S. Hafnor, S. Spiller, M. Guagliano, F. Berto, Fatigue analysis of as-built and heat-treated severely notched AlSi10Mg alloy specimens made by laser powder bed fusion technology, Int. J. Fatigue 179 (2024) 108041, https://doi.org/10.1016/j.ijfatigue.2023.108041.

[237] A. Sterling, N. Shamsaei, B. Torries, S.M. Thompson, Fatigue behaviour of additively manufactured Ti-6Al-4V, Proc. Eng. 133 (2015) 576–589, https://doi.org/10.1016/J.PROENG.2015.12.632.

[238] A.J. Sterling, B. Torries, N. Shamsaei, S.M. Thompson, D.W. Seely, Fatigue behavior and failure mechanisms of direct laser deposited Ti-6Al-4V, Mater. Sci. Eng. A 655 (2016) 100–112, https://doi.org/10.1016/J.MSEA.2015.12.026.

[239] R. Shrestha, J. Simsiriwong, N. Shamsaei, S.M. Thompson, L. Bian, Effect of build orientation on the fatigue behavior of stainless steel 316L manufactured via a laser-powder bed fusion process, in: 27th Annual Solid Freeform Fabrication Symposium Proceedings, 2016.

[240] O. Andreau, E. Pessard, I. Koutiri, J.D. Penot, C. Dupuy, N. Saintier, P. Peyre, A competition between the contour and hatching zones on the high cycle fatigue behaviour of a 316L stainless steel: analyzed using X-ray computed tomography, Mater. Sci. Eng. A 757 (2019) 146–159, https://doi.org/10.1016/J.MSEA.2019.04.101.

[241] E. Beevers, A.D. Brandão, J. Gumpinger, M. Gschweitl, C. Seyfert, P. Hofbauer, T. Rohr, T. Ghidini, Fatigue properties and material characteristics of additively manufactured AlSi10Mg – effect of the contour parameter on the microstructure, density, residual stress, roughness and mechanical properties, Int. J. Fatigue 117 (2018) 148–162, https://doi.org/10.1016/j.ijfatigue.2018.08.023.

[242] B. Torries, N. Shamsaei, S.M. Thompson, Effects of Build Orientation on Fatigue Performance of Ti-6Al-4V Parts Fabricated via Laser-Based Powder Bed Fusion, 2017.

[243] N.W. Hrabe, P. Heinl, B. Flinn, C. Körner, R.K. Bordia, Compression-compression fatigue of selective electron beam melted cellular titanium (Ti-6Al-4V), J. Biomed. Mater. Res., Part B, Appl. Biomater. 99B (2011) 313–320, https://doi.org/10.1002/jbm.b.31901.

[244] Y. Liu, H. Wang, S. Li, S. Wang, W. Wang, W. Hou, Y. Hao, R. Yang, L. Zhang, Compressive and fatigue behavior of beta-type titanium porous structures fabricated by electron beam melting, Acta Mater. 126 (2017) 58–66, https://doi.org/10.1016/j.actamat.2016.12.052.

[245] S. Ahmadi, R. Hedayati, Y. Li, K. Lietaert, N. Tümer, A. Fatemi, C. Rans, B. Pouran, H. Weinans, A. Zadpoor, Fatigue performance of additively manufactured meta-biomaterials: the effects of topology and material type, Acta Biomater. 65 (2018) 292–304, https://doi.org/10.1016/j.actbio.2017.11.014.

[246] C.N. Kelly, J. Francovich, S. Julmi, D. Safranski, R.E. Guldberg, H.J. Maier, K. Gall, Fatigue behavior of As-built selective laser melted titanium scaffolds with sheet-based gyroid microarchitecture for bone tissue engineering, Acta Biomater. 94 (2019) 610–626, https://doi.org/10.1016/J.ACTBIO.2019.05.046.

[247] M.-W. Wu, J.-K. Chen, B.-H. Lin, P.-H. Chiang, M.-K. Tsai, Compressive fatigue properties of additive-manufactured Ti-6Al-4V cellular material with different porosities, Mater. Sci. Eng. A 790 (2020) 139695, https://doi.org/10.1016/j.msea.2020.139695.

[248] S. Raghavendra, A. Molinari, V. Fontanari, G. Zappini, M. Benedetti, Evaluation of static and fatigue properties of regular lattice and trabecular cellular structures, Proc. Struct. Integr. 28 (2020) 517–524, https://doi.org/10.1016/j.prostr.2020.10.061.

[249] S. Raghavendra, A. Molinari, A. Cao, C. Gao, F. Berto, G. Zappini, M. Benedetti, Quasi-static compression and compression–compression fatigue behavior of regular and irregular cellular biomaterials, Fatigue Fract. Eng. Mater. Struct. 44 (2021) 1178–1194, https://doi.org/10.1111/ffe.13422.

[250] S. Ahmadi, R. Kumar, E. Borisov, R. Petrov, S. Leeflang, Y. Li, N. Tümer, R. Huizenga, C. Ayas, A. Zadpoor, V. Popovich, From microstructural design to surface engineering: a tailored approach for improving fatigue life of additively manufactured meta-biomaterials, Acta Biomater. 83 (2019) 153–166, https://doi.org/10.1016/j.actbio.2018.10.043.

[251] D. Tang, X. He, B. Wu, L. Dang, H. Xin, Y. Li, Anisotropic fatigue performance of directed energy deposited Ti-6Al-4V: effects of build orientation, Mater. Sci. Eng. A 876 (2023) 145112, https://doi.org/10.1016/j.msea.2023.145112.

[252] X. Liang, A. Hor, C. Robert, F. Lin, F. Morel, Effects of building direction and loading mode on the high cycle fatigue strength of the laser powder bed fusion 316L, Int. J. Fatigue 170 (2023) 107506, https://doi.org/10.1016/j.ijfatigue.2023.107506.

[253] W. Yuan, W. Hou, S. Li, Y. Hao, R. Yang, L.C. Zhang, Y. Zhu, Heat treatment enhancing the compressive fatigue properties of open-cellular Ti-6Al-4V alloy prototypes fabricated by electron beam melting, J. Mater. Sci. Technol. 34 (2018) 1127–1131, https://doi.org/10.1016/J.JMST.2017.12.003.

[254] M.-W. Wu, J.-K. Chen, B.-H. Lin, P.-H. Chiang, Improved fatigue endurance ratio of additive manufactured Ti-6Al-4V lattice by hot isostatic pressing, Mater. Des. 134 (2017) 163–170, https://doi.org/10.1016/j.matdes.2017.08.048.

[255] L. Yang, C. Yan, W. Cao, Z. Liu, B. Song, S. Wen, C. Zhang, Y. Shi, S. Yang, Compression–compression fatigue behaviour of gyroid-type triply periodic minimal surface porous structures fabricated by selective laser melting, Acta Mater. 181 (2019) 49–66, https://doi.org/10.1016/j.actamat.2019.09.042.

[256] Y. Xiong, W. Wang, R. Gao, H. Zhang, L. Dong, J. Qin, B. Wang, W. Jia, X. Li, Fatigue behavior and osseointegration of porous Ti-6Al-4V scaffolds with dense core for dental application, Mater. Des. 195 (2020) 108994, https://doi.org/10.1016/j.matdes.2020.108994.

[257] L. Bai, C. Gong, X. Chen, J. Zheng, L. Xin, Y. Xiong, X. Wu, M. Hu, K. Li, Y. Sun, Quasi-Static compressive responses and fatigue behaviour of Ti-6Al-4V graded lattice structures fabricated by laser powder bed fusion, Mater. Des. 210 (2021) 110110, https://doi.org/10.1016/j.matdes.2021.110110.

[258] W. Radlof, C. Polley, H. Seitz, M. Sander, Influence of structure-determining parameters on the mechanical properties and damage behavior of electron beam melted lattice structures under quasi-static and fatigue compression loading, Mater. Lett. 289 (2021) 129380, https://doi.org/10.1016/J.MATLET.2021.129380.

[259] A. Cutolo, B.V. Hooreweder, Fatigue behaviour of diamond based Ti-6Al-4V lattice structures produced by laser powder bed fusion: on the effect of load direction, Mater. Today Commun. 33 (2022) 104661, https://doi.org/10.1016/J.MTCOMM.2022.104661.

[260] M. Tilton, A. Borjali, J.C. Griffis, K.M. Varadarajan, G.P. Manogharan, Fatigue properties of Ti-6Al-4V TPMS scaffolds fabricated via laser powder bed fusion, Manuf. Lett. 37 (2023) 32–38, https://doi.org/10.1016/j.mfglet.2023.06.005.

[261] M. Pisati, M.G. Corneo, S. Beretta, E. Riva, F. Braghin, S. Foletti, Numerical and experimental investigation of cumulative fatigue damage under random dynamic cyclic loads of lattice structures manufactured by laser powder bed fusion, Metals 11 (9) (2021) 1395, https://doi.org/10.3390/MET11091395.

[262] M. Gavazzoni, S. Beretta, L. Boniotti, E.D. Carmine, L. Gallazzi, R. Iazurlo, S. Foletti, Structural assessment of a multi-functional additively manufactured space component with bulk-lattice hybrid architecture, Thin-Walled Struct. 192 (2023) 111158, https://doi.org/10.1016/j.tws.2023.111158.

[263] K. Lietaert, A. Cutolo, D. Boey, B. Van Hooreweder, Fatigue life of additively manufactured Ti6Al4V scaffolds under tension-tension, tension-compression and compression-compression fatigue load, Sci. Rep. 8 (2018) 4957, https://doi.org/10.1038/s41598-018-23414-2.

[264] M. Gavazzoni, L. Boniotti, S. Foletti, Influence of specimen size on the mechanical properties of microlattices obtained by selective laser melting, 235 (2019) 1774–1787, https://doi.org/10.1177/0954406219869741.

[265] E.G. Brodie, T. Wegener, J. Richter, A. Medvedev, T. Niendorf, A. Molotnikov, A mechanical comparison of alpha and beta phase biomedical TiTa lattice structures, Mater. Des. 212 (2021) 110220, https://doi.org/10.1016/j.matdes.2021.110220.

[266] N. Soro, N. Saintier, J. Merzeau, M. Veidt, M.S. Dargusch, Quasi-static and fatigue properties of graded Ti-6Al-4V lattices produced by Laser Powder Bed Fusion (LPBF), Addit. Manuf. 37 (2021) 101653, https://doi.org/10.1016/J.ADDMA.2020.101653.

[267] A. Coluccia, G.D. Pasquale, Strain-based method for fatigue failure prediction of additively manufactured lattice structures, Sci. Rep. 13 (2023) 22775, https://doi.org/10.1038/s41598-023-49846-z.

[268] Y. Li, K. Lietaert, W. Li, X.-Y. Zhang, M. Leeflang, J. Zhou, A. Zadpoor, Corrosion fatigue behavior of additively manufactured biodegradable porous iron, Corros. Sci. 156 (2019) 106–116, https://doi.org/10.1016/j.corsci.2019.05.003.

[269] Y. Li, W. Li, F. Bobbert, K. Lietaert, J.-H. Dong, M. Leeflang, J. Zhou, A. Zadpoor, Corrosion fatigue behavior of additively manufactured biodegradable porous zinc, Acta Biomater. 106 (2020) 439–449, https://doi.org/10.1016/j.actbio.2020.02.001.

[270] W. Radlof, H. Panwitt, C. Benz, M. Sander, Image-based and in-situ measurement techniques for the characterization of the damage behavior of additively manufactured lattice structures under fatigue loading, Proc. Struct. Integr. 38 (2022) 50–59, https://doi.org/10.1016/J.PROSTR.2022.03.006.

[271] A. Timercan, P. Terriault, V. Brailovski, Axial tension/compression and torsional loading of diamond and gyroid lattice structures for biomedical implants: simulation and experiment, Mater. Des. 225 (2023) 111585, https://doi.org/10.1016/j.matdes.2022.111585.

[272] D. Zhao, C. Han, B. Peng, T. Cheng, J. Fan, L. Yang, L. Chen, Q. Wei, Corrosion fatigue behavior and anti-fatigue mechanisms of an additively manufactured biodegradable zinc-magnesium gyroid scaffold, Acta Biomater. 153 (2022) 614–629, https://doi.org/10.1016/j.actbio.2022.09.047.

[273] G. Li, D. Chen, Y. Mine, K. Takashima, Y. Zheng, Fatigue behavior of biodegradable Zn-Li binary alloys in air and simulated body fluid with pure Zn as control, Acta Biomater. 168 (2023) 637–649, https://doi.org/10.1016/j.actbio.2023.07.030.

[274] ISO 13.314 - Mechanical testing of metals — Ductility testing — Compression test for porous and cellular metals.

[275] ASTM E466 - Standard Practice for Conducting Force Controlled Constant Amplitude Axial Fatigue Tests of Metallic Materials.

[276] M. Benedetti, S. Raghavendra, R.D. Biasi, F. Russo, G. Zappini, F. Berto, Characterization of compressive fatigue behavior and acoustic emission analysis of Ti6Al4V cellular lattice materials fabricated by laser powder bed fusion [Conference presentation], in: ESIAM23 the Third European Conference on the Structural Integrity of Additively Manufactured Materials, 2023.

[277] A. Wormsen, A. Fjeldstad, G. Härkegård, The application of asymptotic solutions to a semi-elliptical crack at the root of a notch, Eng. Fract. Mech. 73 (2006) 1899–1912, https://doi.org/10.1016/J.ENGFRACMECH.2006.02.006.
[278] A. Fjeldstad, A. Wormsen, G. Härkegård, Approximate stress intensity factors for cracked V-notched specimens based on asymptotic solutions with application to T-joints, Eng. Fract. Mech. 75 (2008) 1083–1098, https://doi.org/10.1016/J.ENGFRACMECH.2007.04.028.
[279] P. Kumar, U. Ramamurty, High cycle fatigue in selective laser melted Ti-6Al-4V, Acta Mater. 194 (2020) 305–320, https://doi.org/10.1016/j.actamat.2020.05.041.
[280] P. Kumar, U. Ramamurty, Microstructural optimization through heat treatment for enhancing the fracture toughness and fatigue crack growth resistance of selective laser melted Ti 6Al 4V alloy, Acta Mater. 169 (2019) 45–59, https://doi.org/10.1016/j.actamat.2019.03.003.
[281] B. Atzori, D. Rigon, G. Meneghetti, An analysis of the dependence of the material length parameter a_0 on the stress ratio, IOP Conf. Ser., Mater. Sci. Eng. 1275 (2023) 012019, https://doi.org/10.1088/1757-899X/1275/1/012019.
[282] K.J. Miller, The short crack problem, Fatigue Fract. Eng. Mater. Struct. 5 (1982) 223–232, https://doi.org/10.1111/J.1460-2695.1982.TB01250.X.
[283] S. Romano, E. Peradotto, S. Beretta, D. Ugues, L. Barricelli, G. Maculotti, L. Patriarca, G. Genta, Fatigue strength estimation of net-shape L-PBF Co–Cr–Mo alloy via non-destructive surface measurements, Int. J. Fatigue 178 (2024) 108018, https://doi.org/10.1016/j.ijfatigue.2023.108018.
[284] A. Karolczuk, A. Kurek, M. Böhm, S. Derda, M. Prażmowski, K. Kluger, K. Żak, Łukasz Pejkowski, J. Seyda, Heterogeneous effect of aging temperature on the fatigue life of additively manufactured thin-walled 18Ni300 maraging steel tubular specimen, Mater. Des. 237 (2024) 112561, https://doi.org/10.1016/j.matdes.2023.112561.
[285] F.J. Kalahroudi, M. Sadek, P. Krakhmalev, T. Berglund, J. Bergström, M. Grehk, On the microstructure and high cycle fatigue of near-net shape PM-HIPed Inconel 625, Mater. Sci. Eng. A 886 (2023) 145671, https://doi.org/10.1016/j.msea.2023.145671.
[286] C. Shi, N. Nouri, V. Schulze, S. Dietrich, High cycle fatigue behaviour of AISI 4140 steel manufactured by laser-powder bed fusion, Int. J. Fatigue 168 (2023) 107469, https://doi.org/10.1016/j.ijfatigue.2022.107469.
[287] ASTM E647 - Standard Method for Measurement of Fatigue Crack Growth Rates.
[288] BS ISO 12108 - Metallic materials - Fatigue testing - Fatigue crack growth method.
[289] U. Zerbst, M. Vormwald, R. Pippan, H.-P. Gänser, C. Sarrazin-Baudoux, M. Madia, About the fatigue crack propagation threshold of metals as a design criterion – A review, Eng. Fract. Mech. 153 (2016) 190–243, https://doi.org/10.1016/j.engfracmech.2015.12.002.
[290] G. Meneghetti, P. Lazzarin, Significance of the elastic peak stress evaluated by FE analyses at the point of singularity of sharp V-notched components, Fatigue Fract. Eng. Mater. Struct. 30 (2007) 95–106, https://doi.org/10.1111/j.1460-2695.2006.01084.x.
[291] G. Meneghetti, A. Campagnolo, State-of-the-art review of peak stress method for fatigue strength assessment of welded joints, Int. J. Fatigue 139 (2020) 105705, https://doi.org/10.1016/j.ijfatigue.2020.105705.
[292] B. Atzori, L. Susmel, Notch and defect sensitivity under any kind of fatigue loading: an unifying approach, in: Proc. of the 11th International Conference on Fracture, 2005.
[293] S. Beretta, Y. Murakami, Statistical analysis of defects for fatigue strength prediction and quality control of materials, Fatigue Fract. Eng. Mater. Struct. 21 (9) (1998) 1049–1065, https://doi.org/10.1046/j.1460-2695.1998.00104.x.
[294] S. Beretta, Y. Murakami, Largest-extreme-value distribution analysis of multiple inclusion types in determining steel cleanliness, Metall. Mater. Trans. B 32 (2001) 517–523, https://doi.org/10.1046/j.1460-2695.1998.00104.x.
[295] J.C. Fox, A.L. Pintar, Prediction of extreme value areal parameters in laser powder bed fusion of nickel superalloy 625, Surf. Topogr., Metrol. Prop. 9 (2) (2021) 025033, https://doi.org/10.1088/2051-672X/ac0061.
[296] ASTM E2283-08 - Standard Practice for Extreme Value Analysis of Nonmetallic Inclusions in Steel and Other Microstructural Features.